VESTNIK
of
DON STATE
TECHNICAL
UNIVERSITY

Vol. 19, № 2

Theoretical
and scientific-practical journal

Published since 1999

4 issues a year
April-June 2019

ISSN 1992-5980
eISSN 1992-6006
DOI: 10.23947/1992-5980

Founder and publisher — Don State Technical University

Included in the list of peer-reviewed scientific editions where the basic research results of doctoral, candidate's theses should be published (State Commission for Academic Degrees and Titles List) in the following research areas:

01.02.01 – Analytical Mechanics (Engineering Sciences)
01.02.04 – Deformable Solid Mechanics (Engineering Sciences)
01.02.04 – Deformable Solid Mechanics (Physicomathematical Sciences)
01.02.06 – Dynamics, Strength of Machines, Gear, and Equipment (Engineering Sciences)
05.02.02 – Engineering Science, Drive Systems and Machine Parts (Engineering Sciences)
05.02.04 – Machine Friction and Wrear (Engineering Sciences)
05.02.07 – Technology and Equipment of Mechanical and Physicotechnical Processing (Engineering Sciences)
05.02.08 – Engineering Technology (Engineering Sciences)
05.02.10 – Welding, Allied Processes and Technologies (Engineering Sciences)
05.02.11 – Testing Methods and Diagnosis in Machine Building (Engineering Sciences)
05.13.11 – Software and Mathematical Support of Machines, Complexes and Computer Networks (Engineering Sciences)
05.13.17 – Foundations of Information Science (Engineering Sciences)
05.13.18 – Mathematical Simulation, Numerical Methods and Program Systems (Engineering Sciences)

The journal is indexed and archived in the Russian Science Citation Index (RSCI), and in EBSCO International Database
The journal is a member of Directory of Open Access Journals (DOAJ), Association of Science Editors and Publishers (ASEP) and Cross Ref

Certificate of mass media registration ПИ № ФС 77-66004 of 06.06.2016 is issued by the Federal Service for Supervision of Communications, Information Technology, and Mass Media

The subscription index in Rospechat catalogue is 35578

The issue is prepared by:
Inna V. Boyko, Marina P. Smirnova (English version)
Passed for printing 28.06.2019,
imprint date 30.06.2019.
Format 60×84/8. Font «Times New Roman».
C.p.sh. 22.6. Circulation 1000 cop. Order no. 28/06 Free price.

Founder's, Publisher's and Printery Address:
Gagarin Sq. 1, Rostov-on-Don, 344000, Russia. Phone: +7 (863) 2-738-372
E-mail: vestnik@donstu.ru http://vestnik.donstu.ru/

CONTENT

MECHANICS

Zakovorotny V. L., Gvindzhiliya V. E., Kolodkin P. S. Effect of dynamic properties of interacting subsystems on evolution of selective transfer formation in friction units 104

Safonova M. N., Arkhangelskaya E. A., Fedotov A. A. On specifics of hardening mechanisms in metalli matrix composition 113

MACHINE BUILDING AND MACHINE SCIENCE

Strelnikov V. N., Voloshin A. I., Sukov M. G. Development of a power model for large wave gear toothing 120

Bordatchev E. V., Lapshin V. P. Mathematical temperature simulation in tool-to-work contact zone during metal turning 130

Fomin N. E., Khasan I. Kh., Kyashkin V. M. Effect of electrospark doping on mechanical properties of Al-Si-Cu alloys 138

Madorsky V. V., Rogov I. E., Kruglov A. K. Study on frequency dependence of polarized piezoceramics constants in equivalent circuits at weak electric fields (part III) 143

Zhukova I. Yu., Kashparov I. I., Kucherenko S. V., Kagan E. Sh. Comparative characteristics of sterically hindered phenols and nitroxide radicals as stabilizers of polyethylene photodegradation 151

Kobzev K. O. Study of the working body mechanism in forging-and-stamping equipment 158

Kireev S. O., Stepanov V. N., Korchagina M. V., Yefimov A. V. Effectiveness analysis of external heating system of gauge tank of pumping unit using exhaust piping of the IC engine 164

Pilyushina G. A., Pyrikov P. G., Pamfilov E. A., Kapustin V. V. On ensuring joint tightness on the basis of technological induction 170

INFORMATION TECHNOLOGY, COMPUTER SCIENCE, AND MANAGEMENT

Tsibirova I. M. Formation of similarity criteria for physical objects and processes based on NonDimCritFormer 1.0 computer program 179

Razumov P. V., Smirnov I. A., Pilipenko I. A., Selyova A. V., Cherkesova L. V. Comparative analysis of NTRUEncrypt modified post-quantum cryptographic system and standard RSA cryptosystem 185

Korolev S. A., Maykov D. V. Optimization of two-stage methanogenesis regime based on the Pontryagin's maximum principle 195

МЕХАНИКА
MECHANICS

UDC 621.89 https://doi.org/10.23947/1992-5980-2019-19-2-104-112

Effect of dynamic properties of interacting subsystems on evolution of selective transfer formation in friction units *

V. L. Zakovorotny[1], V. E. Gvindzhiliya[2], P. S. Kolodkin[3]**
[1, 2, 3] Don State Technical University, Rostov-on-Don, Russian Federation

Влияние динамических свойств взаимодействующих подсистем на эволюцию формирования избирательного переноса в узлах трения***

В. Л. Заковоротный[1], В. Е. Гвинджилия[2], П. С. Колодкин[3]**
[1, 2, 3] Донской государственный технический университет, Ростов-на-Дону, Российская Федерация

Introduction. Selective transfer is a typical example of the self-organization processes in tribosystems. In this case, joint surfaces of the servovite film are formed in the contact area, which changes fundamentally the friction and wear conditions. To form selective transfer in the area of mating surfaces, some power of the irreversible transformations of the input energy is needed, which depends on the elastic-dissipative properties of the contact surfaces.
Materials and Methods. The mathematical model of the dynamic system considering the evolutionarily changing servovite film is given. Its formation depends on the phase path of the irreversible transformations power in the area of surface matching, and it is represented by the Volterra integral operator of the second kind.
Research Results. The outcome analysis including dependences of the servovite film formation on the dynamic parameters of interacting subsystems is provided. The mathematical simulation of the evolution of the friction unit properties with the formation or destruction of the servovite film is first considered.
Discussion and Conclusions. During the evolutionary process of the servovite film formation, the dynamic coupling parameters generated in the friction unit, change. Consequently, the dynamic properties of the system also change. The tribosystem dynamics is first considered under the process of forming the selective transfer.

Keywords: dynamic friction system, selective transfer, servovite film, evolution.

For citation: V. L. Zakovorotny, et al. Effect of dynamic properties of interacting subsystems on evolution of selective transfer formation in friction units. Vestnik of DSTU, 2019, vol. 19, no. 1, pp. 104−112. https://doi.org/10.23947/1992-5980-2019-19-2-104-112

Введение. Типичным примером процессов самоорганизации в трибосистемах является избирательный перенос. В этом случае в области контакта формируются сопрягающие поверхности сервовитной пленки, что принципиально меняет условия трения и изнашивания. Для образования избирательного переноса в зоне сопряжения контактирующих поверхностей необходима некоторая мощность необратимых преобразований подводимой энергии, которая зависит от упруго-диссипативных свойств контактирующих поверхностей.
Материалы и методы. Приводится математическая модель динамической системы с учетом эволюционно изменяющейся сервовитной пленки. Ее формирование зависит от фазовой траектории мощности необратимых преобразований в зоне сопряжения поверхностей и представляется в виде интегрального оператора Вольтерры второго рода.
Результаты исследования. Приводится анализ результатов исследования, в том числе зависимости формирования сервовитной пленки от динамических параметров взаимодействующих подсистем. Впервые рассматривается проблема математического моделирования эволюции свойств узла трения с образованием или разрушением сервовитной пленки.
Обсуждение и заключение. В ходе эволюционного процесса образования сервовитной пленки меняются параметры динамической связи, формируемой в узле трения. Следовательно, меняются и динамические свойства системы. Впервые проанализирована динамика трибосистемы в процессе образования избирательного переноса.

Ключевые слова: динамическая система трения, избирательный перенос, сервовитная пленка, эволюция.

Образец для цитирования: Заковоротный, В. Л. Влияние динамических свойств взаимодействующих подсистем на эволюцию формирования избирательного переноса в узлах трения / В. Л. Заковоротный, В. Е. Гвинджилия, П. С. Колодкин // Вестник Дон. гос. техн. ун-та. — 2019. — Т. 19, № 2. — С. 104−112. https://doi.org/10.23947/1992-

* The research is done on RFFR grant no. 19-08-00022 of 09.01.2019.
**E-mail: vzakovorotny@dstu.edu.ru, sinedden@yandex.ru, Goodman.2012@yandex.ru
*** Работа выполнена при финансовой поддержке гранта РФФИ 19-08-00022 от 09.01.2019 г.

5980-2019-19-2-104-112

Introduction. After publication of the papers by I. Prigogine [1–3] and G. Haken [4, 5], lots of issues on the operation of technical systems interacting with different media are considered from the view point of their self-organization [6–12]. If you follow the synergetic analysis paradigm, then when studying such systems, you should first perform the procedure for extending the state space dimension [7, 8]. That means that it is necessary to additionally consider a model of environment in the coordinates of the system state. There is an exchange of information, material, energy, etc., with the environment. Here, coherent interactions of various physical nature are possible, that is, synergetic phenomena. A typical example of self-organization is the effect of selective transfer discovered by I.V. Kragelsky and D.N. Garkunov in 1956 [13].

The ideas of self-organization were formulated by B.I. Kostetsky [14] in the 60s of the XX century, and then developed in papers on structural adaptability together with L.I. Bershadsky [15] and N.A. Bushe [16]. In a number of papers, the formation of a servovite film in the tribosystem when it enters the selective transfer mode is studied [17–22]. It is shown that definite tribochemical reactions are necessary for the formation of selective transfer, as well as some power trajectory of irreversible transformations in the system-environment interface [17–24]. When entering the selective transfer mode, self-oscillations are observed. In some cases, chaotic attracting sets of deformation displacements of the contacting pairs are formed [17, 22–24].

Materials and Methods. Thus, when studying the transition to the selective transfer mode, it is necessary to consider the tribosystem dynamics in the unity of the subsystems interacting through friction and the dynamic coupling formed by the friction node. The parameters of such a dynamic link and the formation of a servovite film depend on the power path of irreversible transformations on the work done. The mathematical modeling of such an evolutionary system is considered, and the dependence of evolution on the dynamic parameters of interacting subsystems is analyzed.

Research Results

Mathematical system modeling. In mathematical modeling, we use the previously obtained results. In [17, 23, 24–26] it was shown that the basic dynamic properties of the friction system can be disclosed on the basis of the following assumptions:

- the sample is absolutely tough;
- indenter deformations are considered in the plane normal to the contacting surface and passing through the direction of the relative slip velocity.

When studying the dynamics, we can limit ourselves to the first vibration modes. Then, the system model is represented by the equation

$$m\frac{d^2X}{dt^2}+h\frac{dX}{dt}+cX=F_\Sigma(t), \tag{1}$$

where $m=\begin{bmatrix} m & 0 \\ 0 & m \end{bmatrix}$, $h=\begin{bmatrix} h_{1,1} & h_{2,1} \\ h_{1,2} & h_{2,2} \end{bmatrix}$, $c=\begin{bmatrix} c_{1,1} & c_{2,1} \\ c_{1,2} & c_{2,2} \end{bmatrix}$ are positively defined, symmetric matrices of inertial, velocity, and elastic coefficients; $X=\{X_1,X_2\}^T$ is vector of the deformation displacements of the indenter tip; $F_\Sigma(t)=\{F_{1,\Sigma}(t),F_{2,\Sigma}(t)\}^T$ is vector of forces affecting the indenter tip (Fig. 1).

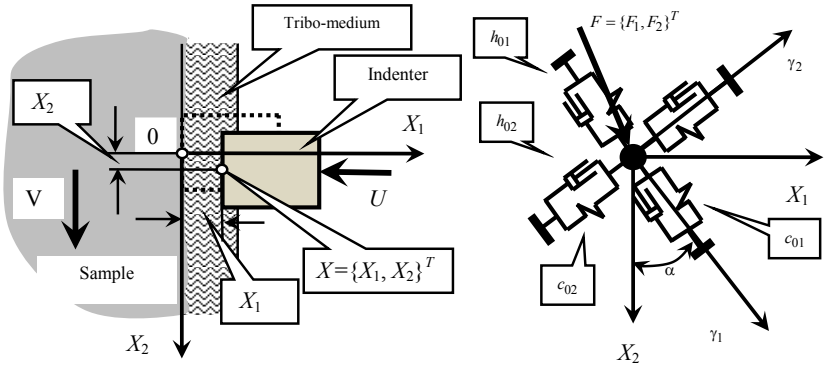

Fig. 1. Dynamic friction system schematic

We will follow the synergistic concept of the analysis, that is, we will represent $F_\Sigma(t)$ forces in the coordinates of the state. To do this, we introduce the concept of tribo-medium - this is the third body that is formed in the transition zone between the contacting surfaces. When approaching, the conditions of their interactions change, which phys-

ically manifests itself in changing parameters such as the actual contact area, heat production, friction coefficient, molecular interaction conditions, diffusion processes, etc. [27–30]. However, the primary reasons for all changes are interactions due to the contact mechanics.

In this case, due to changing the actual contact area, the normal pressure forces grow disproportionately fast, which prevent the surfaces from approaching. It is convenient to consider modeling these forces [23, 24] as the following function of approach

$$F_1(X_1) = F_{1,0}\exp[-\alpha(X_1)] - U, \quad X_1 \in (0, +\infty), \tag{2}$$

where α is coefficient of the contact force rate in $\left[mm^{-1}\right]$; U is an external force.

The above papers show that when a servovite film is being formed, a potential barrier appears in the function of approach, which actually determines the carrying capacity of the servovite film of the friction unit. The formation of a potential barrier can be conveniently represented as

$$\Phi_1(X_1) = \Phi_{1,0}\exp[-\alpha_1(X_1 - X_{1,0})^2], \tag{3}$$

where α_1 is the parameter characterizing the potential barrier slope in $\left[mm^{-2}\right]$; $X_{1,0}$ is the potential barrier coordinate; $\Phi_{1,0}$ is the evolutionary parameter in $[kg]$. Thus, the function of convergence is $F_{1,\Sigma}(X_1) = \Phi_1(X_1) + F_1(X_1)$ sum. On modeling the tangential component of the force, let us take into account that when forming a servovite film, the friction force is by an order of magnitude less. Therefore

$$F_{2,\Sigma}(t) = \begin{cases} k_T^{(1)} F_{1,\Sigma}(t), at: X_1 \langle X_{1.0}; \\ k_T^{(2)} F_{1,\Sigma}(t), at: X_1 \rangle X_{1.0}, \end{cases} \tag{4}$$

where $k_T^{(1)} \rangle\rangle k_T^{(2)}$.

For example, in the steel – glycerin – brass friction system, after the formation of a servovite film, the friction coefficient decreases by more than an order of magnitude. Previously it was shown that the forces of contact interaction are characterized by a lag in the tangential component of the force (friction force) with respect to the normal pressure forces. In this case, instead of (4), the following relation occurs

$$F_{2,\Sigma}(t) = \begin{cases} k_T^{(1)} F_{1,\Sigma}(t - T^{(1)}), at: X_1 \langle X_{1.0}; \\ k_T^{(2)} F_{1,\Sigma}(t - T^{(2)}), at: X_1 \rangle X_{1.0}, \end{cases} \tag{5}$$

where $T^{(1)}$, $T^{(2)}$ are time-lag constants depending on the properties of the tribo-medium formed in the contact area, and on the relative slip velocity. In (5), $T^{(1)} \rangle\rangle T^{(2)}$ condition is always satisfied. In addition, $T^{(1)}$ and $T^{(2)}$ decrease with increasing the relative slip velocity. Later, the hypothesis was adopted, according to which the potential barrier is formed depending on the work paths and the power of irreversible transformations as the indenter moves relative to the sample in the direction of the relative slip velocity. Moreover, $\Phi_{1.0}$ is affected not only by the current value of power, but also by the preceding values of power. Therefore the following is true:

$$\Phi_{1.0}(N) = \beta \int_0^t w(t - \xi) N(\xi) d\xi, \tag{6}$$

where $N = F_2(V + dX_2 / dt)$ is the power of irreversible transformations; $w(t-\xi) = \{\beta \exp[-\frac{1}{T}(t-\xi)]\}$ is the core of the integral operator considering the effect of the preceding power values; T is the parameter in $[s]$ characterizing a long-time impact of power on the potential barrier; β is the parameter in $\left[m^{-1}\right]$.

The equations (1) - (6) characterize the mathematical model of a dynamic friction system considering the evolution of its properties during the formation of a servovite film.

Dynamic properties change depending on the potential barrier parameters and the dynamic properties of the indenter. First, consider the properties of the frozen system on the assumption that the parameters of the servovite film are preset and constant. Suppose also that $T^{(1)} = 0$ and $T^{(2)} = 0$. Consider an example of changing system properties depending on the stages of the evolutionary transformation (Fig. 2).

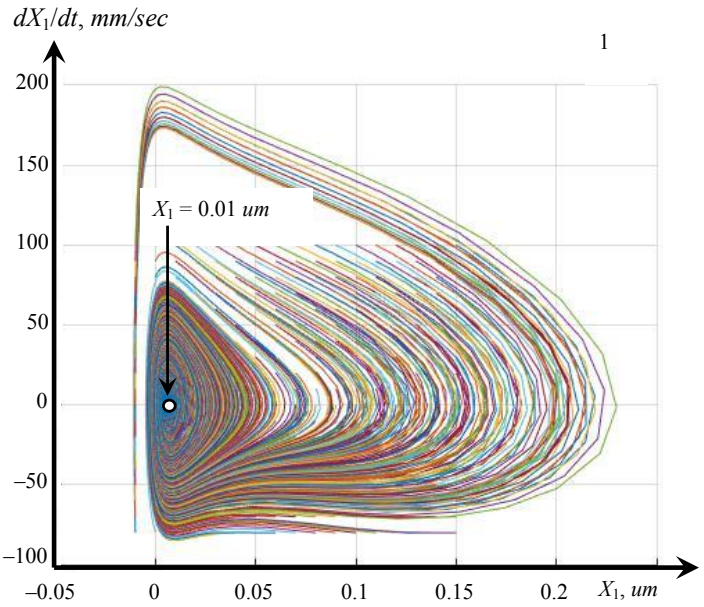
dX_1/dt, *mm/sec*
1
200
150
100
50
0
–50
–100
X_1 = 0.01 *um*
–0.05
0
0.05
0.1
0.15
0.2
X_1, *um*

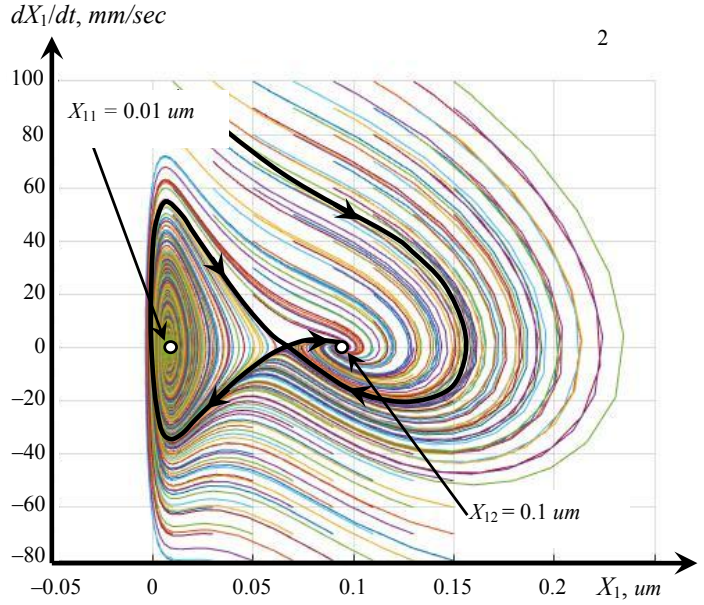
dX_1/dt, *mm/sec*
2
100
80
60
40
20
0
–20
–40
–60
–80
X_{11} = 0.01 *um*
X_{12} = 0.1 *um*
–0.05
0
0.05
0.1
0.15
0.2
X_1, *um*

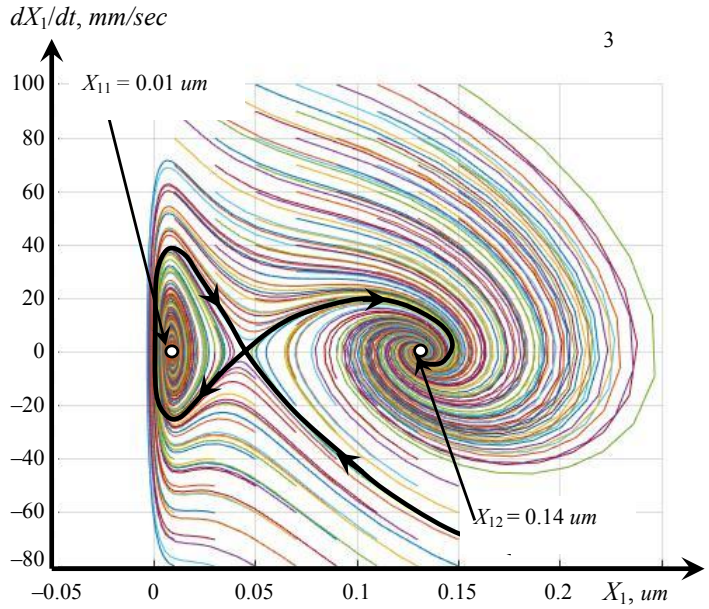
dX_1/dt, *mm/sec*
3
100
80
60
40
20
0
–20
–40
–60
–80
X_{11} = 0.01 *um*
X_{12} = 0.14 *um*
–0.05
0
0.05
0.1
0.15
0.2
X_1, *um*

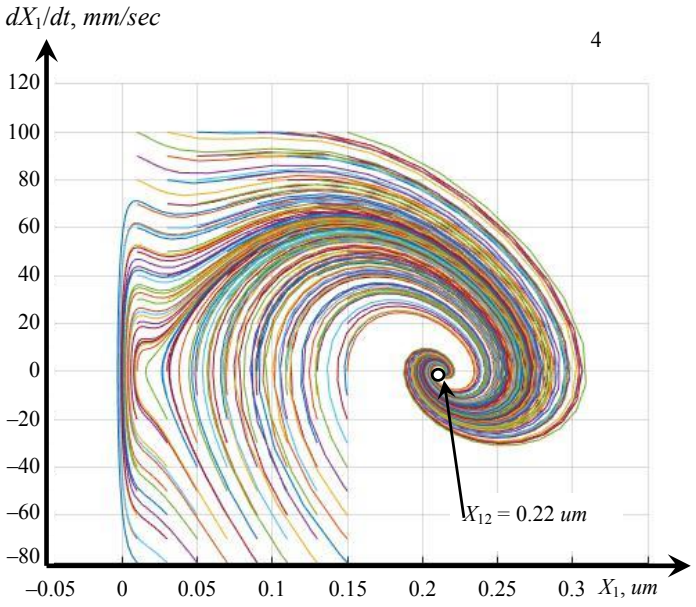

Fig. 2. Transformation of phase path projections onto X_1 — dX_1/dt plane

At the initial stage of transformations (Fig. 2-1), a unique equilibrium point is formed in the system, which corresponds to the friction with a traditional coefficient in the range of 0.2–0.3. Moreover, this point has the property of global attraction. Then (Fig. 2-2), two equilibrium points ($X_{1.1}, X_{1.2}$) are formed during the formation of a servovite film at the initial stage. The domain of attraction of $X_{1.1}$ point is bounded by a saddle-shaped separatrix. The rest of the domain is characterized by the attraction to $X_{1.2}$ point. It is important that at $X_{1.2}$ point of equilibrium, a servovite film is already formed, but its value and properties (determined by $\Phi_{1.0}$) do not allow for the attraction of the trajectories of the whole phase space. Therefore, depending on the initial conditions or disturbances (for example, fluctuations or formable attracting sets of deformation displacements in variations relative to the equilibrium point), it is possible to generate properties of a friction unit that differ fundamentally from each other. Subsequently (Fig. 2-3), the domain bounded by the saddle separatrix decreases and disappears (Fig. 2-4). In the latter case, the servovite film thickness and its carrying capacity increase. In the model, this is shown as an increase in the potential barrier, and the second equilibrium point acquires the properties of global attraction. In this case, a stable selective transfer is formed in the system.

The illustrations characterize the system dynamics considering that the servovite film properties are frozen, that is, they do not evolve. However, even in this case, the domains of attraction of equilibrium points corresponding to the friction with a servovite film and without it depend fundamentally on the dynamic parameters of the indenter, primarily, on the matrices of its stiffness (c) and dissipation (h) (1). In actual practice, there is a time evolution of the system. It depends on the relative slip velocity

(V_0), the force (U), the initial state of the surface of the contacting bodies, etc. The evolution simulated by an integral operator (6) is affected by many physical factors the integral count of which is determined by the kernel of the operator. Therefore, when varying the external conditions (for example, relative slip velocity), it is necessary to consider the velocity – integral operator parameters relationship, as well as the velocity – the power trajectory of irreversible transformations relationship. It is experimentally shown that with increasing speed, $T_i, i = 1,2$ parameter in (6) decreases. In addition, frictional forces (and, consequently, the power path of irreversible transformations) depend on the relative slip velocity. Note that it is the time required to establish a stationary servovite film that determines one of the indicators which allow identifying the parameters of the integral operator kernel.

Cursorily, we give an example of changing the phase trajectories of deformation displacements in X_1-direction as the indenter dynamic parameters and the tribological medium properties vary (Fig. 3).

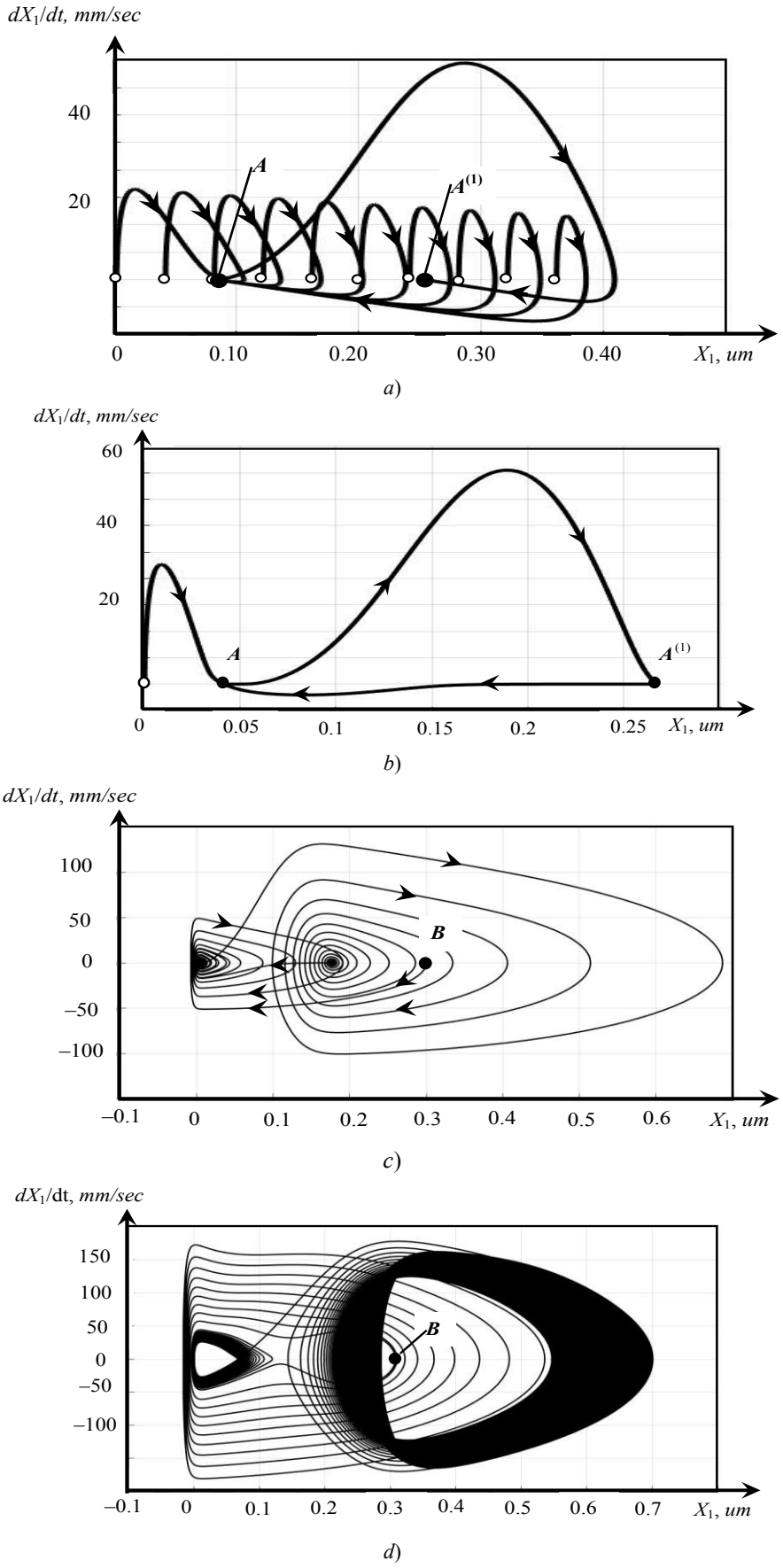

Fig. 3. Transformation of phase path projections onto X_1 — dX_1/dt plane depending on system parameters and friction conditions

First, consider friction with a sufficiently high velocity of relative slip $V_0 = 2.0\ м/с$. In this case, when forming a servovite film, the power of irreversible transformations decreases and the destruction is not observed, since the relative slip velocity is rather high (Fig. 3, *a*). At the initial stage, under various conditions, the trajectories are asymp-

totically attracted to the equilibrium point without a servovite film (point A in Fig. 3, *a*). After the potential barrier has been established, all trajectories evolve to $A^{(1)}$ equilibrium point on the servovite film. Fig. 3, *b*, *c*, and *d* show evolutionary curves with one initial value corresponding to *B* point. At this, the deformation displacements and the corresponding properties of the friction system deform to one of the two equilibrium points. However, evolutionary curves differ depending on the properties of the tribo-media and the Q-factor of the oscillatory circuits of the indenter subsystem without friction. Fig. 3, *b* shows an example of the evolutionary trajectory under *a* conditions, but at the relative slip velocity of $V_0 = 1.0\ m/s$. In this case, the power released in the friction zone is not enough to maintain the servovite film, and friction is periodically observed in the system with a servovite film and without it. In the deformation displacements, this causes the effect of low-frequency oscillations. Specifically, the formation time and the destruction time of the servovite film differ essentially. In Fig. 3, this is indicated through a significant decrease in the rate at which the indenter tip returns from $A^{(1)}$ point to *A* point.

The Q-factor of the indenter subsystem can be increased (Fig. 3, *c*). In this case, complex oscillatory displacements are formed in the system. Some of their components characterize the low-frequency material exchange between the lubricant and the friction surface, as well as vibration displacements at the frequencies of the indenter oscillators.

In the direction orthogonal to the relative slip velocity, cyclic forces are generated. Due to this, and also due to the dynamic interaction, a short-term formation of forces exceeding the potential barrier is possible. The situation is even more complicated if we additionally consider the lag in the variations of the tangential force components to their normal components (Fig. 3, *d*). Depending on the lag, various attracting sets of deformation displacements and, consequently, the forces of contact interaction are formed. The generation of chaotic dynamics in the system, which introduces great uncertainty in the regularities of servovite film formation, is also observed.

Discussion of the results. It is known that moving of the tribosystem to the selective transfer mode is determined by tribochemical reactions and the material exchange between the contacting surfaces and the lubricant. In order for the tribosystem to enter the selective transfer mode with the formation of a servovite film and to maintain it in the process of friction, some particular power of irreversible transformations of the input energy of the mechanical system is required [17, 21–24]. During the evolution of the dynamic friction system, the carrying capacity of the servovite film varies, which is simulated by the size of $\Phi_{1.0}$ potential barrier preventing direct contact of the friction surfaces. If the forces of contact interaction in the direction normal to this surface exceed $\Phi_{1.0}$, then a dynamic restructuring of the friction system with partial destruction of the servovite film is observed. Therefore, the friction conditions in the selective transfer mode depend not only on tribochemical reactions and the power of irreversible transformations, but also on the dynamic mode. Here, the stability of the equilibrium point and various attracting sets of deformation displacements (limit cycles, invariant tori, chaotic attractors) formed in its neighborhood are of fundamental importance. In addition, the dynamic system is perturbed, for example, by the out-of-true-running. Moreover, due to a fundamental change in the friction conditions during the direct contact and at the contact through a servovite film, the power of irreversible transformations in the surface matching changes, which changes the evolution and the maintenance conditions of the formed servovite film.

Conclusion. So, in conclusion: the stability of selective transfer is affected by both the dynamic parameters of the subsystems interacting through the friction node, and by disturbances that always occur in a real machine. Therefore, when studying selective transfer to ensure the friction unit wearlessness, it is required to obtain identity of the dynamic systems on a friction machine and in a real machine. For this purpose, the well-known techniques [27, 31] can be used.

The data show that the formation of a servovite film in a tribocontact node is affected not only by the tribochemical characteristics of the mating surfaces, but also by the parameters of the indenter and sample subsystems interacting through the tribology. Therefore, in each specific case, there is a bounded domain of parametric space of the dynamical systems, as well as disturbances in which the formation of selective transfer is a rule.

References

1. Prigogine, I., Stengers, I. Poryadok iz khaosa. [Order out of Chaos.] Moscow: Progress, 1986, 432 p. (in Russian).

2. Prigogine, I., Stengers, I. Poryadok iz khaosa. Novyy dialog cheloveka s prirodoy. [Man's New Dialogue with Nature.] Moscow: URSS Editorial, 2003, 432 p. (in Russian).

3. Prigogine, I. Ot sushchestvuyushchego k voznikayushchemu. [From being to becoming.] Moscow: Nauka, 1985, 296 p. (in Russian).

4. Haken, G. Sinergetika. Ierarkhiya neustoychivostey v samoorganizuyushchikhsya sistemakh i ustroystvakh. [Synergetics: Instability Hierarchies of Self-Organizing Systems and Devices.] Moscow: Mir, 1985, 424 p. (in Russian).

5. Haken, G. Tayny prirody. Sinergetika: uchenie o vzaimodeystvii. [Secrets of Nature. Synergetics: Doctrine of Interaction.] Moscow; Izhevsk: Institute of Computer Sciences, 2003, 320 p. (in Russian).

6. Ebeling, V., Engel, A., Feistel, R. Fizika protsessov evolyutsii. Sinergeticheskiy podkhod. [Physics of evolution processes. Synergetic approach.] Moscow: URSS, 2001, 328 p. (in Russian).

7. Kolesnikov, A.A. Sinergeticheskaya teoriya upravleniya. [Synergetic Control Theory.] Moscow: Energoatomizdat, 1994. — 344 c. (in Russian).

8. Kolesnikov, A.A., ed. Sinergetika i problemy teorii upravleniya. [Synargetics and control theory problems.] Moscow: Fizmatlit, 2004, 504 p. (in Russian).

9. Zakovorotny, V.L., Gvindzhiliya, V.E. Bifurkatsii prityagivayushchikh mnozhestv deformatsionnykh smeshcheniy rezhushchego instrumenta v khode evolyutsii svoystv protsessa obrabotki. [Bifurcations of attracting sets of cutting tool deformation displacements at the evolution of treatment process properties.] Izvestia VUZ. Applied Nonlinear Dynamics, 2018, vol. 26, no. 5, pp. 20–38. DOI: 10.18500/0869-6632-2018-26-5-20-38 (in Russian).

10. Zakovorotny, V.L., Gvindzhiliya, V.E. Vliyanie fluktuatsiy na ustoychivost' formoobrazuyushchikh traektoriy pri tochenii. [The influence of fluctuation on the shape-generating trajectories stability with a turning.] University News. North-Caucasian region. Technical Sciences Series. 2017, no. 2, pp. 52–61. DOI: 10.17213/0321-2653-2017-2-52-61(in Russian).

11. Zakovorotny, V.L., et al. Bifurcation of stationary manifolds formed in the neighborhood of the equilibrium in a dynamic system of cutting. Journal of Sound and Vibration, 2016, vol. 368, pp. 174–190.

12. Zakovorotny, V.L., Gubanova, A.A., Lukyanov, A.D. Ispol'zovanie sinergeticheskoy kontseptsii dlya izucheniya ustoychivosti formoobrazuyushchikh traektoriy poputnogo frezerovaniya. [Use of synergetic concept for studying stability of forming trajectories of climb cutting.] STIN, 2016, no. 4, pp. 32–40 (in Russian).

13. Garkunov, D.N., Kragelskiy, I.V. Effekt beziznosnosti: nauchnoe otkrytie. [Wearlessness effect: scientific discovery.] Available at: http://ross-nauka.narod.ru/06/06-041.html (accessed 01.05.19) (in Russian).

14. Kostetsky, B.I. Strukturno-energeticheskaya prisposablivaemost' materialov pri trenii. [Structural and energy adaptability of materials at friction.] Journal of Friction and Wear, 1985, no. 2 (6), pp. 201–212 (in Russian).

15. Bershadskiy, L.I. Samoorganizatsiya tribosistem i kontseptsiya iznosostoykosti. [Tribosystem self-organization and the concept of wear resistance.] Journal of Friction and Wear, 1992, no. 6 (13), pp. 1077–1094 (in Russian).

16. Bushe, N.A., Kopytko, V.V. Sovmestimost' trushchikhsya poverkhnostey. [Compatibility of rubbing surfaces.] Moscow: Nauka, 1981, 128 p. (in Russian).

17. Kuzharov, A.S., Zakovorotny, V.L. Samoorganizatsiya pri trenii. [Self-organization during friction.] Tribologiya. Sostoyanie i perspektivy: sb. nauch. tr. [Tribology. State and prospects: coll.of sci.papers.] Ufa: USATU EPC, 2016, pp. 68–82 (in Russian).

18. Gershman, I. S. Formation of secondary structures and the self-organization process of tribosystems during friction with the collection if electric current. Self-Organization during Friction: Advanced Surface Engineered Materials and Systems Designed. German S. Fox-Rabinovich, George E. Totten, eds. Boca Raton; London; New York: Taylor & Francis, 2006, pp. 197–230.

19. Gershman, I. S. Sinergeticheskiy podkhod k opisaniyu i upravleniyu iznashivaniem. [Synergetic approach to the description and management through wear.] Tribologiya. Sostoyanie i perspektivy: sb. nauch. tr. [Tribology. State and prospects: coll.of sci.papers.] Ufa: USATU EPC, 2016, pp. 82–87 (in Russian).

20. Gershman, I.S., Bushe, N.F. Thin films and self-organization during friction under the current collection conditions. Surface and Coating Technology, 2004, no. 185, pp. 405–411.

21. Kuzharov, A.S., Marchak, R. Osobennosti evolyutsionnogo perekhoda tribologicheskoy sistemy latun'-glitserin-stal' v rezhime beziznosnogo treniya. [Features of evolutionary transition of brass-glycerin-steel tribological system in the wearless friction regime.] Doklady Akademii Nauk, 1997, no. 5 (354), pp. 642–644 (in Russian).

22. Kuzharov, A.S. Kontseptsiya beziznosnosti v sovremennoy tribologii. [The concept of wearless in modern tribology.] University News. North-Caucasian region. Technical Sciences Series, 2014, no. 2, pp. 23–31 (in Russian).

23. Zakovorotny, V.L. Dinamika tribosistem. Samoorganizatsiya, evolyutsiya. [Dynamics of tribosystems. Self-organization, evolution.] Rostov-on-Don: DSTU Publ. Centre, 2003, 502 p. (in Russian).

24. Zakovorotny, V.L. Nelineynaya tribomekhanika. [Nonlinear tribomechanics.] Rostov-on-Don: DSTU Publ. Centre, 2000, 293 p. (in Russian).

25. Lyapunov, A.M. Obshchaya zadacha ob ustoychivosti dvizheniya. [General problem on stability of motion.] Moscow: Gostekhizdat, 1950, 494 p. (in Russian).

26. Appell, P. Teoreticheskaya mekhanika. [Theoretical mechanics.] Moscow: Fizmatgiz, 1960, vol. 2, 487 p. (in Russian).

27. Zakovorotny, V.L., Shapovalov, V.V. Dinamika transportnykh tribosistem. [Dynamics of transportation tribosystems.] Assembling in Mechanical Engineering and Instrument-Making, 2005, no. 12, pp. 19–29 (in Russian).

28. Goryacheva, I.G. Mekhanika friktsionnogo vzaimodeystviya. [Mechanics of friction interaction.] Moscow: Nauka, 2001, 478 p. (in Russian).

29. Goryacheva, I.G., Makhovskaya, Yu.Yu. Adgezionnoe vzaimodeystvie uprugikh tel. [Adhesive interaction of elastic bodies.] Journal of Applied Mathematics and Mechanics, 2001, vol. 65, no. 2, pp. 279–289 (in Russian).

30. Myshkin, N.K., Petrokovets, M.I. Trenie, smazka i iznos. [Friction, lubrication and wear.] Moscow: Fizmatlit, 2007, 368 p. (in Russian).

31. Zakovorotny, V.L, Bordachev, E.V. Informatsionnoe obespechenie sistemy dinamicheskoy diagnostiki iznosa rezhushchego instrumenta na primere tokarnoy obrabotki. [Information support of the dynamic diagnostic system for cutting tool wear by the example of lathing.] Journal of Machinery Manufacture and reliability, 1995, no. 3, pp. 95–103 (in Russian).

Submitted 25.02.2019
Scheduled in the issue 05.04.2019

Authors:

Zakovorotny, Vilor L.,
professor of the Production Automation Department, Don State Technical University
(1, Gagarin Square, Rostov-on-Don, 344000, RF), Dr.Sci. (Eng.), professor,
ORCID: https://orcid.org/0000-0003-2187-9897
vzakovorotny@dstu.edu.ru

Gvindzhiliya, Valeria E.,
postgraduate of the Production Automation Department, Don State Technical University
(1, Gagarin Square, Rostov-on-Don, 344000, RF),
ORCID: https://orcid.org/0000-0003-1066-4604
sinedden@yandex.ru

Kolodkin, Pavel S.,
graduate student of the Production Automation Department, Don State Technical University
(1, Gagarin Square, Rostov-on-Don, 344000, RF),
ORCID: https://orcid.org/0000-0002-6361-4750

МЕХАНИКА
MECHANICS

UDC 539.375.6 https://doi.org/10.23947/1992-5980-2019-19-2-113-119

On specifics of hardening mechanisms in metallic matrix composition*

M. N. Safonova[1], E. A. Arkhangelskaya[2], A. A. Fedotov[3]**
[1,2,3]North-Eastern Federal University, Yakutsk, Russian Federation

К вопросу об особенностях механизмов упрочнения в металлической матричной композиции***

М. Н. Сафонова[1], Е. А. Архангельская[2], А. А. Федотов[3]**
[1,2,3] Северо-Восточный федеральный университет им. М. К. Аммосова, г. Якутск, Российская Федерация

Introduction. Functional properties of diamond powders are determined by a large-scale structural factor since it affects the formation of structurally sensitive mechanical properties — stress limit and yield value. Considering the qualitative correlation between yield value and hardness, it is possible to predict an increase in hardness including highly rigid materials.

Materials and Methods. Physical characteristics of the basic types of fillers that make up the reinforcers are considered, systematized and tabulated. M2-01 tin bronze (20 wt. % tin, 80% copper) was used as a bond. Ultradisperse natural diamond (UDND, 0.5–4 wt. %) was added to it, as well as powders of natural diamond (3/2 μm fraction, 7/5 μm, –40 μm) obtained through processing diamonds at the enterprise of "Sakha Daimond" JSC. The above materials were made on the crushing and screening equipment and shaking tables. The stages of obtaining powders were recorded using the raster electron microscopy. Vibroscreens were applied for the grain-size classification of diamond powders. Physical and mechanical characteristics of the produced samples were tested by standard methods. VLTE-500 electronic fourth-class laboratory balance was used for weighing. Density was determined by MK 0–25 mm micrometer according to GOST 6507-78.

Research Results. Porosity was calculated through the actual and theoretical density. It was found that with a decrease in the filler size, an improvement in the physicomechanical properties of the binder modified with a diamond powder is observed. The best performance was observed in the samples with the UDND filler.

Discussion and Conclusions. As a result of the study, it was recorded that the calculated data differ from the experimental data since they show an increase in the material hardening pro rata to the amount of the diamond particles introduced into the volume. An assumption has been made that the considered hardening model (Orowan model) does not take into

Введение. Функциональные свойства алмазных порошков обусловлены масштабным структурным фактором, поскольку он влияет на формирование структурно-чувствительных механических свойств — пределов прочности и текучести. Учитывая качественную корреляцию между пределом текучести и твердостью, можно прогнозировать повышение твердости, в том числе высокотвердых материалов.

Материалы и методы. Рассмотрены, систематизированы и представлены в виде таблицы физические характеристики основных типов наполнителей, входящих в состав упрочнителей. В качестве связки использована оловянистая бронза М2-01 (20 мас. % олова, 80 % меди). В нее добавляли ультрадисперсный природный алмаз (УДПА, 0,5–4 мас. %), а также порошки природного алмаза (фракции 3/2 мкм, 7/5 мкм, –40 мкм), полученные при переработке алмазов на предприятии ОАО «Сахадаймонд». Названные материалы изготавливались на дробильно-классификационном оборудовании и вибростолах. Стадии получения порошков фиксировались с помощью растровой электронной микроскопии. Для классификации алмазных порошков по зернистости применяли вибросита. Физические и механические характеристики изготовленных образцов испытывали по стандартным методикам. Для взвешивания использовали лабораторные электронные весы четвертого класса ВЛТЭ-500. Плотность определяли микрометром МК 0–25 мм по ГОСТ 6507-78.

Результаты исследования. Через фактическую и теоретическую плотности рассчитана пористость. Выяснилось, что с уменьшением размера фракции наполнителя наблюдается улучшение физико-механических свойств связки, модифицированной алмазным порошком.

Наилучшие показатели отмечены у образцов с наполнителем из УДПА.

Обсуждение и заключения. В результате проведенного исследования отмечено, что расчетные данные отличаются от экспериментальных, т. к. показывают увеличение упрочнения материала пропорционально количеству вводимых в объем частиц алмаза. Выдвинуто предположение, что рассмотренная модель упрочнения (модель Оро-

* The research is done within the frame of the independent R&D.
** E-mail: marisafon_2006@mail.ru, arkhangelskaya@yandex.ru, Fedot_andrey@mail.ru
*** Работа выполнена в рамках инициативной НИР.

account the formation of carbon and the agglomeration of diamonds into larger objects in the matrix volume under an increase in the number of input diamonds. If the UDND particle volume reaches 3%, the carbon con
tent in the material increases. As a result, the filler particles are not fully oxidized, thus increasing the number of pores in the material.

Keywords: bond, metal matrix, composite, hardener, ultrafine particles, hardening mechanisms.

For citation: M.N. Safonova, et al. On specifics of hardening mechanisms in metallic matrix composition. Vestnik of DSTU, 2019, vol. 19, no. 2, pp. 113−119. https://doi.org/10.23947/1992-5980-2019-19-2-113-119

вана) не учитывает образование углерода и агломерацию алмазов в более крупные объекты в объеме матрицы при повышении количества вводимых алмазов. Если объем частиц УДПА достигает 3 %, в материале растет содержание углерода. В результате частицы наполнителя полностью не окисляются, тем самым увеличивая количество пор в материале.

Ключевые слова: связка, металлическая матрица, композит, упрочнитель, ультрадисперсные частицы, механизмы упрочнения.

Образец для цитирования: Сафонова, М. Н. К вопросу об особенностях механизмов упрочнения в металлической матричной композиции / М. Н. Сафонова, Е. А. Архангельская, А. А. Федотов // Вестник Дон. гос. техн. ун-та. — 2019. — Т. 19, № 2. — С. 113−119. https://doi.org/10.23947/1992-5980-2019-19-2-113-119

Introduction. It is known that the physicomechanical properties of diamond powders are determined by a larger specific surface area and grain dispersion. In particular, this is shown by the Hall – Petch equation which is performed over a wide range of grain sizes (up to 1 um). Functional properties of these materials are determined by the large-scale structure factor since it affects the formation of structure-sensitive mechanical properties – stress limit and yield value [1, 2]. Given the qualitative correlation between yield strength and hardness, it is possible to predict an increase in hardness including highly rigid materials: the finer the filler, the fewer defects it has and, accordingly, the higher the strength.

Materials and Methods. Strengthening mechanisms in highly rigid materials depend on the interaction pattern of the introduced particles or hardener fibers and the matrix material. A successful application of the dispersion strengthening effect is shown in [3–6, 7]. Under such strengthening, a structure that makes the dislocation motion harder is created in the materials. Discrete particles of the second phase characterized by high strength and melting point inhibit the dislocation motion especially strongly. Considering the two-phase structure and high hardness of the materials obtained, it should be expected that their wear resistance will also be higher than that of the nonhardenable matrix materials. Besides, the strength of the components interface is an important factor for the wear resistance of composites. A strong adhesive bond at the interface ensures a composite with high rigidity and higher static strength [3, 6–8].

According to the mechanism described by Orowan, ultrafine diamond particles distributed in the binder volume affect the strain hardening of the composite material. Particles of the particulate filler introduced into the matrix inhibit the dislocation motion in a metal increasing its strength at the standard and elevated temperatures. In addition, they represent a mechanical obstacle in the path of crack propagation that may appear in the matrix, and increase the fracture resistance of the composite material.

Another characteristic that determines the reinforcing filler – matrix relationship is the thermal linear expansion coefficient. For solids at constant pressure and temperature, the thermodynamic equilibrium criterion is Gibbs minimum potential (or energy). This value shows an energy change during a chemical reaction and demonstrates the possibility of chemical reactions between the material components [5]. Thus, a minimum change in Gibbs energy corresponds to a stable equilibrium between the components of the system (Table 1).

Table 1

Physical characteristics of the main types of fillers [9, 10, 11]

Substance and state	$\Delta G^{o}_{обр.,}$ 298,15, kJ/mol Gibbs energy change	Microhardness, $\times 10^2$ Mpa	Temperature stability, °C
C (diamond)	2.377	1000	650–700
W	0	258	3300–3400
Al_2O_3	–1582.3	180–220	1500–1700
BN	–226.8	800–900	1100–1300
SiC	–60	300–320	1200–1300
BeO	–579.9	152	2500
Be_2C	–948	780	2150

The table shows that the optimal filler is diamond. It has a fairly low value of Gibbs energy change, the highest microhardness value, but the lowest temperature stability. Diamond has a high adsorption capacity [12] and is the least chemically active compared to other forms of carbon. These properties are important advantages when using diamond as a hardener.

The work objective is to study features of the mechanisms of forming the metal-matrix composition structure.

Objects of Study. We used M2-01 tin bronze (20 wt. % tin, 80% copper) as a basic binder. Ultradisperse natural diamond (UDND, 0.5–4 wt. %) was added to it, as well as powders of natural diamond (3/2 μm fraction, 7/5 μm, –40 μm).

Research Methodology. Natural diamond powders (NDP, 3/2 μm fractions, 7/5 μm, –40 μm) and the UNDN submicropowder were obtained during the processing of diamonds at the enterprise of "Sakha Diamond" JSC. The powders were made on the crushing and screening equipment and shaking tables under the optimum conditions. Fig. 1 shows the stages of obtaining the powders. The images were taken using the scanning electron microscopy (SEM).

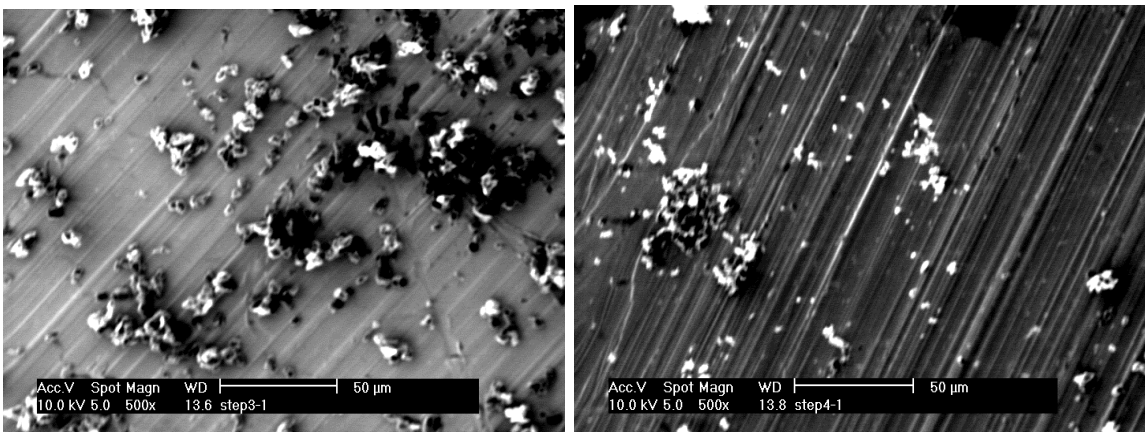

a) *b*)

Fig. 1. SEM photographs of: fine-grained powder of 7 um or less (*a*); submicropowder (*b*)

Vibroscreens were applied for the grain-size classification of diamond powders. . Physical and mechanical characteristics of the produced samples were tested through standard methods. VLTE-500 electronic fourth-class laboratory balance was used for weighing. Density (ρ) was determined by MK 0–25 mm micrometer according to GOST 6507-78.

Research Results. Hardness was measured on Equotip 3 device, Proceq, according to the corresponding method of the GOST. The proportionality limit in compression and the elasticity modulus were determined according to GOST 25.503-97. The test results are shown in Table 2.

Table 2

NDP impact on physicomechanical properties of M2-01alloy

ND, %	Porosity, %				Hardness, HB				Proportionality limit in compression $\sigma_{пр}$, MPa				Actual density $\rho_{факт}$, kg/m3				Compressive modulus Ec, MPa
ND Dimensionality um	3/2	7/5	–40	UNDN	3/2	7/5	–40	UNDN	3/2	7/5	–40	UNDN	3/2	7/5	–40	UNDN	UNDN
0	41.0	41.0	41.0	41.0	41	41	41	41	9.7	9.7	9.7	9.7	7560	7560	7560	7560	5735.94
1	29.0	30.0	30.0	28.0	43	47	48	48	10.5	11.5	11.0	11.5	7630	7620	7610	7670	6771.03
2	27.0	28.0	28.0	26.0	43	43	51	53	10.5	11.5	12.0	12.5	7710	7700	7760	7750	6953.50
3	25.0	28.0	27.0	26.0	47	43	51	53	10.2	10.5	12.1	12.2	7730	7720	7770	7750	6580.27

To determine the elasticity modulus and proportionality limit, the samples were compressed on presses to a relative deformation of 15–16%, at a loading rate of 0.2 kN/s.

The porosity (P) was calculated through the actual and theoretical density using the formula:

$$П = (1 - \rho/\rho_т) \times 100\%, \quad (1)$$

where $\rho_т$ is the theoretical (calculated) density of nonporous material; ρ is the actual density of the sample.

The theoretical density was obtained by the formula:

$$\rho_т = 100/(C_1/\rho_1 + C_2/\rho_2 + C_3/\rho_3 + C_4/\rho_4), \quad (2)$$

where C_1, C_2, C_3 and C_4 are concentrations of copper, tin, NDP and UNDN in the powder mixtures according to their density ρ_1, ρ_2, ρ_3 and ρ_4.

The densities taken into account are:

- copper: 8.96 × 103 kg/m^3,
- tin: 7.28 × 103 kg/m^3,
- diamond: 3,5 × 103 kg/m^3,
- UDND: 3.1 × 103 kg/m^3.

The volume of samples was calculated by the formula:

$$V = (m_1 - m_2) / \rho_ж, \quad (3)$$

where V is pressing volume; m_1 is mass in air; m_2 is mass in water; $\rho_ж$ is liquid density.

In the course of the study, it turned out that with a decrease in the filler size, there was an improvement in the physicomechanical properties of the bond modified with diamond powder.

The elasticity modulus values were determined for the samples with the addition of the UDND and a pure binder. The best indicators are shown by the samples with the filler from UDND. At the same time, the physicomechanical properties under consideration deteriorate if the volume of the added UDND particles exceeds 2%.

The metallographic studies of the samples allowed us to establish how diamond particles affect the matrix structure. Fig. 2 shows the images of microstructures of the deformed samples.

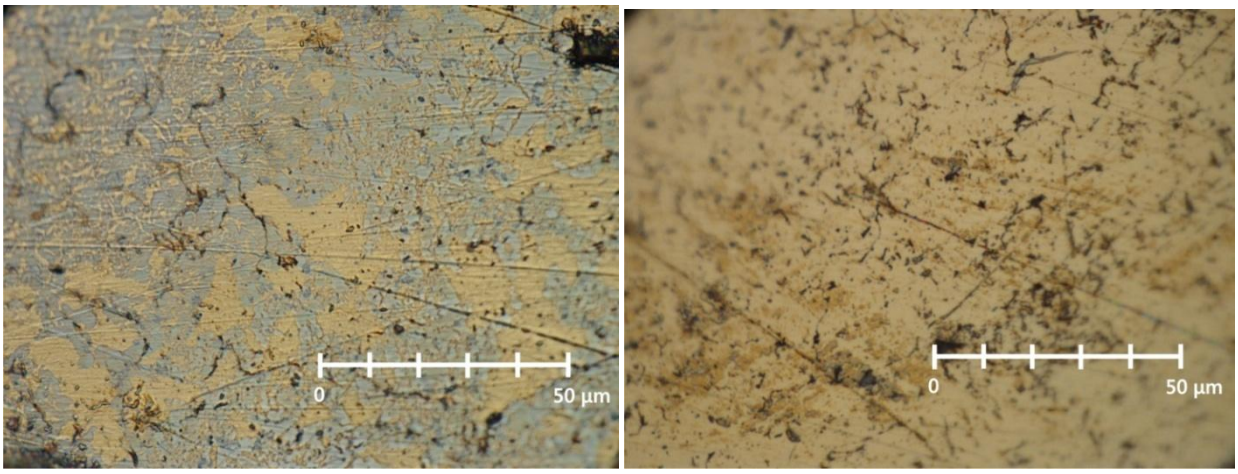

Fig. 2. Images of ground surface of deformed sample with addition of 2% of diamond powder particles under × 1000 magnification.

The pictures show clearly visible narrow and branched microstructure objects. Hypothetically, these are boundaries between the grains or microcracks formed under the deformation.

Inside the grains, there are also point microscopic objects that form a disperse substructure. Compared to the boundary-distributed point objects, their density is much less, but significantly more than in the original matrix which has no diamond fillers.

Based on the results of metallographic studies, it can be argued that the strengthening of the matrix material has two mechanisms – dispersion and grain-boundary ones.

If we are talking about a dispersion mechanism, the volume of NDP introduced into the matrix material can be calculated using Orowan equation [13]:

$$\zeta_N = \frac{Gb}{2\pi\lambda} k_0 \ln\frac{\lambda}{2b}, \quad (4)$$

where λ is the nearest distance between the particles; G is matrix shear modulus; b is Burgers vector; k_0 is coefficient characterizing the pattern of interacting atoms with dislocation.

The following values are chosen: $G = 0.367 \times 10^5$ MPa for bronze; $b = 2.564$ Å for copper; k_0 coefficient is equal to 0.85.

The nearest average distance between the particles, depending on the content and dispersion, is calculated by the formula proposed in [14]:

$$\lambda = \left[\left(\frac{200+L_H}{1{,}91L_H}\right)^{\frac{1}{3}} - 1\right] d, \quad (5)$$

where L_H is weight fraction of the filler; d is the diameter or thickness of the filler particles.

Table 3 shows the calculations of an average distance between filler particles depending on their volume and size.

Table 3

Nearest average distance between filler particles depending on their volume and size, and hardening according to Orowan equation under introduction of diamond particles

Particle size	7/5			3/2			–40			UDND		
Particle content, %	1	2	3	1	2	3	1	2	3	1	2	3
λ, um	125.3	98.19	85.02	52.19	40.91	35.42	417.56	327.30	283.40	6.26	4.91	4.25
ζ_N, MPa	0.13	0.16	0.18	0.28	0.35	0.40	0.04	0.05	0.06	1.91	2.38	2.70

The calculated data were substituted into Orowan equation, and thus the strengthening was determined through introducing the diamond powder particles into the matrix material.

According to the calculations, the greatest strengthening is provided through introducing the UDND into the matrix, which is generally validated by the experimental data.

When the grain geometry changes due to the agglomeration of filler particles at the interfaces in the material, it is advisable to calculate the material properties change according to the theory of grain-boundary strengthening [15, 16].

To determine the quantitative increase in the strength of the material through adding particles of diamond powders due to the grain-boundary strengthening, calculations were made using Hall – Petch empirical relationship [17]:

$$\Delta\sigma_T = k{d_3}^{-1/2}, \quad (6)$$

where k is Hall – Petch coefficient for this material; d_3 is grain size.

For calculations, we used the samples showing the greatest increase in strength according to Orowan theory. The calculations were performed according to the data obtained from the processing of the surface microstructure images through the technique proposed in [18].

The Hall – Petch coefficient is applied to copper. According to [19], it is a variable value; it depends on the average grain size and varies in the range of 0.01–0.24 MPa × $m^{1/2}$. The calculations show that the greatest strengthening is provided by the introduction of ultrafine NDP into the matrix material. In general, this is confirmed by the experimental data.

The average grain size is calculated according to the metallographic studies of the sample surface:

$$d_3 = \sqrt{\frac{4\left(\frac{S_{общ}}{N_{общ}}\right)}{\pi}}, \quad (7)$$

where $S_{общ}$ is total area of objects; $N_{общ}$ is total number of objects.

With an average grain size of about 10^{-1} μm, the Hall – Petch coefficient is about 0.01 MPa × $m^{1/2}$.

The calculations based on Hall – Petch ratio indicate an increase in the yield strength of the material with the addition of particles of NDP. The yield strength reaches the maximum design value when the content of fillers is 1% (Fig. 3).

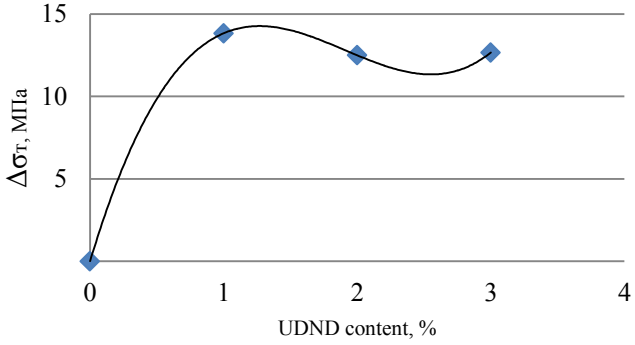

Fig. 3. Yield strength – UDND content dependence

Discussion and Conclusions. The calculations show that the samples with the addition of NDP have a smaller grain size compared to the initial ones. This fact can be explained as follows. The diamond particles, settling at the grain boundaries of the material, help to reduce their average size. As a result, the geometry of the boundaries between the grains changes; barriers to dislocations are formed; and thus, the potential capability of the material to resist plastic deformation is enhanced.

The yield strength increases by about 12–13 MPa which correlates with the calculated data obtained using Orowan theory for dispersion strengthening. If we are talking about polycrystalline material, then, in principle, the yield strength increases with decreasing the grain size. Diamond particles added to the matrix volume increase the yield strength since they change the geometry of grains reducing their average area and size.

The calculated data differ from the experimental results since they show an increase in the material strengthening pro rata to the number of diamond particles introduced into the volume. It can be assumed that the Orowan strengthening model does not consider the formation of carbon and the agglomeration of diamonds into larger objects in the volume of the matrix when increasing the number of diamonds introduced.

The decrease in the number of pores when adding the UDND particles in the amount of 1–2% can be explained by the high sorption properties of the filler. During sintering of compacts obtained through the powder metallurgy, the UDND particles absorb oxygen contained in the powder mixture with the formation of CO and CO_2 reducing gases. These gases destroy the oxide film covering the powder mixture particles and prevent oxidation during sintering, thereby reducing the total volume of gases in the powder mixture. At the same time, reducing gases accelerate the sintering process of the material. The combination of these factors ultimately reduces the residual porosity in the material which is validated by the calculated data. If the UDND particle volume reaches 3%, an increase in the carbon content in the material occurs. As a result, the filler particles are not fully oxidized, thereby increasing the number of pores in the material.

References

1. Yemelyanova, M.A., Romanov, G.N., Noyev, I.N. Formirovanie abrazivnogo materiala na osnove med'-titan-almaz. [Abrasive formation on a basis of copper-titanium-diamond.] Vestnik of NEFU, 2010, vol. 7, no. 1, pp. 64–70 (in Russian).

2. Ivanov, D.A., Sitnikov, A.I., Shlyapin, S.D. Dispersnouprochnennye, voloknistye i sloistye neorganicheskie kompozitsionnye materialy. [Dispersive, fibrous and layered inorganic composite materials.] Moscow: MATI-RSTU Publ. House, 2009, 306 p. (in Russian).

3. Kallip, K., et al. Microstructure and mechanical properties of near net shaped aluminium/alumina nanocomposites fabricated by powder metallurgy. Journal of Alloys and Compounds, 2017, no. 714, pp. 133–143.

4. Jiang, Y., et al. Interface-induced strain hardening of graphene nanosheet/aluminum composites. Carbon, 2017, no. 146, pp. 17–27.

5. Liu, D., et al. Molecular dynamics simulation on formation mechanism of grain boundary steps in microcutting of polycrystalline copper. Computational Materials Science, 2017, no. 126, pp. 418–425.

6. Saba, F., Zhang, F., Liu, S., & Liu, T. Reinforcement size dependence of mechanical properties and strengthening mechanisms in diamond reinforced titanium metal matrix composites. Composites. Part B: Engineering, 2019, no. 167, pp. 7–19.

7. Mokdad, F., et al. Deformation and strengthening mechanisms of a carbon nanotube reinforced aluminum composite. Carbon, 2017, no. 104, pp. 64–77.

8. Loktyushin, V.A., Adamenko, N.A., Gurevich, L.M. Kontaktnye vzaimodeystviya v kompozitsionnykh materialakh. [Contact interactions in composite materials.] Volgograd: VolgGTU, 2004, 74 p. (in Russian).

9. Donald, J. Vaughan Strength of Diamond. Science, 1994, vol. 266, pp. 419–422.

10. Mishchenko, K.P., Ravdel, A.A., eds. Kratkiy spravochnik fiziko-khimicheskikh velichin. [Short critical tables.] Leningrad: Khimiya, 1974, 200 p. (in Russian).

11. Babichev, A.P., et al. Fizicheskie velichiny. Spravochnik. [Physical values. Reference guide.] Moscow: Energoatomizdat, 1991, pp. 363–450 (in Russian).

12. Parkaeva, S.A., Belyakova, L.D., Larionov, O.G. Adsorbtsionnye svoystva modifitsirovannykh poroshkov detonatsionnogo nanoalmaza po dannym gazovoy khromatografii. [Adsorption properties of modified powders of detonated diamond obtained by gas chromatography.] Sorption and Chromatographic Processes, 2010, vol. 10, iss. 2, pp. 283–292 (in Russian).

13. Islamkulov, K.M., Aymenov, Zh.T., Smagulov, D.U. Modelirovanie protsessa uprochneniya malouglerodistykh staley. [Simulation of hardening low-carbon steels.] Advances in Current Natural Sciences, 2014, no. 10, pp. 73-75 (in Russian).

14. Azygaliev, U.Sh. Strukturnaya modifikatsiya organopolimernykh stroitel'nykh kompozitov. [Structural modification of organo-polymeric construction composites.] Vestnik of KSUCTA, 2012, no. 3, pp. 29–33 (in Russian).

15. Maltseva, L.A., Gervasyev, M.A., Kutyin, A.B. Materialovedenie. [Materials science.] Yekaterinburg: UGTU-UPI, 2007, 339 p. (in Russian).

16. Kushner, V.S., et al. Materialovedenie. [Materials science.] Omsk: OmSTU Publ. House, 2008, 232 p. (in Russian).

17. Carlton, C.E., Ferreira, P.J. What is behind the inverse Hall-Petch effect in nanocrystalline materials? Acta Materialia, 2007, vol. 55, pp. 3749–3756.

18. Kim, V.A., et al. Osnovy kolichestvennoy i komp'yuternoy metallografii. [Basics of quantitative and computerized metallography.] Komsomolsk-on-Amur: KnAGTU, 2013, 133 p. (in Russian).

19. Kozlov, E.V., Zhdanov, A.N., Koneva, N.A. Bar'yernoe tormozhenie dislokatsiy. Problema Kholla — Petcha. [Barrier retardation of dislocations. Hall-Petch problem.] Physical Mesomechanics, 2006, vol. 9, no. 3, pp. 81–92 (in Russian).

Submitted 25.04.2019
Scheduled in the issue 20.05.2019

Authors:

Safonova, Maria N.,
associate professor of the Applied Mechanics Department, North-Eastern Federal University in Yakutsk (50, Kulakovsky St.,Yakutsk, 677000, RF), Cand.Sci. (Eng.),
marisafon_2006@mail.ru

Arkhangelskaya, Ekaterina A.,
associate professor of the Property Survey, Management and Cadastral Register Department, North-Eastern Federal University in Yakutsk (50, Kulakovsky St.,Yakutsk, 677000, RF), Cand.Sci. (Eng.),
arkhangelskaya@yandex.ru

Fedotov, Andrey A.,
senior lecturer of the Applied Mechanics Department, North-Eastern Federal University in Yakutsk (50, Kulakovsky St.,Yakutsk, 677000, RF),
ORCID:http://orcid.org/0000-0003-8885-1885
Fedot_andrey@mail.ru

МАШИНОСТРОЕНИЕ И МАШИНОВЕДЕНИЕ
MACHINE BUILDING AND MACHINE SCIENCE

UDC 621.833 https://doi.org/10.23947/1992-5980-2019-19-2-120-129

Development of a power model for large wave gear toothing *

V. N. Strelnikov[1], A. I. Voloshin[2], M. G. Sukov[3]**

[1] Belgorod State Technological University named after V.G. Shukhov, Belgorod, Russian Federation
[2, 3] "Novokramatorsky Mashinostroitelny Zavod" PJSC, Kramatorsk, Ukraine

Разработка силовой модели зубчатого зацепления крупной волновой передачи ***

В. Н. Стрельников[1], А. И. Волошин[2], М. Г. Суков[3]**

[1] Белгородский государственный технологический университет, г. Белгород, Российская Федерация
[2, 3] Частное акционерное общество «Новокраматорский машиностроительный завод», г. Краматорск, Донецкая обл., Украина

Introduction. The development of computational-and-experimental methods for evaluating the force distribution pattern across the width of the toothed rim and in the circumferential direction of the toothing of a large wave gear is considered. The study is based on the results of the test tooth tensometry using scale modeling of prototype units. The work objective is to create a reliable experimental-theoretical model of the teeth force interaction in a large wave gearing. Such a solution involves the transformation of model sample deformations into a distributed load between teeth which will eliminate the basic uncontrollable nonlinear errors and improve the accuracy of estimation of force factors in the toothing area.

Materials and Methods. An improved power analysis procedure of a large wave gearing, optimized by accuracy criteria, is developed. The accuracy of the research results is enhanced through improving physical and computational models. This approach enables to obtain reasonable dependences of the power factors distribution in a large wave gearing.

Research Results. The design shape of the control tooth is simplified; an invariant profile is introduced over the full width of the ring gear. Thus, non-linear distortions of the experimental results introduced by a variable tooth shape across the width of the ring gear are excluded. In this case, the installation of tensoresistors across the full width of the test tooth is possible. In addition, the proposed solution can establish the dependence of the teeth deformation across the full width of the ring gear, and not only in the extreme areas as suggested by the well-known techniques. The development of perfect physical and mathematical models enables to increase accuracy of the results of theoretical and experimental studies on power processes in the large wave gearing. The scientific-based two-parameter dependences of the force distribution in gearing are obtained.

Введение. Статья посвящена разработке расчетно-экспериментальных методов оценки характера распределения сил по ширине зубчатого венца и в окружном направлении зубчатого зацепления крупной волновой передачи. Исследование основано на результатах тензометрии контрольного зуба с использованием масштабного моделирования опытных образцов. Цель работы — создание объективной экспериментально-теоретической модели силового взаимодействия зубьев в зацеплении крупной волновой передачи. Такое решение предполагает преобразование деформаций модельных образцов в распределенную нагрузку между зубьями, что позволит исключить основные неконтролируемые погрешности нелинейного характера, повысить точность оценки силовых факторов в поле зацепления.

Материалы и методы. Разработана уточненная методика силового анализа зубчатого зацепления крупной волновой передачи, оптимизированная по критериям точности. Точность результатов исследования повышена за счет совершенствования физических и расчетных моделей. Такой подход позволил получить обоснованные зависимости распределения силовых факторов в зубчатом зацеплении крупной волновой передачи.

Результаты исследования. Упрощена конструктивная форма контрольного зуба: по всей ширине зубчатого венца введен неизменный профиль. Таким образом исключены нелинейные искажения результатов экспериментов, вносимые переменной формы зуба по ширине зубчатого венца. В таком случае возможен монтаж тензорезисторов по всей ширине контрольного зуба. Кроме того, предлагаемое решение позволяет установить зависимость деформации зубьев по всей ширине зубчатого венца, а не только на крайних участках, как предлагают известные методики. Разработка совершенных физических и математических моделей позволила повысить точность результатов теоретических и экспериментальных исследований силовых процессов в зубчатом зацеплении крупной волновой передачи. Получены научно обоснованные двухпараметрические зависимости рас-

* The research is done with the financial support from "Novokramatorsky Mashinostroitelny Zavod" PJSC and at its production facilities.
** E-mail: strelnikov2019@mail.ru, ztm@nkmz.donetsk.ua, maxgs@yandex.ru
*** Работа выполнена при финансовой поддержке и на производственных площадях частного акционерного общества «Новокраматорский машиностроительный завод».

Discussion and Conclusions. Approximation of the involute-tooth profile in the trapezoidal profile has simplified evidence of identity of the elasticity equations and the boundary conditions of mathematical models. The results obtained are applicable in the mathematical simulation of the planar stress state of teeth with nonlinear profiles. Comparative evaluation of errors introduced by deviations of geometry and dimensions of physical models and mathematical analogues supports the experiment correctness and the validity of the quantitative data obtained. The research results can be used in the improved calculation of the design parameters of the gear components in the engineering process of large heavily loaded wave reducers.

Keywords: wave gear, gearwheel, power analysis, load distribution

For citation: V.N. Strelnikov, et al. Development of a power model for large wave gear toothing. Vestnik of DSTU, 2019, vol. 19, no. 2, pp. 120−129. https://doi.org/10.23947/1992-5980-2019-19-2-120-129

пределения сил в зубчатом зацеплении.

Обсуждение и заключения. Аппроксимация эвольвентного профиля зуба в трапецеидальный профиль упростила доказательство тождественности уравнений упругости и граничных условий математических моделей. Полученные результаты применимы при математическом моделировании плосконапряженного состояния зубьев с нелинейными профилями. Сравнительная оценка погрешностей, вносимых отклонениями геометрических форм и размеров физических моделей и математических аналогов, подтверждает корректность постановки эксперимента и обоснованность полученных количественных данных. Результаты работы могут быть использованы при уточненном расчете конструктивных параметров элементов зубчатого зацепления в процессе проектирования крупных тяжело нагруженных волновых редукторов.

Ключевые слова: волновая передача, зубчатое зацепление, силовой анализ, распределение нагрузки.

Образец для цитирования: Стрельников, В. Н. Разработка силовой модели зубчатого зацепления крупной волновой передачи / В. Н. Стрельников, А. И. Волошин, М. Г. Суков // Вестник Дон. гос. техн. ун-та. — 2019. — Т. 19, № 2. — С. 120−129. https://doi.org/10.23947/1992-5980-2019-19-2-120-129

Introduction. The intermediate transformation of the rotational motion into a continuous wave deformation of the flexible wheel has changed the established principles and forms of conjugation of the engagement elements of higher kinematic pairs. At this, a small tooth difference in the internal gearing of wave transmission (two teeth) differs from the traditional ideas on the conditions of geometric synthesis and functioning of a gear pair. Therefore, from the viewpoint of interference of the teeth, the engagement of the wave transmission is beyond the permissible limits of the existence of an involute internal gear with rigid tooth-wheels. The interference of second-type teeth arising in clamping is enhanced by the deformation of the flexible wheel from the transmitted load, which limits the carrying capacity of wave gear. The negative impact of the scale factor contributes to the occurrence of tooth interference in large wave transmissions, which causes jamming and slipping of teeth in the gearing.

The basic concept of wave gear (strain wave gearing, SWG) was patented by K. W. Musser in 1957. The solution remains unchanged for the stock-produced designs of limited capacity despite many design improvements. This is confirmed by wave gears manufactured by the leading companies in the USA (Harmonic Drive Technologies Inc., United Shoe Machinery Corp.), Japan (Harmonic Drive Systems Inc.), Germany (Harmonic Drive AG), and others including licensed products of Harmonic Drive Systems Inc., China [1, 2]. In large wave gearheads, high capacities are realized, and torques exceed (0.3 ... 1.5) $\times 10^6$ Nm. Mining, metallurgical equipment and large machines produced by Novokramatorsk Machine Building Plant (NKMZ) are completed with such parts. The standard design of a cam wave generator with a flexible ball bearing is inoperative and inapplicable in such products of heavy engineering [3]. Large wave gears use a disk wave generator. In contrast to the cam generator which simultaneously contacts along the entire perimeter of the flexible wheel, the disk wave generator interacts with the flexible wheel in diametrically opposite areas. This creates a higher level of freedom of deformation of the flexible wheel and increases possible deviations from the specified position.

Under the action of the wave generator discs and torque, the flexible wheel becomes curved in the form of a slightly twisted taper. This causes tooth misalignment over the width of the ring gear relative to the rigid wheel. The uniformity of the gap setting in the gearing across the width of the gear rims is disturbed.

Under heavy-duty service, the deformations of the flexible wheel exceed the gaps in the gearing and create interference conditions for the teeth of the second kind. With wide toothed crowns, a small module of the teeth under heavy loads, the gaps in the local zones of the deformed gearing take on negative values, activate the interference, cause jamming and breakthrough. Constructive features of large wave gears are mainly due to the scale. This factor exacerbates the negative processes observed in the gearing of higher kinematic pairs, and reduces the specifications and performance of heavily loaded wave gearboxes.

The work objective is to increase the load capacity, the specifications and performance of large wave gear reducers that meet the technical requirements of heavy engineering.

Theoretical and practical developments in the study of large wave transmissions are limited, the results obtained are contradictory, and they cannot always be repeated. Besides, we note significant construction features, lack of geometric similarity in the size series of kinematic and large wave transmissions among others. All this does not allow using well-known computational methods in the design of wave transmissions for the purposes of heavy engineering [4–6]. Synthesis of gearing is subject to the condition of constancy of a given gear ratio, governed by the Euler – Savary formula. Permanent deformation of the flexible wheel does not agree with the fundamental gearing theorem, which contributed to the development of conflicting methods for the synthesis of wave gearing [7–11]. In some papers, a general case of gearing is taken as the basis [12], while others consider a wedge mechanism with a complex relative movement of links [13–15]. In some techniques, the geometry and kinematics of wave gearing are simplified [16, 17]. The combined approach is synthesis of the general theory of gearing with elements of the wedge mechanism [1].

To satisfy the conditions of the fundamental theorem of gearing in relation to the synthesis of wave transmission, E.G. Ginzburg used the kinematic approach [18]. The concept of "angular velocity of a point" introduced by him is wrong, the arguments based on it are incorrect.

In the monograph by N.A. Kovalev [19], complexity of the force and kinematic processes occurring in wave transmissions, absence of reliable dependencies that can adequately reflect the impact of external factors on internal processes in kinematic pairs are specified. It prevents from developing an effective method for synthesis of wave gear that optimizes the basic parameters of the bearing links. According to N.A. Kovalev, with an inextensible middle surface, only the point of intersection of the tooth axis and the middle surface moves uniformly, which contradicts the conclusions of E.G. Ginzburg [18].

Maximum radial elastic displacement (w_o) on the middle surface of the flexible wheel is set by the wave generator in the absence of torque. The w_o offset must exceed half the working height of the tooth. The toothing dimensions should be adjusted by w_o value, not vice versa [19].

There is no consensus on the value of w_o parameter. Some authors associate maximum radial deformation (w_{max}) with the transmission ratio of wave gear [20] and a disk wave generator. To increase efficiency, it is recommended to assume $w_{max} = m$. E.G. Ginzburg recommends to determine $w_{\max}$ through m_y conditional module, different from m module [18].

Materials and Methods. To prevent the interference of teeth, the following well-known techniques are used in the stock-produced wave gearboxes:

- tooth correction,
- widening of the tooth space,
- angle increase in the original tooth contour.

This, along with a narrow width of the gear rims and relatively small transmitted torques, in many ways settles practical issues of the approximate gearing synthesis in terms of eliminating the tooth interference for the stock-produced low-loaded wave gears. However, theoretical studies on these issues are far from complete. So far, there is no satisfactory solution regarding the engagement of higher kinematic pairs of large wave gears with the gear rim width of 100–200 mm, a tooth module of 1.5–3 mm and a disk wave generator. Large wave gearboxes, designed by well-known methods and manufactured at NKMZ, turned out to be inoperable due to the tooth interference. Solving such problems requires new technical solutions based on reliable results of the theoretical and experimental research.

A scientific research has been carried out to assess the boundary conditions for the interference phenomena and tooth breakthrough in the gearing, as well as to prevent these negative developments. Their results enable to create a generalized model of the tooth interaction in the engagement of a large wave transmission. A refined power analysis procedure of such toothing is developed. The research results accuracy is enhanced through improving the physical and computational models. This allows obtaining reasonable dependences of the distribution of power factors in the gearing of a large wave transmission.

Deformation of stressed structural elements, including teeth, is usually measured using strain gauge methods. However, it is impossible to fix strain gages on the wave transmission teeth with a small module. According to the known methods [20, 21], two parallel slots are made in the rim of the hard wheel removing two adjacent teeth (Fig. 1).

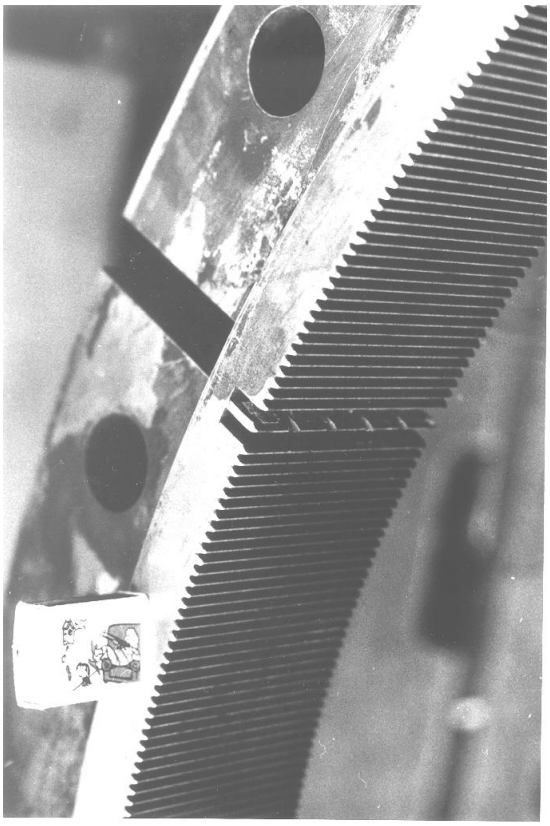

Fig. 1. Localized tooth elements of rigid wheel tilt gear of MP-600AC mobile mixer

Across the wheel width, the slots can be end-to-end or blind, made at both ends of the rim so that the middle part remains intact. According to the authors of common methods, through deep slots can reduce significantly the wheel stiffness, which is unacceptable. In the known papers, an experimental model is used, where the middle part of the teeth is not removed and it works alongside with all others.

The ideas of an unacceptable reduction in wheel stiffness through end-to-end slots [22] are inconclusive, since the thickness of the rim of a rigid wheel is not regulated; and it can be taken sufficient under the experimental conditions that the slots have no real impact on rigidity. In addition, the hard wheel is pressed into the hull design and, when evaluating stiffness, is considered together with the gearbox housing. .

According to the methods [20, 21], the slots of the rigid wheel increase the deformation of the control tooth relative to its middle part. The change in the rigidity of the control tooth along the length increases the deformation of the selected elements at the ends, distorts the deformed state of the control tooth and does prevents with sufficient accuracy the estimation of the force characteristics of the gearing along the crown width and in the circumferential direction. A multiple decrease in the rigidity of the selected tooth elements is not considered by the well-known methods [22], which violates the objectivity of the experimental results and complicates their analysis.

Standard techniques for measuring the tooth deformation of the wave transmission [8] differ little from the method of conventional gears [23]. In [22], it is shown that the difference in rigidity of the model, due to blind slots on the hard wheel, distorts the deformation of the control tooth under load and is considered when conducting the experiment and processing of the data obtained. This reduces the accuracy and reliability of the results.

The strain gauge is not mounted in the middle of the control tooth, so it is impossible to get a full picture of its deformation, qualitative and quantitative characteristics of the force distribution in the toothing. Moreover, when considering the stepwise change in the rigidity of a physical model by the known methods, the boundary conditions are not taken into account, the impact of which is enhanced by the scale factor [18].

Consider VZ-1120 wave reducer of the tilt drive of MP-600AC mobile mixer with the capacity of 600 tons of molten metal. Assume that load in the gearing of the wave transmission is applied in the middle of the tooth height, because there is ~ 20÷25% of teeth in the internal gearing of one wave.

Let us determine a possible error of allowance in the experiment. Consider a rigid annulus internal gear:

- modulus of teeth m = 1.5 mm;
- number of teeth of the rigid wheel Z_2 = 762;
- number of cutter teeth Z_4 = 68;

– wheel pitch circle diameter d = 1143 mm;
– wheel tooth depth H = 2.985 mm;
– wheel outside diameter D = 1155.12 mm;
– root diameter of wheel teeth D_b = 1161.09 mm;
– pressure angle at the tooth point on the pitch circle d, $\alpha_0 = 20$ °;
– tool addendum modification coefficient x = +4.953 mm;
– face width b = 100 mm;
– normal rack tooth profile as per GOST 13755-81 standard;
– accuracy degree 7D (GOST 1643-81).

The relative error of R assumption concerning the conditional application of normal force in the middle of the tooth depth:

$$R = \frac{2H}{D + D_b} \cdot 100\% = \frac{2 \cdot 2.985}{1155.12 + 1161.09} \cdot 100\% = 0.3\%.$$

The accepted assumption has no real impact on the transmission of forces in gearing, since it changes slightly the diameter of the loading appliance. For approximation of the involute tooth profile in a straight line shape, we determine the thickness of the tooth (S_x) of the rigid wheel along an arbitrary circle of radius (r_x):

$$S_x = m\frac{cos\,\alpha_0 \pi}{cos\,\alpha_x^2} + \Delta_2 + Z_2\left(inv\alpha_x - inv\alpha_0\right), \quad cos\,\alpha_x = \frac{r}{r_x} cos\,\alpha_0,$$

where α_x is pressure angle at the tooth point, where radius is r_x vector; Δ_2 is ratio of the tooth thickness on any wheel circumference in the normal section under toothing by the cutter of medium wear:

$$\Delta_2 = \left(Z_2 - Z_4\right)\left(inv\,a_0 - inv\,a_{C2}\right). \quad (1)$$

The relative error is defined as the modulus of ratio of the absolute error to the approximation value. In this case, maximum possible absolute error is equal to $H/2$. The approximate value is the radius of the middle tooth circle of the rigid wheel: $\left(D + D_b\right)/4$. The angle cosine of the machine tool α_{C2} in the expression (1) when cutting a rigid wheel by the cutter of medium wear is determined considering the addendum modification coefficient of the cutter:

$$cos\alpha_{C2} = cos\alpha_0 \frac{z_2 - z_4}{z_2 - z_4 + 2\varepsilon_2}.$$

The tooth thickness values (S_X) along the arc of an arbitrary radius (r_x) of the rigid wheel are given in Table 1.

Table 1

Arc tooth thickness S_X of rigid wheel in different sections with radius r_X, mm

r_x	579.239	579.426	579.612	579.799	579.985	580.172	580.358	580.545
S_x	2.613	2.765	2.918	3.071	3.223	3.377	3.530	3.685

Arc tooth thickness differs from the chordal tooth thickness at the given parameters of a rigid wheel by $5 \cdot 10^{-5}$ mm, so with sufficient accuracy, we can equate the arc tooth thickness with r_x radius and the corresponding chordal tooth thickness.

We determine the tooth thickness S_{ax} approximated in a straight profile at the radius of r_X = 579.799 mm. It is equal to the half-sum of the extreme tooth thickness values along the radii r_x = 579.053 mm and r_x = 580.545 mm: $S_{\alpha x}$ = 3.074 mm.

The tooth thickness of the involute profile of the rigid wheel on the circle of radius r_x = 579.799 mm is equal to S_x = 3.071 mm. Absolute error of the approximation of the tooth profile of a rigid wheel in a straight-line profile:

$$A_x = S_x - S_{ax} = -0.003 \text{ mm}.$$

Relative error of the straight-line approximation of the involute tooth profile of a rigid wheel:

$$R = \left|\frac{S_x - S_{ax}}{S_{ax}}\right| \cdot 100 = 0.1\,\%.$$

The approximation of the involute tooth profile of a rigid wheel with a straight-line profile does not introduce a detectable error in the design scheme. The equation of the straight-line profile of the tooth model in the *XOY* coordinates is shown in Fig. 2.

$$\frac{Y-Y_2}{X-X_2}=\frac{Y_1-Y_2}{X_1-X_2}. \tag{2}$$

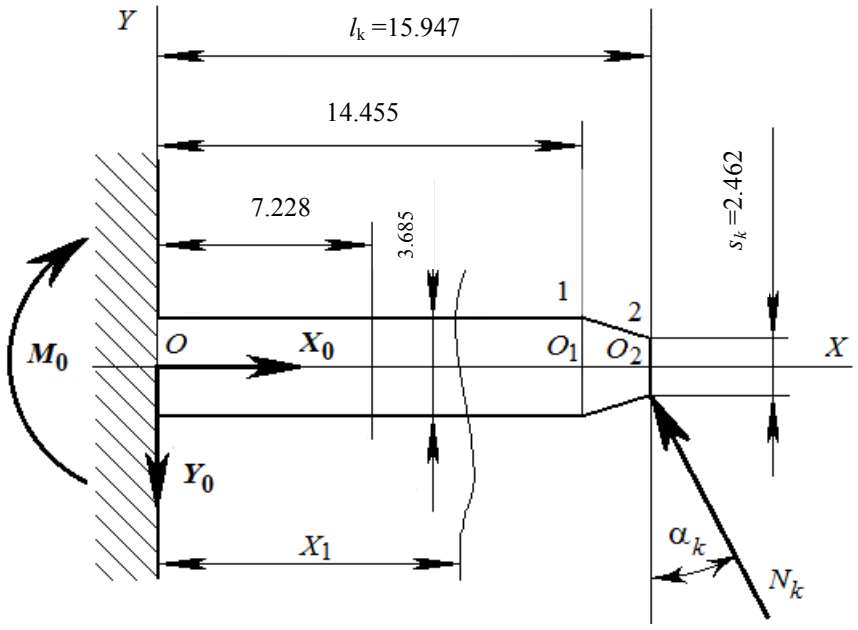

Fig. 2. Design model of control tooth of rigid wheels approximated by straight-lineprofile

In Fig. 2, 1 and 2 indices indicate membership of the coordinate functions X and Y to the extreme 1 and 2points of the straight-line tooth profile. X and Y values are inserted in the equation (2) at 1 and 2 points as shown in Fig. 2, and the equation of the straight tooth profile with linear dimensions in millimeters is written:

$$Y = 7.767 - 0.410\,X.$$

Thickness and rigidity of the approximated straight tooth of a rigid wheel in an arbitrary section, mm:

$$S_{ax} = 2Y = 15.534 - 0.820\,X\,. \tag{3}$$

$$EI_z = 2.1\cdot 10^5\,\frac{l\,S_x^3}{12}. \tag{4}$$

Specific rigidity of the approximated straight tooth of a rigid wheel in an arbitrary cross section is determined by substituting the values (3) at l = 17.5 mm into the expression (4):

$$EI_{z_0} = 0.169\cdot 10^6\cdot(18.943 - X)^3\,.$$

Deflection of the elastic line of the control tooth model under N_k force is determined at $X = l_к$ = 15.947 mm:

$$Y_2 = 0.819\cdot 10^{-4}\,N_k\ [\text{мм}]. \tag{5}$$

Tension stresses σ^+ and compression σ^- of the control tooth model in the area of installation of strain gages at the distance of $a_т$ = 7.2275 mm from the cantilever fastening (pinching) of the model:

$$\sigma^+ = \frac{M_И}{W_Z} - \frac{X_0}{F} = 0.1867N_k, \frac{H}{mm^2}, \tag{6}$$

$$\sigma^- = \frac{M_И}{W_Z} + \frac{X_0}{F} = 0.1983N_k, \frac{H}{mm^2}, \tag{7}$$

Here, $M_и$ is bending moment in the area of installation of strain gauges; $M_и = M_о - Y_о \cdot a_т$; W_z is section modulus of the linear tooth model:

$$W_z = \frac{bh^2}{6} = 39.61\ \text{mm}^3.$$

Using the ratio

$$\sigma = E\varepsilon,$$

where ε is the relative deformation of the strain gauge, as well as the formulas (5–7), a relationship is established between the relative deformation of the strain gauges on the stretched and compressed surfaces of the control tooth model and the deflection of the elastic line under the force:

$$Y_2 = 5013.33 \cdot \varepsilon^{+}, \; Y_2 = 472.07 \cdot \varepsilon^{-}. \quad (8)$$

Research Results. Theoretical and experimental studies, practical developments are mainly associated with the development, production and operation of relatively small wave gearboxes [25–32]. The accumulated experience cannot be used without considering the scale factor for large wave gears with torques of $5 \cdot 10^5$ Nm and more.

The flexible link enhances the negative effect of the scale factor through disturbing the regular operation of the gearing of higher kinematic pairs. Under heavy-duty service, interference of the second kind can cause jamming and breakthrough of the teeth. Interference also activates force processes in the wave generator area increasing energy losses

The fragment of the oscillograph pattern corresponds to the turnover of 2π wave generator (Fig. 3).

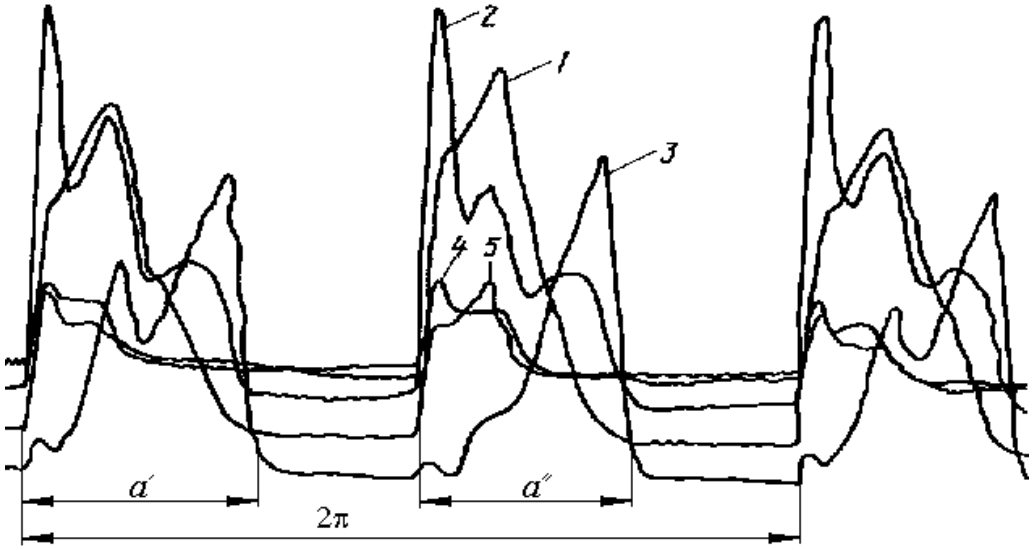

Fig. 3. Oscillogram of rigid wheel tooth deformation under load $M_2 = 3 \cdot 10^5$ Nm and rotation frequency $\omega_1 = 1.667$ s^{-1}; 1, 2, 3, 4, 5 are deformation oscillograms of localized control tooth elements

The number of tooth pairs in Z_Σ gearing is determined by the duration of the engagement of the control tooth under a complete rotation of the wave generator $(\alpha' + \alpha'')$:

$$Z_\Sigma = \frac{a' + a''}{2\pi} Z_B \cdot 100\,\%. \quad (9)$$

The number of simultaneously engaging tooth pairs and the load shape across the width of the ring gear depend on the design parameters of the wave transmission, which determine the conditions of toothing, and represent some torque functions.

The technique of power analysis of gearing for large wave transmission is developed. Two advantages differ it from the known solutions.

1) It enables to eliminate the distortion of the deformed state of the control tooth under load due to the stiffness constancy lengthwise. For this purpose, through parallel slots are made on a rigid wheel symmetrically to the axis of the control tooth.

2) It becomes possible to significantly improve the accuracy of the evaluation of gearing power characteristics across the width of the crown and in the circumferential direction due to the rigidity reduction of the control tooth. For this purpose, physical models of a control tooth and a scaled tooth of a rigid wheel are developed.

Discussion and Conclusions. The control tooth shape is taken invariant across the full width of the ring gear (this differs the presented approach from the techniques [20–22]). Hence, the distortion of the experimental results introduced by the variable width of the tooth shape is eliminated.

The solution provides the installation of strain gauges across the full width of the control tooth, which establishes a complete dependence of the tooth deformation across the full width of the ring gear, and not just in the outermost sections, as the well-known technique suggests.

The updating of physical and mathematical models made it possible to improve the accuracy of the theoretical and experimental results of force processes in the gearing of a large wave transmission [8–10]. The scientific-based two-parameter dependences of the force distribution in gearing are obtained.

References

1. Musser, C.W. Breakthrough in mechanical design: The Harmonic Drive. Machine Design, 1960, no. 32 (8), pp. 160–172.

2. Malogabaritnye reduktory CSF ot Harmonic Drive. [CSF Compact gearboxes from Harmonic Drive.] "Market of microelectronics" LLC. Available at: http://catalog.gaw.ru/index.php?page=document&id=37585 (accessed: 02.05.19) (in Russian).

3. Timofeev, G.A., Samoylova, M.V. Sravnitel'nyy analiz skhemnykh resheniy privodov s volnovymi zubchatymi peredachami dlya sledyashchikh system. [Comparative analysis of the wave gear drive kinematic diagram for servo-type mechanisms.] Vestnik MSTU (Series Machine Building), 2015, no. 4 (103), pp. 109–118 (in Russian).

4. Strelnikov, V.N., Sukov, M.G. Analysis of axial forces of heavy-duty harmonic gear drive. Actual Issues of Mechanical Engineering (AIME 2018): Int. Conf.: Advances in Engineering Research (AER), 2018, vol. 157, pp. 584–589. Available at: https://www.atlantis-press.com/proceedings/aime-18.

5. Strelnikov, V.N, Sukov, M.G. Experimental investigation on interaction of wave disk generator with flexible gear. Proc. Int. Conf. on Innovations and Prospects of Development of Mining Machinery and Electrical Engineering, 12–13 April 2018, Saint-Petersburg, IOP Publishing. IOP Conference Series: Earth and Environmental Science, 2018, vol. 194, no. 3. Available at: http://iopscience.iop.org/volume/1755-1315/194 (accessed 02.05.19).

6. Strelnikov, V.N., Sukov, M.G. Stressed state of heavy-duty harmonic gear drive flexspline. Proc. Int. Conf. on Aviamechanical Engineering and Transport (AviaENT 2018). Advances in Engineering Research, 2018, vol. 158, pp. 391–398. Available at: https://www.atlantis-press.com/proceedings/avent-18/articles (accessed 02.05.19).

7. Kyzykhanov, Kh.R. O linii zatsepleniya volnovoy zubchatoy peredachi. [On the pressure line of wave gear.] Proceedings of Higher Educational Institutions. Machine Building, 1968, no. 1, pp. 5–8 (in Russian).

8. Kovalev, N.A., Shapochkina, I.M. Kinematicheskoe issledovanie evol'ventnoy volnovoy peredachi, u kotoroy zub'ya gibkogo kolesa narezany v nedeformirovannom sostoyanii. [Kinematic study of an involute wave transmission in which flexible wheel teeth are cut in the undeformed state.] Proceedings of Higher Educational Institutions. Machine Building,1967, no. 1, pp. 21–27 (in Russian).

9. Rubtsov, V.K. Nekotorye osobennosti vybora profilya zuba volnovoy peredachi. [Some features of the tooth profile selection of wave gear.] Mechanics of Machines, 1967, iss. 9, pp. 98–105 (in Russian).

10. Rubtsov, V.K. Nekotorye osobennosti vybora profilya zuba volnovoy peredachi. [Some features of the tooth profile selection of wave gear.] Mechanics of Machine, 1967, iss. 10, pp. 112–109 (in Russian).

11. Shenderova, E.N. Vybor nekotorykh geometricheskikh parametrov zatsepleniya zub'yev volnovoy peredachi na osnove analiza krivoy odnoparnogo kontakta. [Selection of some geometrical parameters of teeth gearing of wave transmission based on the one-pair contact curvature analysis.] Wave gear. Moscow: Stankin, 1975, pp. 115–125 (in Russian).

12. Shuvalov, S.A., Dudko, V.D. Prostranstvennoe predstavlenie zatsepleniya volnovoy peredachi. [Spatial representation of wave gearing.] Proceedings of Higher Educational Institutions. Machine Building,1972, no. 10, pp. 45–47 (in Russian).

13. Tseitlin, N.M., Zuckermann, E.M. Metodika geometricheskogo rascheta volnovykh zubchatykh peredach. [Method of geometric calculation of wave gears.] Wave and chain gears. Moscow: Stankin, 1967, pp. 9–20 (in Russian).

14. Tseitlin, N.M., Zuckermann, E.M. Raschet parametrov zatsepleniya volnovoy peredachi. [Wave gear parameter determination.] Wave gear. Moscow: Stankin, 1970, pp. 13–25 (in Russian).

15. Zuckermann, E.M. Vybor geometricheskikh parametrov volnovoy zubchatoy peredachi. [Selection of wave gear geometry.] Vestnik Mashinostroeniya,1964, no. 11, pp. 23–28 (in Russian).

16. Shuvalov, S.A. Grafoanaliticheskiy metod analiza geometrii zatsepleniya v volnovoy zubchatoy peredache. [Grapho-analytical method for analyzing the wave gear geometry.] Proceedings of Higher Educational Institutions. Machine Building, 1965, no. 2, pp. 89–93 (in Russian).

17. Yastrebov, V.M., Voronin, N.A., Borovikov, N.A. Sintez priblizhennogo zatsepleniya volnovoy zubchatoy peredachi s odnoventsovym gibkim kolesom. [Synthesis of approximate engagement of wave gearing with unilateral flexible gear.] Wave gearing: Abstract. Leningrad: LVIKA after A.F. Mozhaisky; Mashprom NTO, 1969, pp. 228–235 (in Russian).

18. Ginzburg, E.G. Volnovye zubchatye peredachi. [Wave gear.] Leningrad: Mashinostroenie, 1969, 160 p. (in Russian).

19. Kovalev, N.A. Peredachi gibkimi kolesami. [Flexible gearing.] Moscow: Mashinostroenie, 1979, 200 p. (in Russian).

20. Finogenov, V.A. O raspredelenii nagruzki po zub'yam volnovoy peredachi. [On load distribution over the wave gear teeth.] Proceedings of Higher Educational Institutions. Machine Building,1971, no. 12, pp. 51–54 (in Russian).

21. Ivanov, M.N., Shuvalov, S.A., Finogenov, V.A. Eksperimental'noe opredelenie kolichestva odnovremenno zatseplyayushchikhsya zub'yev i velichin ikh deformatsii v volnovoy peredache. [Experimental determination of the number of simultaneously engaging teeth and their deformation values in wave gear.] Proceedings of Higher Educational Institutions. Machine Building, 1968, no. 9, pp. 37–40 (in Russian).

22. Ivanov, M.N. Volnovye zubchatye peredachi. [Wave gear.] Moscow: Vysshaya shkola, 1981, 184 p. (in Russian).

23. Gadolin, V.L., et al. Mashiny i stendy dlya ispytaniya detaley. [Machines and stands for part testing.] D.N. Reshetov, ed. Moscow: Mashinostroenie, 1979, 343 p. (in Russian).

24. Ivanov, M.N., Sorokin, A.N. Raschet nagruzki na kulachkovyy generator i napryazheniy rastyazheniya v gibkom kolese volnovoy peredachi. [Load calculation on the cam generator and tensile stresses in the flexible wave gear.] Proceedings of Higher Educational Institutions. Machine Building,1980, no. 6, pp. 15–19 (in Russian).

25. Buchakov, Yu.V. O parametrakh kontakta zub'yev koles pri prirabotke volnovoy zubchatoy peredachi. [On contact parameters of the wheel teeth during brake-in period of wave gear.] Mekhanika protsessov i mashin: sb. nauch. tr. [Mechanics of processes and machines: coll.of sci.papers.] Omsk: OmSTU Publ. House, 2002, pp. 54–59 (in Russian).

26. Yemelyanov, A.F. Eksperimental'noe obosnovanie vozniknoveniya vozmushchayushchego momenta v volnovoy zubchatoy peredache. [Experimental verification of occurrence of a disturbing torque in wave gear.] Teoriya, metody i sredstva izmereniy, kontrolya i diagnostiki: mat-ly mezhdunar. nauch.-prakt. konf. [Theory, methods and means of measurement, control and diagnostics: Proc. Int. Sci.-Pract. Conf.] Novocherkassk: SRSTU Publ. House, 2000, Part 5, pp. 14–15 (in Russian).

27. Yemelyanov, A.F., Rumyantsev, P.O. Vozniknovenie vozmushchayushchego momenta v volnovoy zubchatoy peredache. [Occurrence of disturbing moment in wave gear.] Avtomatizatsiya i progressivnye tekhnologii: tr. 3-y mezhotrasl. nauch-tekhn. konf. [Automation and advanced technologies: Proc. 3rd Int. Sci.-Tech. Conf.] Novouralsk: NSTU Publ. House, 2002, pp. 401–402 (in Russian).

28. Nepomnyashchikh, V.N., Tatishchev, V.N. Diskovyy generator bystrokhodnoy volnovoy zubchatoy peredachi s malym peredatochnym chislom. [High-speed gearwheel disk generator with low gear ratio.] Wave gear. Moscow: Stankin, 1975, pp. 187–201(in Russian).

29. Skvortsova, N.A., Semin, Yu.I., Fursyak, F.I. K voprosu polucheniya bezzazornogo volnovogo zubchatogo soedineniya. [To the issue of backlash-free wave gear.] Proceedings of Higher Educational Institutions. Machine Building,1972, no. 7, pp. 64–67 (in Russian).

30. Timofeev, G.A., Tarabarin, V.B. Proektirovanie privodov s planetarno-volnovymi mekhanizmami dlya sledyashchikh system. [Design of drives with planetary-wave mechanisms for servo systems.] Proektirovanie tekhnologicheskikh mashin, 1999, no. 16, pp. 61–67 (in Russian).

31. Ghorbel, F.H., Gandhi, P.S. On the Kinematic Error in Harmonic Drive Gears. Journal of Mechanical Design, 1998, no. 123 (1), pp. 90–97.

32. Zhong, Liang-Wei, Xiao-Jing Zeng, Xu-Ping Zou. Research on harmonic gear transmission CAD system. Journal of University of Shanghai for Science and Technology, 2002, no. 2, pp. 149–152.

Submitted 01.03.2019
Scheduled in the issue 02.04.2019

Authors:

Strelnikov, Victor N.,
professor of the Engineering Mechanics and Strength of Materials Department, Belgorod State Technological University named after V.G. Shukhov (46, Kostyukov St., Belgorod,308012, Russia), Dr.Sci. (Eng.), professor,
ORCID: https://orcid.org/0000-0002-1752-4279
strelnikov2019@mail.ru

Voloshin, Alexey I.,
chief engineer, "Novokramatorsky Mashinostroitelny Zavod" PJSC" (5,Ordzhonikidze St., Kramatorsk, Donetsk region, 84305, Ukraine),
ORCID: https://orcid.org/0000-0002-8493-4067
ztm@nkmz.donetsk.ua

Sukov, Maxim G.,
workshop supervisor, "Novokramatorsky Mashinostroitelny Zavod" PJSC" (5,Ordzhonikidze St., Kramatorsk, Donetsk region, 84305,Ukraine),
ORCID: https://orcid.org/0000-0001-5817-9056
maxgs@yandex.ru

МАШИНОСТРОЕНИЕ И МАШИНОВЕДЕНИЕ
MACHINE BUILDING AND MACHINE SCIENCE

UDC 621.9:531.3 https://doi.org/10.23947/1992-5980-2019-19-2-130-137

Mathematical temperature simulation in tool-to-work contact zone during metal turning*

E. V. Bordatchev[1], V. P. Lapshin[2]**
[1] Don State Technical University, Rostov-on-Don, Russian Federation
[2] National Research Council Canada, Ottawa, Canada

Математическое моделирование температуры в зоне контакта инструмента и изделия при токарной обработке металлов***

Е. В. Бордачев[1], В. П. Лапшин[2]**
[1] Национальный научно-исследовательский совет Канады, Оттава, Канада
[2] Донской государственный технический университет, Ростов-на-Дону, Российская Федерация

Introduction. Two factors of metal turning are compared: the dissipated temperature and the power of irreversible transformations in the material of the product and the tool. The paper is devoted to the issues of mathematical modeling of their link.

Materials and Methods. The mathematical apparatus is based on the modification of the Volterra equation which involves the use of double integral. It shows how the thermal energy released earlier during cutting affects the current state of temperature in the tool-to-work contact zone. In addition to the proposed new basic mathematical model, the processing effect of the observed data on the power of irreversible transformations and the measured temperature in the tool-to-work contact zone under metal turning are used. The experiments were carried out on 1K625 machine and STD.201-1 stand. A specialized software tool for processing information arrays describing the processes occurring during cutting (reaction forces, tool vibrations and power of irreversible transformations) was created in the Matlab package. The same tool has performed the temperature calculation in the tool-to-work contact zone.

Research Results. The procedure of parametric identification of the proposed basic mathematical model is carried out. The resulting model showed a high degree of proximity of the experimental data on the temperature in the cutting zone and the simulated level of thermal energy; but in the initial section of the measurable temperature dependence, the results of these two approaches are in rather poor agreement. This can be explained by an error of the experimental temperature measurement based on the estimate of the thermoelectromotive force (thermal EMF) output which is generated as a result of the dynamic thermocouple formation in the tool-to-work contact zone.

Введение. Сопоставлены два фактора токарной обработки металлов резанием: рассеиваемая температура и мощность необратимых преобразований в материале изделия и инструмента. Статья посвящена вопросам математического моделирования их связи.

Материалы и методы. Математический аппарат основан на модификации уравнения Вольтерры, которая предполагает использование двукратного интеграла. Он показывает, как выделенная ранее при резании тепловая энергия влияет на текущее состояние температуры в зоне контакта инструмента с обрабатываемой деталью. В работе помимо предложенной новой базовой математической модели использованы результаты обработки экспериментальных данных о мощности необратимых преобразований и об измеряемой температуре в зоне контакта инструмента с деталью при токарной обработке металла. Эксперименты проводились на станке 1К625 и стенде STD.201-1. В пакете Matlab была создана специализированная программа для обработки массивов информации, описывающих процессы, протекающие при резании (силы реакции, вибрации инструмента и мощность необратимых преобразований). В этой же программе выполнен расчет температуры в зоне контакта инструмента и детали.

Результаты исследования. Проведена процедура параметрической идентификации предлагаемой базовой математической модели. Полученная модель показала высокую степень близости экспериментальных данных о состоянии температуры в зоне резания и моделируемого уровня тепловой энергии, однако на начальном участке измеряемой температурной зависимости результаты двух этих подходов не вполне согласуются. Это можно объяснить погрешностью экспериментального измерения температуры на основе оценки вырабатываемой термоэлектродвижущей силы (термоЭДС), которая формируется в результате образования естественной термопары в зоне контакта инструмента и детали.

* The research is done with the financial support from RFFI (grant no. 19-08-00022 A).
** E-mail: Lapshin1917@yandex.ru, Evgueni.Bordatchev@nrc-cnrc.gc.ca
*** Работа выполнена при финансовой поддержке гранта РФФИ №19-08-00022 А.

Discussion and Conclusions. The proposed mathematical model enables to adequately describe the conversion of the mechanical component of the cutting energy into the thermal component through the indicator of the total output power of the mechanical interaction in the cutting zone for all the processing time.

Обсуждение и заключения. Предлагаемая математическая модель позволяет адекватно описывать процесс преобразования механической составляющей энергии резания в тепловую составляющую через показатель суммарной выделяемой мощности механического взаимодействия в зоне резания за все время обработки.

Keywords: turning, cutting, power of irreversible transformations, metal working, thermal conductivity of metals, Volterra integral equation, thermoelectromotive force (thermal EMF).

Ключевые слова: точение, резание, мощность необратимых преобразований, обработка металлов, теплопроводность металлов, уравнение Вольтерры, термоэлектродвижущая сила (термоЭДС).

For citation: E. Bordatchev, V.P. Lapshin. Mathematical temperature simulation in tool-to-work contact zone during metal turning. Vestnik of DSTU, 2019, vol. 19, no. 2, pp. 130–137. https://doi.org/10.23947/1992-5980-2019-19-2-130-137

Образец для цитирования: Бордачев, Е. Математическое моделирование температуры в зоне контакта инструмента и изделия при токарной обработке металлов / Е. Бордачев, В. П. Лапшин // Вестник Дон. гос. техн. ун-та. — 2019. — Т. 19, № 2. — С. 130–137. https://doi.org/10.23947/1992-5980-2019-19-2-130-137

Introduction. Thermal processes occurring under metal processing on the machine tools (both in metals and in other environments) are hard to describe. Their analysis is based on the Fourier heat condition equation [1]. In cases related to metal cutting, you need to have an idea about the temperature in the tool-to-work contact zone [2–5]. At that, there is no need to control the heat propagation beyond this zone since it does not affect the processing conditions. Similar reasoning can be applied to another widely used method for describing thermal processes, which considers the formation of heat source-drains in a workpiece [6]. Such approaches do not allow using the cutting process dynamics in the description of emerging thermal phenomena in the contact zones and developing a system of equations to represent the conversion of mechanical energy into thermal energy.

During operations with metals on the machine tools, irreversible transformations in workpieces and tools cause the heat generation, which, according to the second law of thermodynamics, is dissipated in space. Thermal processes in metals are more inertial than the treatment process dynamics, therefore dissipation lasts long enough. In the case in hand, the heat generation itself is associated with the power of irreversible transformations [11], which depends on the magnitude of the reaction forces to the tool forming movements [2–5] in the tool-to-work contact zone. At the same time, heat generation is the primary mechanism of dissipation of the released energy of material conversion [12].

The cutting process dynamics and the issues of its simulation are directly related to the representation of forces and reactions in the coordinates of the process state. In this case, as a rule, only the mechanical component is considered, as can be seen from foreign [13–18] and national [19–21] papers. Thus, it is advisable to introduce coordinates describing the temperature variation in the tool-to-work contact zone into the simulation of dynamics of the metal processing processes through consideration of the irreversible transformations. This approach will increase adequacy of the used mathematical apparatus.

Materials and Methods

Mathematical Model Validation. The forces preventing the tool from penetrating into the workpiece material have a complex spatial arrangement in the coordinate system associated with the tool strain axes. In the papers on the analysis of the reaction forces occurring in the cutting zone, it is mostly common to resolve such a reaction into components [4–6, 10, 19–21]. In the case under consideration, the following relations between the components of the reaction forces will be valid [5]:

$$R = \sqrt{P_x^2 + P_y^2 + P_z^2}, \quad (1)$$

where R is general force response from the cutting process to the forming movements of the tool; P_x is projection of the force response on the axis of the main rotational cutting movement in the feed direction; P_y is projection of force reaction directed along the radius of the main rotational cutting movement of at the cutting top; P_z is projection of the force reaction on the axis coinciding with the main movement speed at the tool tip.

The relationship between P_x, P_y, P_z forces introduced depends on many factors: the tool geometry, the tool wear factor, etc. [4]. Thus, in [5], when machining with a sharp cutter with the parameters of $\gamma = 15^0$, $\varphi = 45^0$ and $\lambda = 0^0$, the ratio is on average equal to

$$P_x, P_y, P_z = (0{,}3 - 0{,}4), (0{,}4 - 0{,}5). \quad (2)$$

Similar reasoning can be provided on analyzing the speeds of the relative tool movement along the workpiece, and we obtain the total speed of such movement:

$$V = \sqrt{V_x^2 + V_y^2 + V_z^2}. \quad (3)$$

With these arguments in view, we define the power of irreversible transformations:

$$N = \sqrt{P_x^2 + P_y^2 + P_z^2}\sqrt{V_x^2 + V_y^2 + V_z^2}. \quad (4)$$

Suppose that heat generation during cutting in the metal-cutting machines linearly depends on the power of irreversible transformations:

$$T_p = k_T N. \quad (5)$$

Here, T_p is the value describing the temperature increments in the cutting zone (^{0}C); k_T is the coupling coefficient between the power of irreversible transformations in the cutting zone and the magnitude of the increment of thermal energy in the tool-to-work contact zone with c^{0}C/Nm dimension. However, the total temperature value at a specific instant in time and in a given tool-to-work contact zone will be determined not only by the current value of heat gain. Due to the heat dissipation of in the material of the workpiece and tool, the impact of the following should be considered:

- power of irreversible transformations throughout the previous path,
- product processing time.

Imagine processing in the form of a discrete process graph where $N(n)$ is current value of the power of irreversible transformations; $L(n)$ is current value of the tool path during machining; $t(n)$ is current value of the processing time. According to (5), at each point of the discrete graph of the treatment process, heat increment proportionate to the power of non-reversible transformations at this point in space and time will be generated. The current temperature value at n point will be determined by both the heat gain at that point and the effect of temperature increments that previously occurred on the tool path (L) during processing (t). With the increase in time and distance passed, the impact of these factors on the process of heat generation in the contact zone under study weakens; therefore, an approach based on the use of the Volterra operator of the second kind is convenient for the mathematical description [10]. It cannot be applied directly because of the complexity of describing the heat propagation in metals; therefore, we will take the multiplicative criterion for assessing the effect of the previous heat gain on the current value in the form of a double integral as a basic model:

$$T_z = \Theta_s + k_T \iint_D w_L(\gamma - L) w_t(\eta - t) N(\gamma, \eta) d\gamma d\eta. \quad (6)$$

Here, T_z is heat value in the tool-to-work contact zone; Θ_s is ambient temperature; $w_L(\gamma - L)$ is the kernel which characterizes the effect of the previously generated power of irreversible transformations along the processing path on the current temperature value; $w_t(\eta - t)$ is the kernel which characterizes the impact of the previously generated power of irreversible transformations in terms of processing time on the current temperature value; D is the domain of integration characterizing the space-time heat dissipation; γ has the distance dimension, m; η has the processing time dimension, s. The kernels of the integral operator themselves are dimensionless gain constants.

The integral operator represented as a double integral (6), can be reduced to a multiple integral of the following form:

$$T_z = \Theta_s + k_T \int_0^{L(t)} w_L(\gamma - L)\, d\gamma \int_0^t w_t(\eta - t) N(\eta) d\eta. \quad (7)$$

The tool path is a function of time because each time value can be assigned the value of the distance passed. Therefore, the approach (7) is valid.

It is convenient to use exponential functions of the following form [10] as kernels of the integral operator proposed in (7):

$$\begin{cases} w_L(\gamma - L) = e^{\alpha_1(\gamma - L)} \\ w_t(\eta - t) = e^{\alpha_2(\eta - t)} \end{cases}, \quad (8)$$

where α_1, α_2 are scaling parameters of the integral operator to be identified.

Thus, the integral operator proposed in (7) takes the following form:

$$T_z = \Theta_s + k_T \int_0^{L(t)} e^{\alpha_1(\gamma - L)} d\gamma \int_0^t e^{\alpha_2(\eta - t)} N(\eta) d\eta. \quad (9)$$

This operator has the solution for the stationary case when the power of irreversible transformations is constant: $N_0 = N(t)$.

$$T_z = \Theta_s + \frac{k_T N_0}{\alpha_1 \alpha_2}(1 - e^{-\alpha_1 L})(1 - e^{-\alpha_2 t}). \quad (10)$$

As can be seen from (10), under a stationary machining process, temperature in the

$$T_z = \Theta_s + \frac{k_T N_0}{\alpha_1 \alpha_2}. \quad (11)$$

We illustrate these arguments by setting $\Theta_S = 25$ ^{0}C; $k_T = 0.0026$ s^{0}C / Nm; $\alpha_1 = 0.03$; $\alpha_2 = 0.01$; $N_0 = 20$ Nm/s (Fig. 1).

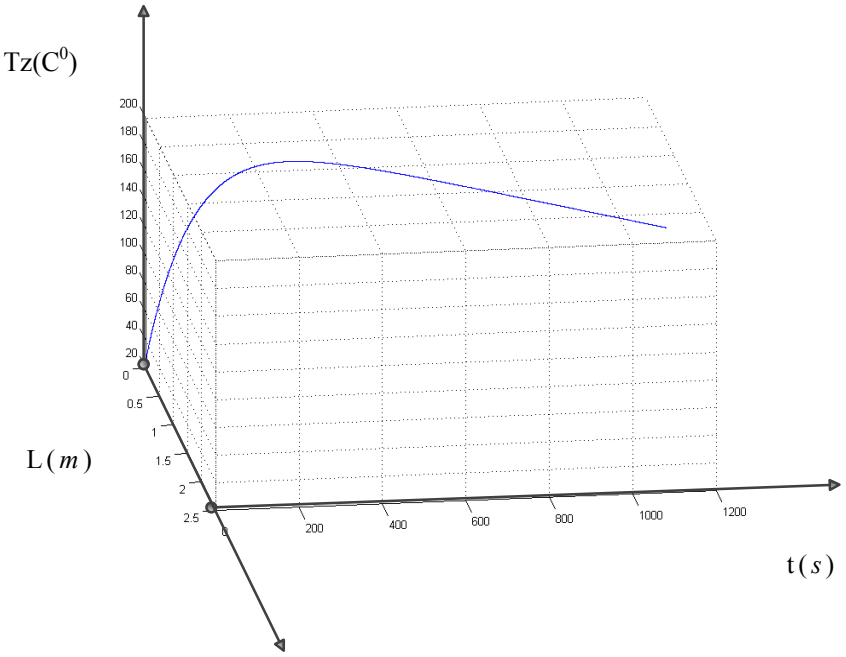

Fig. 1. Implementation of stationary temperature increase in the cutting zone

Fig. 1shows that the stationary heat process in the cutting zone increases exponentially and – having reached some equilibrium state – does not change anymore. Real processes occurring in machine tools are not stationary [11–12]. Based on these considerations, the process shown in Fig. 1 can be regarded as a movement towards which the temperature of the tool-to-work contact zone tends in a steady case. At that, the equation (10) is a generator equation for the integral operator (9).

Research Results

Parametric identification of the model from experimental data and simulation results. For the parametric identification of the model, a full-scale experiment was conducted on 1K625 lathe with the installed STD.201-1 stand. The stand is designed to study dynamic and thermal processes occurring during metal cutting on lathes in various modes.

The basic objective of the experiment was to study the impact of cutting dynamics on thermal processes in the tool-to-work contact zone. The change in cutting dynamics is understood as the cross effect of tool wear and cutting process associated with the force reaction occurring in the cutting zone. Measurement of this reaction and temperature through thermoelectromotive force (thermal EMF) generated in the tool-to-work contact zone allows evaluating the impact of the cutting dynamics on the thermal processes in the specified zone.

During the experiment, continuous turning of a shaft-type part was performed. At this, all processing parameters were preserved and the change in the force response from the cutting process was monitored. The conditions and the basic results of the experiment are described in detail in [22].

The data obtained as a result of a full-scale experiment are of discrete nature; therefore, it is impossible to directly apply the model represented by the integral operator (9) to them. For this reason, it is required to modify the basic mathematical model that describes the thermal process dynamics in the tool-part contact. To begin with, we leave in reasoning only a member of the integral operator depending on the power of irreversible transformations:

$$T_z^N = k_T \int_0^{L(t)} e^{\alpha_1(\gamma - L)} d\gamma \int_0^t e^{\alpha_2(\eta - t)} N(\eta) d\eta . \quad (12)$$

Since the experiment is already carried out, its completion time (t_k) and $L(t_k)$ path value corresponding to it are constants. Therefore, it will be valid to factor the exponents with these values outside the integrals:

$$T_z^N = k_T e^{-\alpha_1 L(t_k)} e^{-\alpha_1 t_k} \int_0^{L(t_k)} e^{\alpha_1 \gamma} d\gamma \int_0^{t_k} e^{\alpha_2 \eta} N(\eta) d\eta . \quad (13)$$

Assume that there is a certain discrete set of the calculated power values of irreversible transformations obtained as a result of analyzing discrete experimental information on the cutting process dynamics, that is $N(t) = N_1, N_2, N_3, N_4 \ldots\ldots$ On this basis, the integral operator (13) takes the form of the following sum:

$$\begin{aligned} T_z^N = k_T e^{-\alpha_1 L(t_k)} e^{-\alpha_1 t_k} [N_1 \int_0^{L_1} e^{\alpha_1 \gamma} d\gamma \int_0^{t_1} e^{\alpha_2 \eta} d\eta + N_2 \int_{L_1}^{L_2} e^{\alpha_1 \gamma} d\gamma \int_{t_1}^{t_2} e^{\alpha_2 \eta} d\eta + \Leftrightarrow \\ \Leftrightarrow + N_3 \int_{L_2}^{L_3} e^{\alpha_1 \gamma} d\gamma \int_{t_2}^{t_3} e^{\alpha_2 \eta} d\eta + N_4 \int_{L_3}^{L_4} e^{\alpha_1 \gamma} d\gamma \int_{t_3}^{t_4} e^{\alpha_2 \eta} d\eta + \ldots\ldots] \end{aligned} . \quad (14)$$

Assuming that $N_1 = 0$, we get the final solution for the case described by the expression (14):

$$\begin{aligned} T_z^N = \frac{k_T e^{-\alpha_1 L(t_k)} e^{-\alpha_1 t_k}}{\alpha_1 \alpha_2} [N_2 (e^{\alpha_1 L(t_2)} - e^{\alpha_1 L(t_1)})(e^{\alpha_2 t_2} - e^{\alpha_2 t_1}) + \Leftrightarrow \\ \Leftrightarrow + N_3 (e^{\alpha_1 L(t_3)} - e^{\alpha_1 L(t_2)})(e^{\alpha_2 t_3} - e^{\alpha_2 t_2}) + \ldots\ldots] \end{aligned} . \quad (15)$$

The expression (15) is very convenient for processing large arrays of discrete information on the cutting process. In fact, this is a sum of powers of irreversible transformations weighted relative to the final value.

Consider only one experiment from the series in which there was no wear on the back surface of the tool. In the following cases, the tool wear changed, and hence, the process dynamics (from both a mechanical and a thermodynamic point of view). Note that the results obtained in this experiment are generalized for all other cases, but the length of the paper does not allow them to be considered.

Fig. 2 shows the process response to the forming movements of the tool along *x* axis.

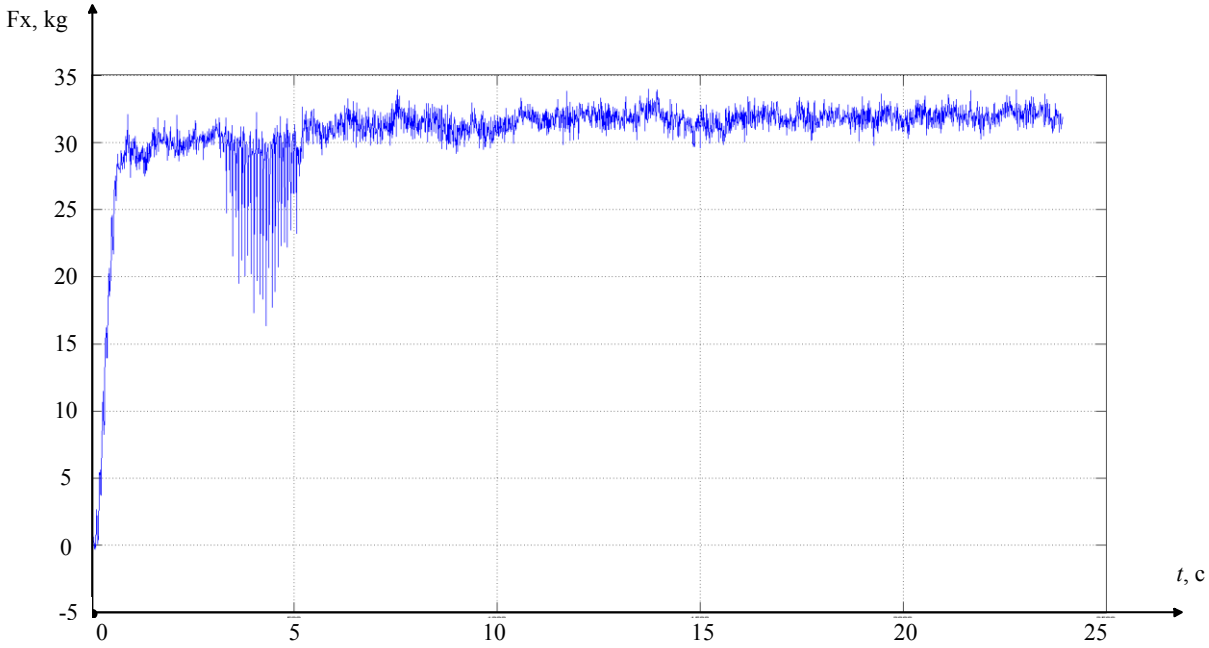

Fig. 2. Process response to forming movements of the tool along *x* axis in the first experiment step

As can be seen from Fig. 2, the reaction to the forming tool movements during turning is essentially non-stationary, but there is a certain attracting variety around which a perturbed toolpath is generated. Similar to that shown in Fig. 2, reactions to the shape-forming tool movements along the remaining axes were obtained in the experiment. In addition, information is available on tool accelerations relative to the workpiece. Integration of these data with consid-

eration of the known cutting elements allowed us to obtain the values of the machining speeds and the toolpath along the workpiece.

A specialized software tool for processing information arrays to describe the processes occurring during cutting (reaction forces, tool vibrations and power of irreversible transformations) was created in the Matlab package. The same tool has performed the temperature calculation in the tool-to-work contact zone according to (15). The model parameters are presented in Table 1.

Table 1

Parameters of the identified model

α_1	α_2	k_T c^{0}C/Нм	Θ_s ^{0}C
0.00099	0.00078	0.000159	24.8

Fig. 3 shows the simulation results of the expression (15) considering the parameters of Table 1, as well as the experimentally measured characteristic.

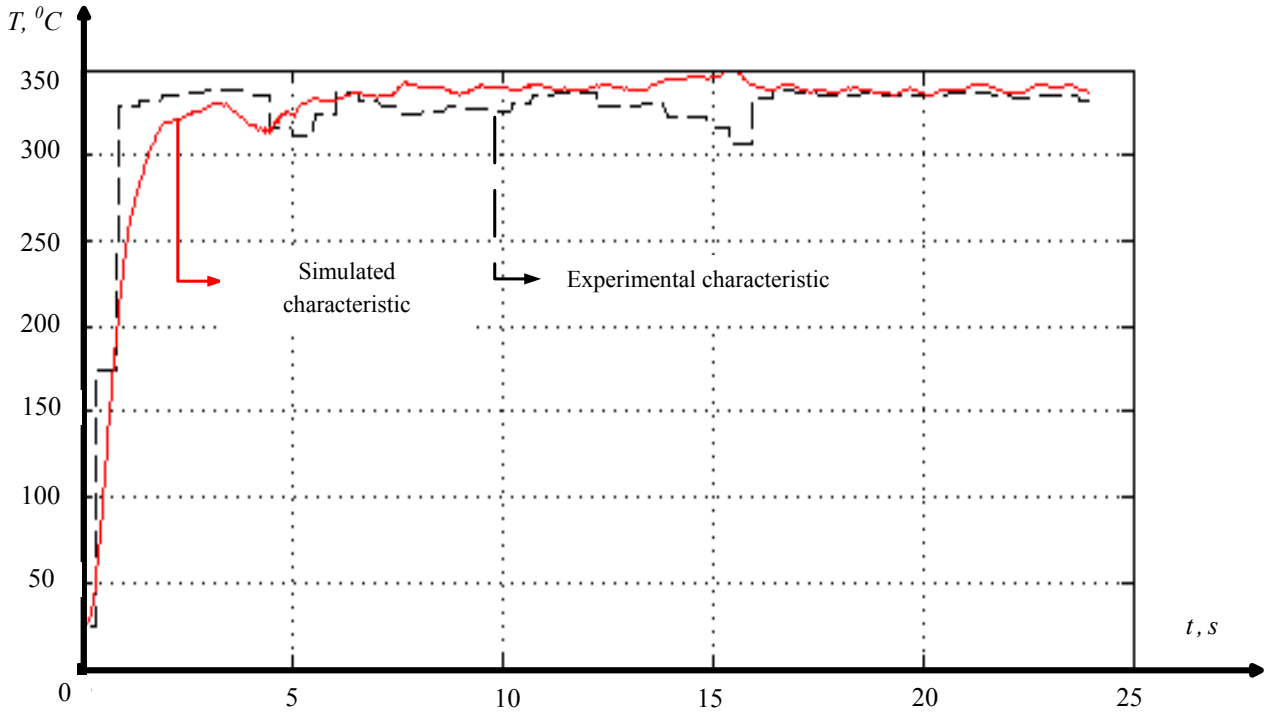

Fig. 3. Comparison of the results obtained in the experiment and calculated from the model

Comparison of Fig. 3 and Fig. 2 shows that the measured temperature value, when the tool enters the workpiece, increases from 25° C (ambient temperature) to 330–340 ° C. According to Fig. 3, first, a faster growth of the measured thermal EMF value is observed, and at the end of the process, the thermal EMF is stabilized.

This is explained by the fact that at STD.201-1 stand, it is not the temperature as such is measured in the contact zone, but the thermal EMF of the natural thermocouple formed at the tool-workpiece contact. At the beginning of the experiment, due to an overshot of the temperature gradients, the thermal EMF shows too large and fast temperature rise, and then, as the temperature gradients diverge, it is stabilized. This effect is widely known. For example, in [5], it is said: "The method of a natural thermocouple is unreliable since the cutting temperature is stabilized within 2–3 s".

In view of dynamics, the temperature variation (see Fig. 3) obtained as a result of simulating the expression (15) is close to the processes occurring during cutting (see Fig. 2). The graph shows the continuing growth of temperature due to the continuing increase in reaction forces (see Fig. 2). The graph also reflects all the dynamic features of the process including low-amplitude power jumps.

From this we can deduce the following: the proposed model describes the cutting temperature variation more accurately than the data of a dynamic thermocouple. Fig. 3 also shows that the simulated characteristic describing the change in the cutting zone temperature, in general, coincides qualitatively with the experimental dependence. The experimental and simulated characteristics coincide most fully after stabilization of the cutting process, within 15-24 seconds.

Discussion and Conclusions. The study results provide an answer to the following question: how to make the description of the hereditary nature of the heat transfer and accumulation during metal turning be adequate to the experimental data. For this purpose, it is required to simulate the temperature in the tool-to-work contact zone on the basis of the proposed modified Volterra operator.

In science terms, the proposed basic mathematical model and the results of its identification on the basis of the experiment on real metal processing are of the main interest. Here, there is a high degree of coincidence of the simulated values of thermal energy in the tool-to-work contact zone in the period of steady-state processing.

References

1. Reznikov, A.N., Reznikov, L.A. Teplovye protsessy v tekhnologicheskikh sistemakh. [Thermal processes in technological systems.] Moscow: Mashinostroenie, 1990, pp. 187–190 (in Russian).
2. Loladze, T.N. Prochnost' i iznosostoykost' rezhushchego instrumenta. [Durability and wear resistance of the cutting tool.]. Moscow: Mashinostroenie, 1982, 320 p. (in Russian).
3. Makarov, A.D. Optimizatsiya protsessov rezaniya. [Optimization of cutting processes.] Moscow: Mashinostroenie, 1976, 178 p. (in Russian).
4. Wolf, A.M. Rezanie metallov. [Metal cutting.] Leningrad: Mashinostroenie, 1973, 496 p. (in Russian).
5. Ryzhkin, A.A., Shuchev, K.G., Klimov, M.M. Obrabotka materialov rezaniem. [Cutting materials.] Rostov-on-Don: Feniks, 2008, 411 p. (in Russian).
6. Zakovorotny, V.L., Vinokurova, I.A. Vliyanie proizvodstva tepla na dinamiku protsessa rezaniya. [Effect of heat generation on dynamics of cutting process.] Vestnik of DSTU, 2017, vol. 17, no. 3 (90), pp. 14–26 (in Russian).
7. Volterra, V. Teoriya funktsionalov, integral'nykh i integro-differentsial'nykh uravneniy. [Theory of Functionals and of Integral and Integro-differential Equations.] Moscow: Nauka, 1982, 304 p. (in Russian).
8. Rabotnov, Yu.N. Elementy nasledstvennoy mekhaniki tverdykh tel. [Elements of hereditary mechanics of solids.] Moscow: Nauka, 1977, 284 p. (in Russian).
9. Smirnov, V.I. Kurs vysshey matematiki. T. 2. [The course of higher mathematics. Vol. 2.] Moscow: Nauka, 1974, 479 p. (in Russian).
10. Zakovorotny, V.L., Lapshin, V.P., Babenko, T.S. Modelirovanie iznosa po rabote i moshchnosti neobratimykh preobrazovaniy energii. [Simulation of work wear and power of irreversible energy transformations.] STIN, 2018, no. 3,pp. 9–10 (in Russian).
11. Yakubov, F.Ya., Kim, V.A., Timofeev, S.M. K termodinamike uprochneniya i iznashivaniya rezhushchego instrumenta. [To thermodynamics of hardening and wear of cutting tools.] Rezanie i instrument v tekhnologicheskikh sistemakh. [Cutting and tooling in technological systems.] 1996, iss. 50, pp. 211–216 (in Russian).
12. Yakubov, F.Ya. Sinergetika i protsessy samoorganizatsii pri trenii i iznashivanii. [Synergetics and self-organization processes in friction and wear.] Sovremennye tekhnologii v mashinostroenii: sb. nauch. tr. [Modern technologies in mechanical engineering: coll. of sci. papers.] 2010, no. 5, pp. 122–133 (in Russian).
13. Zakovorotny, V.L., Lapshin, V.P., Babenko, T.S. Assessing the Regenerative Effect Impact on the Dynamics of De-formation Movements of the Tool during Turning. Procedia Engineering, 2017, vol. 206, pp. 68–73.
14. Lapshin, V.P., Turkin, I.A. Dynamic influence of the spindle servo drive on the drilling of deep narrow holes. Russian Engineering Research, 2015, no. 35 (10), pp. 795–797.
15. Yildiz, A.R. A comparative study of population-based optimization algorithms for turning operations. Information Sciences, 2012, vol. 210, no. 1, pp. 81–88.
16. Faga, M.G., Mattioda, R., Settineri, L. Microstructural and mechanical characteristics of recycled hard metals for cutting tools. CIRP Annals-Manufacturing Technology, 2010, vol. 59, no. 1, pp. 133–136.
17. Hu, J., Chou, Y.K. Characterizations of cutting tool flank wear-land contact. Wear, 2007, vol. 263, no. 7, pp. 1454–1458.
18. Igolkin, A.A., Musaakhunova, L.F., Shabanov, K.Y. Method development of the vibroacoustic characteristics calculation of the gas distribution stations elements. Procedia Engineering, 2015, vol. 106, pp. 309–315.
19. Lapshin, V.P., Turkin, I.A. Vliyanie svoystv servoprivoda shpindelya na dinamiku sverleniya glubokikh otverstiy malogo diametra. [Effect of spindle servo drive properties on drilling dynamics of deep pinholes.] Vestnik of DSTU, 2013, no. 5/6 (74), pp. 125–130 (in Russian).
20. Zakovorotny, V.L., Turkin, I.A., Lapshin, V.P. Vliyanie parametrov servodvigateley na dinamicheskie svoystva sistemy sverleniya glubokikh otverstiy spiral'nymi sverlami. [Servomotor parameter effect on dynamic properties of twist drilling deephole machining system.] Vestnik of DSTU, 2014, vol. 14, no. 2 (77), pp. 56–65 (in Russian).

21. Lapshin, V.P., Turkin, I.A. Modelirovanie dinamiki formoobrazuyushchikh dvizheniy pri sverlenii glubokikh otverstiy malogo diametra. [Modeling of the dynamics of form-building movements in drilling deep openings of small diameter.] Bulletin of Adyghea State University, 2012, no. 4 (110), pp. 226–233 (Mathematical - Natural and Technical Sciences) (in Russian).

22. Lapshin, V.P., Babenko, T.S., Sanygin, I.A. Effektivnost' primeneniya vysokotochnogo izmeritel'nogo oborudovaniya dlya otsenki kachestva vypuskaemoy produktsii. [Effectiveness of high-precision measuring equipment for assessing product quality.] Innovatsii i inzhiniring v formirovanii investitsionnoy privlekatel'nosti regiona: sb. tr. [Innovation and engineering in shaping the region's investment attractiveness: coll. papers.] Rostov-on-Don: DSTU Publ. Centre, 2017, pp. 425–431 (in Russian).

Submitted 22.01.2019
Scheduled in the issue 12.04.2019

Authors:

Lapshin, Victor P.,
associate professor of the Production Automation Department, Don State Technical University (1, Gagarin sq., Rostov-on-Don, 344000, RF), Cand.Sci. (Eng.), associate professor,
ORCID: https://orcid.org/0000-0002-5114-0316
lapshin1917@yandex.ru

Bordatchev, Evgueni V.,
professor of the National Research Council Canada (1200 Montreal Road, Ottawa ON, Canada), Ph.D.,Dr.Eng.Sc., professor,
ORCID: https://orcid.org/0000-0003-2347-6338
Evgueni.Bordatchev@nrc-cnrc.gc.ca

МАШИНОСТРОЕНИЕ И МАШИНОВЕДЕНИЕ
MACHINE BUILDING AND MACHINE SCIENCE

UDC 621.9.648.4 https://doi.org/10.23947/1992-5980-2019-19-2-138-142

Effect of electrospark doping on mechanical properties of Al-Si-Cu alloys*

N. E. Fomin[1], I. Kh. Khasan[2], V. M. Kyashkin[3]**
[1, 2, 3] Ogarev Mordovia State University, Saransk, Russian Federation

Влияние электроискрового легирования на механические свойства Al-Si-Cu сплавов***

Н. Е. Фомин[1], И. Х. Хасан[2], В. М. Кяшкин[3]**
[1, 2, 3] ФГБОУ ВО «Национальный исследовательский государственный университет им. Н. П. Огарева», Саранск, Российская Федерация

Introduction. Microhardness and wear resistance of the aluminum alloy (AK5M7) after its surface treatment through electrospark doping (ESD) using A (Cu) and P (Cu+P) electrodes with different applied energy is considered. The work objective is to study the relationship of the physicomechanical and strength properties of the surface of AK5M7 alloy obtained after ESD with copper and copper-phosphorus electrodes.

Materials and Methods. X-ray diffraction and X-ray fluorescence analysis methods were used to determine the phase composition, coherent-scattering regions (CSR), and the surface microstrain.

Research Results. It is established that with increasing energy, the values of microhardness and wear resistance increase when using both electrodes. The sample was modified by P electrode with the energy of 0.79 J. In this case, the maximum value of microhardness increased 5.3 times, wear resistance - 1.6 times. It is found that with ESD, new intermetallic phases of Al2Cu and Cu3P are formed on the surface of the alloy under study. If the value of the energy used is maximum (0.79 J), the concentration of the Al2Cu phase increases 5 and 9 times with A and P electrodes, respectively, and the concentration of the Cu3P phase increases more than 4 times when using P electrode. The experimental data obtained suggest size reduction of the CSR and an increase in the microstrain values for all the Al, Al2Cu, and Cu3P phases on the surface.

Discussion and Conclusions. An increase in energy with the ESD involves an increase in the defective factors and a change in the phase composition of the newly obtained surfaces. This may explain the increase in wear resistance of the surface.

Keywords: electrospark doping (ESD), coherent-scattering region (CSR), microstrain, aluminum alloys, wear rate.

Введение. Статья посвящена исследованию микротвердости и износостойкости алюминиевого сплава (АК5М7) после обработки его поверхности электроискровым легированием (ЭИЛ) электродами **А** (Cu) и **Р** (Cu + P) с разной приложенной энергией.

Цель работы — исследование взаимосвязи физико-механических и прочностных свойств поверхности сплава АК5М7, полученной после ЭИЛ медным и медно-фосфорным электродами.

Материалы и методы. Использованы методы рентгенодифракционного и рентгенофлуоресцентного анализа для определения фазового состава, областей когерентного рассеяния (ОКР) и микродеформации поверхности.

Результаты исследования. Установлено, что при использовании обоих видов электродов с увеличением энергии возрастают микротвердость и износостойкость. Образец был модифицирован электродом Р с энергией 0,79 Дж. В этом случае максимальное значение микротвердости увеличилось в 5,3 раза, износостойкости — в 1,6 раза. Установлено, что при ЭИЛ на поверхности исследуемого сплава образуются новые интерметаллические фазы Al_2Cu и Cu_3P. Если значение используемой энергии максимально (0,79 Дж), то концентрация фазы Al_2Cu увеличивается в 5 и 9 раз с электродами А и Р соответственно, а концентрация фазы Cu_3P увеличивается более чем в 4 раза при использовании электрода Р. Полученные экспериментальные данные свидетельствуют об уменьшении размеров ОКР и увеличении значений микродеформации для всех имеющихся на поверхности фаз Al, Al_2Cu и Cu_3P.

Обсуждение и заключения. Увеличение энергии при ЭИЛ приводит к повышению дефектности и изменению фазового состава вновь полученных поверхностей. Этим можно объяснить повышение износостойкости данной поверхности.

Ключевые слова: электроискровое легирование (ЭИЛ), область когерентного рассеяния (ОКР), микродеформация, алюминиевые сплавы, интенсивность изнашивания.

* The research is done within the frame of the independent R&D.
** E-mail: vice-rector@adm.mrsu.ru, srorismael@gmail.com, Kyachkin@mail.ru
*** Работа выполнена в рамках инициативной НИР.

For citation: N.E. Fomin, et al. Effect of electrospark doping on mechanical properties of Al-Si-Cu alloys. Vestnik of DSTU, 2019, vol. 19, no. 2, pp. 138−142. https://doi.org/10.23947/1992-5980-2019-19-2-138-142

Образец для цитирования: Фомин, Н. Е. Влияние электроискрового легирования на механические свойств Al-Si-Cu сплавов / Н. Е. Фомин, И. Х. Хасан, В. М. Кяшкин // Вестник Дон. гос. техн. ун-та. — 2019. — Т. 19, № 2. — С. 138−142. https://doi.org/10.23947/1992-5980-2019-19-2-138-142

Introduction. Various coatings and surface modification methods are used to increase the wear resistance of workpieces. One of them is electrospark doping (ESD) of conductive materials (authors: B.R. Lazarenko and N.I. Lazarenko [1–4]).

Al-Si-Cu alloys are widely used in the automobile industry. They are well molded, have all the necessary mechanical properties, and are characterized by a low coefficient of thermal expansion and a high ratio of strength and weight. However, the hardness and wear resistance of aluminum alloys are relatively low. This is the reason for the urgency of the problem of improving these properties through surface hardening [5–10]. The point is that it is required to create hardened layers with improved mechanical-and-physical properties. In the present paper, the results of ESD by various electrodes at different energies to harden the surface of AK5M7 alloy are shown.

Materials and Methods. Samples of AK5M7aluminum alloy with dimensions of 15×15×4 mm were made for research. Their surfaces were processed through the ESD method with copper and copper-phosphorus electrodes. The elemental composition of the alloy and electrodes was determined through X-ray fluorescence analysis on an ARL Perform'X 4200 instrument. The results are shown in Table 1.

Table 1

Elemental composition of alloy and electrodes

	Al, %	Cu, %	Si, %	P, %
AK5M7alloy	88	7	5	
P-electrode		92.9		7.1
A-electrode	0.1	99.9		

Electrospark doping was carried out on ALIER-31 installation (SCINTI, Moldova), which allows performing the ESD in a wide energy range.

X-ray phase analysis was performed to determine the phase composition of coatings applied to aluminum alloy through the ESD technique.

The PANalytical EMPYREAN X-ray diffractometer with CuKα radiation equipped with a nickel filter with an automatic primary beam divergence slit was used for the survey. The radiograph was decoded using the HighScorePlus program. We studied:

- quantitative content of phases detected on the surface;
- the average dimension of coherent-scattering regions (CSR);
- values of microdeformations after ESD of samples.

The microhardness of the modified layer was measured on the surface obtained after ESD. The research complex based on HVS-1000 microhardness meter and a digital video camera were used. The measurements were carried out according to GOST 9450–76 with the Vickers pyramid indenter (the load was P = 25 g). At least ten measurements were performed for each sample. The base alloy and the surfaces of its samples after the ESD treatment were subjected to tribological tests (a lubricant was preliminarily applied on the surfaces of the samples).

Research Results. The results obtained are presented in Table 2 and in Fig. 1–4.

Table 2

Phase concentration of base alloy and surfaces after ESD depending on energy

Energy, J	Phase concentration									
	AK5M7alloy			A-electrode			P-electrode			
	Al	Al_2Cu	Si	Al	Al_2Cu	Si	Al	Al_2Cu	Si	Cu_3P
0	92	2	4							
0.07				97	2	1	94	3	2	1
0.2				96	3	1	70	22	5	3
0.39				94	5	1	65	25	5	5
0.79				89	10	1	59	28	5	8

Table 2 shows phase concentrations found on the surfaces of the base alloy and samples after the ESD at various energies.

The base alloy has three phases: Al, Al_2Cu and Si. With increasing the ESD energy, an increase in the Al_2Cu concentration is observed when using both electrodes, and a decrease in the Al phase, while the Si phase remains constant for the A- electrode at all energies. In this case, Si concentration increases 2.5 times with the energy rise for the P-electrode. In the samples treated with the P-electrode, the Cu_3P phase appears. Its concentration increases 8 times with the pulse energy rise to 0.79 J.

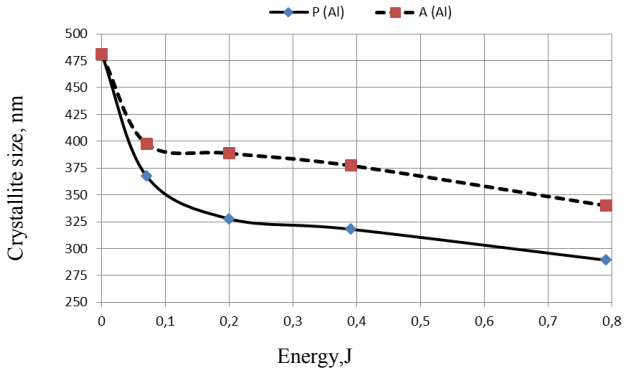

Fig. 1. Dependence of CSR Al-phase size on energy for A and P electrodes

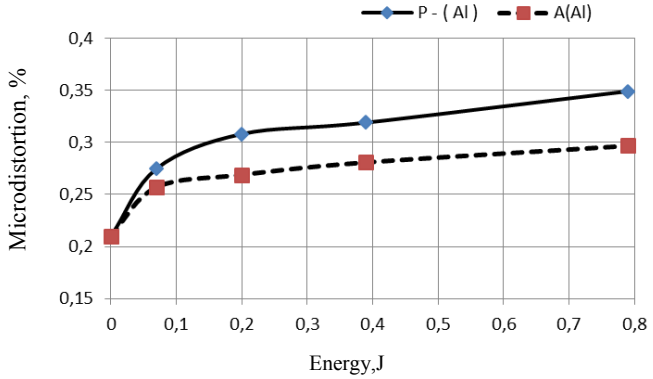

Fig. 2. Dependence of Al-phase microstrain value on energy for A and P electrodes

Fig. 1 and 2 show that when using both electrodes, the CSR decreases with the ESD energy rise, and the microstrain grows. The coherent-scattering regions are practically faultless surface areas. Therefore, an increase in CSR indicates improvement in the microstructure of the modified layer, and reduction of its defect level. However, it is known that a change in the structure imperfection of metallic materials causes a change in their mechanical-and-physical properties [11, 12]. The microstrain value indicates the degree of the crystal lattice distortion, and thus, the structure imperfection ratio can be defined by its value [13, 14]. Similar CSR dependences and microstrain were obtained for the Al_2Cu and Cu_3P phases after the ESD of AK5M7 alloy surface with A and P electrodes. It is found that the patterns of changing the CSR and microstrain are the same as for the Al-based phase. Therefore, the data in Fig. 1, 2 suggest that with increasing energy, the structure of the resulting surface is distorted more heavily.

Fig. 3 shows the measurement results of the surface microhardness after the ESD by the copper and copper-phosphorus electrodes.

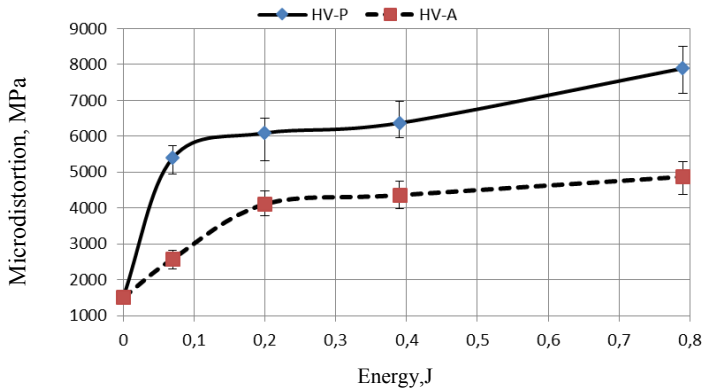

Fig. 3.Ddependence of microhardness on energy for A and P electrodes

It is seen that the microhardness increases with the energy rise, and for A-electrode, at the peak value of energy, nearly 3-fold increase is observed, for P-electrode — 5-fold.

It is known that during the ESD, melting of materials of the anode and the sample surface occurs, and then rapid cooling (quenching). As a result, new phases (in our case, Cu_3P), dislocations, point defects, high degree of surface stress, fine-grained structure, etc., can form on the surface. Accordingly, it can be assumed that with increasing energy, the microhardness grows due to the above-mentioned distortions arisen during the ESD process (see Fig. 3).

Fig. 4 shows the measurement results of the wear rate of AK5M7 alloy and the sample surfaces after the ESD with copper and copper-phosphorus electrodes at the energy of 0.79 J.

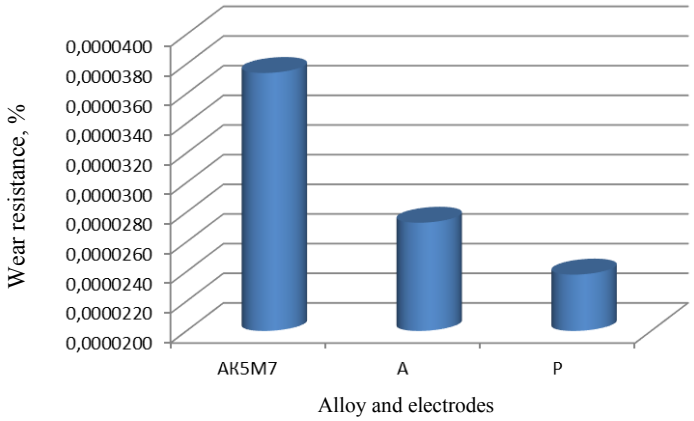

Fig. 4. Wear resistance rate of base AK5M7 alloy and its surface after coating at energy of 0.79 J

Fig. 4 shows that the sample surfaces treated by copper-phosphorus and copper electrodes are worn out much less than the surface of AK5M7alloy.

Discussion and Conclusions. The results obtained validate the efficiency of the ESD of AK5M7 alloy surface by various electrodes and with different energies. Surfaces obtained by this method wear out less. When using a copper electrode, the wear is reduced by 1.37 times, when using a copper-phosphorus electrode — by 1.57 times.

Upon reaching the minimum value of wear after the ESD, the surfaces have the maximum values of microhardness and microstrain, as well as the lowest CSR values. At the same time, there is a significant increase in the concentration of intermetallic phases formed after the ESD: Al_2Cu — from 5 to 9 times with copper and copper-phosphorus electrodes, respectively; Cu_3P — 8 times with a copper-phosphorus electrode. The reason for the increase in wear resistance of surfaces after the ESD can be various distortions and defects formed after melting, as well as the formation of new intermetallic phases.

References

1. Verkhoturov, A.D., et al. Vliyanie prirody elektrodnykh materialov na eroziyu legirovannogo sloya. Kriterii otsenki effektivnosti elektroiskrovogo legirovaniya. [Effect of the nature of electrode materials on erosion and properties of doped layers. The criteria for evaluating the effectiveness of electrospark alloying.] Mordovian University Bulletin, 2018, vol. 28, no. 3, pp. 302-320 (in Russian).

2. Yurchenko, E.V., et al. Izmenenie sostava i svoystv elektroda-instrumenta v usloviyakh elektroiskrovogo legirovaniya splavom Al-Sn. [Changes in composition and properties of tool electrode during electrospark alloying with Al-Sn alloy.] Surface Engineering and Applied Electrochemistry, 2016, no. 52 (2), pp. 157-161 (in Russian).

3. Kozyr, A.V., et al. Issledovanie zharostoykikh svoystv pokrytiy posle elektroiskrovogo legirovaniya stali 45 khromonikelevymi splavami. [Research on heat resistance properties of coatings deposited by electrospark alloying on steel C45 by nickel-chromium alloys.] Letters on Materials, 2018, no. 8 (2), pp. 140–145. DOI: 10.22226/2410-3535-2018-2-140-145 (in Russian).

4. Nemri, Y., et al. Effect of Mg and Zn Contents on the Microstructures and Mechanical Properties of Al–Si–Cu–Mg Alloys. International Journal of Metalcasting, 2017, no. 12 (1), pp. 20–27.

5. Liu, L., et al. Surface Modification of Aluminum Alloys Prepared by Plasma-Based-Ion-Implantation Technique. Solid State Phenomena, 2006, no. 118, pp. 269–274.

6. Medrano-Prieto, H.M., et al. Effect of Nickel addition and solution treatment time on microstructure and hardness of Al-Si-Cu aged alloys. Materials Characterization, 2016, vol. 120, October, pp. 168–174.

7. Giovanni, M.T., et al. Effect of copper additions and heat treatment optimization of Al-7% Si Aluminum Alloy. La Metallurgia Italiana, 2016, no. 11, pp. 43–47.

8. Bogdanoff, T., Dahle, A.K., Seifeddine, S. Effect of Co and Ni addition on the microstructure and mechanical properties at room and elevated temperature of an Al-7% Si alloy. International Journal of Metalcasting, 2018, vol. 12, iss. 3, pp. 434–440. DOI 10.1007/s40962-017-0178-z.

9. GuTao, et al. Microstructure evolution and mechanical properties of laser additive manufacturing of high strength Al-Cu-Mg alloy. Optics and laser technology, 2019, no. 112, pp. 140–150.

10. Oleinik, A., Chuikova, E., Nesterenko, A. Vliyanie kristallizatsii pod davleniem i termoobrabotki na tribotekhnicheskie pokazateli i mikrotverdost' splava AL-25. [The influence of the crystallization under pressure and heat treatment on the tribotechnical indices and microhardness of the Al-25 alloy.] Bulletin of KhSAHTU, 2010, iss. 51, pp. 73–77 (in Russian).

11. Sharenkova, N.V., Kaminskii, V.V., Petrov, S.N. Razmery oblastey kogerentnogo rasseyaniya rentgenovskogo izlucheniya v tonkikh plenkakh SmS i ikh vizualizatsiya. [Sizes of X-ray radiation coherent domains in thin SmS films and their visualization.] Technical Physics, 2011, vol. 81, iss. 9, pp. 144–146 (in Russian).

12. Solntsev, Yu.P., Pryakhin, E.I. Materialovedenie. [Material Sciences.] St. Petersburg: Khimzdat, 2007, 781 p. (in Russian).

13. Melnikov, E.V., Astafurova, E.U., Maier, G.G. Vliyanie temperatury deformatsii na parametry struktury, fazovyy sostav i mikrotverdost' monokristallov stali Fe-28Mn-2.7Al-1.3C, podvergnutykh krucheniyu pod vysokim davleniem. [Effect of deformation temperature on the structural parameters, phase composition and microhardness of Fe-28Mn-2.7Al-1.3C steel single crystals processed by high-pressure torsion.] Letters on Materials, 2018, no. 8 (2), pp. 178–183. DOI: 10.22226/2410-3535-2018-2-178-183 (in Russian).

14. Khasan, I.Kh., Fomin, N.E. Issledovanie fiziko-mekhanicheskikh svoystv alyuminievogo splava posle elektroiskrovoy obrabotki. [Study of physical and mechanical properties of aluminum alloy after electric-spark alloying.] Strengthening Technologies and Coatings, 2019, vol. 15, no. 3, pp. 139–142 (in Russian).

Submitted 16.04.2019
Scheduled in the issue 07.05.2019

Authors:

Fomin, Nikolay E.,
Head of the Solid-State Physics Department, Ogarev Mordovia State University
(68a, Bolshevik St., Saransk, 430005, RF), Cand.Sci. (Phys.-Math.), professor,
ORCID: https://orcid.org/0000-0002-7738-1839
vice-rector@adm.mrsu.ru

Khasan, Ismail Kh.,
postraduate of the Solid-State Physics Department, Ogarev Mordovia State University
(68a, Bolshevik St., Saransk, 430005, RF),
ORCID: https://orcid.org/0000-0002-4560-1016
srorismael@gmail.com

Kyashkin, Vladimir M.,
associate professor of the Solid-State Physics Department, Ogarev Mordovia State University
(68a, Bolshevik St., Saransk, 430005, RF),
ORCID: https://orcid.org/0000-0003-0966-1190
Kyachkin@mail.ru

МАШИНОСТРОЕНИЕ И МАШИНОВЕДЕНИЕ
MACHINE BUILDING AND MACHINE SCIENCE

UDC 621.3 (0.75.8) https://doi.org/10.23947/1992-5980-2019-19-2-143-150

Study on frequency dependence of polarized piezoceramics constants in equivalent circuits at weak electric fields (part III) *

V. V. Madorsky[1], I. E. Rogov[2], A. K. Kruglov[3]**
[1,2]Don State Technical University, Rostov-on-Don, Russian Federation
[3]Southern Federal University, Rostov-on-Don, Russian Federation

Исследование зависимости от частоты констант поляризованной пьезокерамики в схемах замещения при слабых электрических полях (часть III) ***

В. В. Мадорский[1], И. Е. Рогов[2], А. К. Круглов[3]**
[1,2]Донской государственный технический университет, г. Ростов-на-Дону, Российская Федерация
[3]Южный федеральный университет, г. Ростов-на-Дону, Российская Федерация

Introduction. It is acknowledged that electroelastic modules do not depend on the amplitude and frequency of oscillations. This approach is reflected in the Russian and foreign standards for determining the complete set of electro-elastic piezoceramics modules. For example, to determine d_{31} piezo-module of a disc-shaped sample, it is required to take measurements in three frequency domains: in the first and second resonances, in the antiresonance region, and at frequencies much below 1 kHz. Accordingly, it is assumed that when determining d_{31}, the modules of the ceramic under study in the frequency range from 1 KHz to the second resonance are independent of frequency. The work objective is to study the frequency dependence of electro-elastic ceramic modules. In this case, a disc-shaped sample from LZT (lead zirconate titanate) is used.

Materials and Methods. Techniques of setting and solving problems of the stationary electroelasticity and sections of the electrical engineering basics are applied. To implement the finite element method, the perturbation technique and the ANSYS application package are used. The experimental results are processed in the MATLAB environment.

Research Results. For the LZT piezoelectric ceramics, the frequency dependences of various modules (piezoelectric d_{31}, dielectric ε_{33}^T and elastic modules of compliance - s_{11}, s_{12}, s_{13}) were investigated. Radial oscillations of a disc-shaped sample with electrodes on the ends were considered. The sample thickness was 1 mm, the diameter was 40 mm, and the oscillation range was up to 700 KHz. First, the frequency dependence was studied for the elastic ceramic modules from the determination of ten resonance frequencies. Then, the frequency dependence of $d_{31} and\ \varepsilon_{33}^T$ modules was determined from the measured values of the sample conductivity. For this purpose, we used the expression for the electrical conductivity obtained from the solution of the radial oscillations of the disc considering its thickness.

Введение. Принято считать, что электроупругие модули не зависят от амплитуды и частоты колебаний. Это подход отражен в российских и зарубежных стандартах для определения полного набора электроупругих модулей пьезокерамики. Например, для определения пьезомодуля d_{31} образца в форме диска необходимо провести измерения в трех частотных областях: в области первого и второго резонансов, в области антирезонанса и на частотах много ниже 1 кГц. В связи с этим предполагается, что при определении d_{31} модули исследуемой керамики в диапазоне частот от 1 КГц до второго резонанса не зависят от частоты.

Целью данной работы является исследование зависимости от частоты электроупругих модулей керамики. При этом используется образец в форме диска из ЦТС (цирконата-титаната свинца).

*Материалы и методы***.** Использованы методы постановки и решения задач стационарной электроупругости и разделы теоретических основ электротехники. Для реализации метода конечных элементов применены метод возмущений и пакет прикладных программ ANSYS. Результаты экспериментов обработаны в среде MATLAB.

Результаты исследования. Для пьезокерамики ЦТС исследованы зависимости от частоты различных модулей (пьезоэлектрических d_{31}, диэлектрических ε_{33}^T и упругих модулей гибкости s_{11}, s_{12}, s_{13}). Рассмотрены радиальные колебания образца в форме диска с электродами на торцах. Толщина образца — 1 мм, диаметр — 40 мм, диапазон колебаний — до 700 КГц. Сначала исследовалась частотная зависимость для упругих модулей керамики из определения десяти резонансных частот. Затем по измеренным значениям проводимости образца была определена зависимость от частоты модулей d_{31} и ε_{33}^T. С этой целью использовалось полученное в работе выражение для электрической проводимости из решения радиальных колебаний диска с учетом его толщины.

* The research is done within the frame of the independent R&D.
** E-mail: epohrbats@gmail.com, igorro@rambler.ru, kruglov@sfedu.ru
*** Работа выполнена в рамках инициативной НИР.

Discussion and Conclusions. A technique is developed for determining the frequency dependence of LZT piezoelectric ceramic modules. The disc-shaped sample was studied in 15-650 KHz frequency range. It is shown that in the range up to 650 KHz, s_{11}, s_{12}, s_{13} elastic modules with E superscript (it is omitted) or measured at dc field are practically independent of frequency. In the specified range, ε_{33}^{T}, d31, kp constants have an insignificant frequency dependence for the considered radial oscillations.

Keywords: piezoelectric ceramics, electroelastic modules, equivalent circuit, frequency dependence, disc, finite-element technique, perturbation method.

For citation: V.V. Madorsky, et al. Study on frequency dependence of polarized piezoceramics constants in equivalent circuit at weak electric fields s (part III). Vestnik of DSTU, 2019, vol. 19, no. 2, pp. 143−150. https://doi.org/10.23947/1992-5980-2019-19-2-143-150

Обсуждение и заключения. Разработана методика для определения зависимости от частоты модулей пьезоэлектрической керамики ЦТС. Образец в форме диска исследовался при диапазоне частот 15–650 КГц. Показано, что в диапазоне до 650 КГц упругие модули s_{11}, s_{12}, s_{13} с верхним индексом E (он опущен) или измеренные при постоянном электрическом поле практически не зависят от частоты. В указанном диапазоне константы ε_{33}^{T}, d_{31}, k_p для рассматриваемых радиальных колебаний имеют незначительную частотную зависимость.

Ключевые слова: пьезоэлектрическая керамика, электроупругие модули, схема замещения, зависимость от частоты, диск, метод конечных элементов, ANSYS, метод возмущений.

Образец для цитирования: Мадорский, В. В. Исслед ование зависимости от частоты констант поляризованной пьезокерамики в схемах замещения при слабых электрических полях (часть III) / В. В. Мадорский, И. Е. Рогов, А. К. Круглов // Вестник Дон. гос. техн. ун-та. — 2019. — Т. 19, № 2. — С.143−150. https://doi.org/10.23947/1992-5980-2019-19-2-143-150

Introduction. A significant number of papers study and develop mathematical methods for solving problems of piezoelectric body oscillations. Being a component of the piezoelectric devices, piezoelectric elements serve to excite and register oscillations caused by external effects. The selection of piezoelectric material for measuring transducers and the analysis of their characteristics requires a large amount of information on the parameters of materials. Such information includes:

- a complete set of electroelastic modules [1],
- losses,
- analogous electrical circuits, or equivalent circuits of piezoelectric elements [2].

The reactive dynamic parameters (*L, C*) of the equivalent circuits are determined by elastic dielectric and piezoelectric modules, as well as by the density of piezoceramics [3]. It is considered that the electroelastic modules - the equivalent circuit parameters are constant; they do not depend on the amplitude (weak electric fields) and on the oscillation frequency. All this is reflected in the Russian [4] and foreign [5, 6] standards for determining a complete set of electroelastic piezoelectric ceramics modules. For example, to determine d_{31} piezo-module of a disk-shaped sample, it is necessary to carry out measurements in three frequency domains: in the first and second resonances, in the antiresonance region, and at frequencies much below 1 kHz. Accordingly, it is assumed that when determining d_{31}, the modules of the ceramic under study in the frequency range from 1 KHz to the second resonance are independent of frequency.

The work objective is to study the frequency dependence of electro-elastic ceramic modules. In this case, a disc-shaped sample from LZT (lead zirconate titanate) is used, as precisely this type of ceramics is most well known. The ANSYS program [7] is used to verify the correctness of the presented methodology.

Materials and Methods. Consider a piezoelectric disk with the thickness of 2h and the radius a. We introduce a cylindrical coordinate system (r, Θ, z) where z axis coincides with the direction of the polarization axis. The coordinate plane $z = 0$ coincides with the midplane of the disk. Based on the known linear piezoelectric ratios, the equations of the continuum dynamics [1] and Maxwell equations [8], the system of equations for the axisymmetric oscillations of the piezoelectric disk can be written as follows:

$$\partial_1 T_{rr} + \partial_3 T_{rz} + \frac{T_{rr} - T_{\theta\theta}}{r} + \rho\omega^2 U = 0,$$
$$\partial_1 T_{rz} + \partial_3 T_{zz} + \frac{T_{rz}}{r} + \rho\omega^2 W = 0;\ \ \partial_1 D_r + \partial_3 D_z + \frac{D_r}{r} = 0. \qquad (1)$$

Henceforward, the following notations and definitions are introduced: *U, W* are mechanical displacements along *r, z* coordinate axes, respectively; ω is circular frequency; ρ is density; T_{mn} are mechanical stresses; D_r, D_z are components of the electric induction vector; ∂_1 and ∂_3 are operators of derivatives with respect to *r* and *z*.

In case of axial polarization, the linear piezoelectric effect equations for weak electric fields in the cylindrical coordinates can be written as follows [1]:

$$\begin{gathered} T_{rr} = c_{11}\partial_1 U + c_{12}\frac{U}{r} + c_{13}\partial_3 W + e_{31}\partial_3 \varphi, \\ T_{\theta\theta} = c_{12}\partial_1 U + c_{11}\frac{U}{r} + c_{13}\partial_3 W + e_{31}\partial_3 \varphi, \\ T_{zz} = c_{13}\partial_1 U + c_{13}\frac{U}{r} + c_{33}\partial_3 W + e_{33}\partial_3 \varphi, \\ D_z = e_{31}(\partial_1 U + \frac{U}{r}) + e_{33}\partial_3 W - \varepsilon_{33}\partial_3 \varphi; D_r = e_{15}(\partial_3 U + \partial_1 W) - \varepsilon_{11}\partial_1 \varphi. \end{gathered} \quad (2)$$

The following notation is introduced in the relations (2) and further: c_{mn} are elastic constants in the matrix designation measured on samples with shorted electrodes or at the constant electric field E (E upper index of the ceramics constants is omitted here and further); e_{mn} are piezoelectric constants; ε_{mn} are clamped dielectric constants; φ is electric potential where $E = -\text{grad}\,\varphi$ [2, 8].

Assume that the boundary conditions are set at the electrode ends and on the lateral surfaces of the disk [1, 2]:

$$\text{at } z = \pm h \;\; T_{zz} = 0;\; T_{rz} = 0;\; \varphi = 2V, \quad (3)$$

$$\text{at } r = a \;\; T_{rz} = 0;\; T_{rr} = 0;\; D_r = 0. \quad (4)$$

In (3), $2V$ value is electric potential difference applied to the ends [2, 8]. Let us introduce dimensionless coordinates and quantities from the formulas:

$$\xi = \frac{r}{a};\; \zeta = \frac{z}{h};\; \varepsilon = \frac{h}{a};\; \Omega = \omega h\sqrt{\frac{\rho}{c_{44}}};\; \Omega_a = \omega a\sqrt{\frac{\rho}{c_{11}^p}};\; c_{11}^p = c_{11} - \frac{c_{13}^2}{c_{33}}.$$

The solution to the boundary value problem (1-3) consists of the sums of two solutions:

- homogeneous solution at zero boundary conditions at $z = \pm h$;
- particular solution that satisfies only nonzero conditions at the ends (3).

The constructed system of homogeneous solutions will enable to further satisfy the boundary conditions (4) on the lateral surface (as a rule, using variational methods).

It is not difficult to construct the particular solution $D_z^0 = const$ and $D_r^0 \equiv 0$, which satisfies automatically the third equation from the system (1) and the boundary conditions at the ends (3). According to the first two equations of the system (1), the mechanical and electrical components of the particular solution are equal:

$$\begin{gathered} T_{rr}^0 = T_{\theta\theta}^0 = A(e_{31} + \frac{\varepsilon_{33}c_{13}}{e_{33}})\chi\sin(\chi\zeta) + e_{31}K;\; U^0 = 0;\; T_{rz}^0 = 0; \\ \varphi^0 = Kh\zeta + Ah\sin(\chi\zeta);\; D_z^0 = -\varepsilon_{33}K;\; T_{zz}^0 = e_{33}K + e_{33}^p A\chi\cos(\chi\zeta); \\ A = -\frac{V}{h}\frac{e_{33}}{e_{33}^p(\chi\cos(\chi) - k_t^2\sin(\chi))};\; K = \frac{V}{h}\frac{1}{1 - k_t^2\frac{\tan(\chi)}{\chi}}. \end{gathered} \quad (5)$$

The following notation is introduced in (5):

$$\chi = \Omega\sqrt{\frac{c_{44}}{c_{33}^D}};\;\; e_{33}^p = e_{33} + \frac{c_{33}\varepsilon_{33}}{c_{33}^2};\; k_t^2 = 1 - \frac{c_{33}}{c_{33}^D}.$$

If the vector of external forces and the electric potential are zero on the end surfaces, then the construction of homogeneous solutions is associated with the definition of the dispersion equation roots [9]. For symmetric oscillations, the dispersion equation has the following form:

$$a_n M_n \tan^{-1}(\beta_n) = 0, (n = 1, 2, 3). \quad (6)$$

The following notation is introduced in (6):

$$a_n = \alpha^2 c_{13}k_{1n} + c_{33}k_{2n} + e_{33}k_{3n};\;\; b_n = k_{1n}\beta_n + k_{2n};$$

$$M_1 = b_2k_{33} - b_3k_{32};\; M_2 = b_3k_{31} - b_1k_{33};\; M_3 = b_1k_{32} - b_2k_{31}.$$

Here, k_{mn} are algebraic compliments to the elements of the third determinant row of the system for symmetric oscillations (1); β_n is binary cubic root from [9], α is non-dimensional wave number of oscillations along r axis.

To find the roots (α) at the given values of Ω, it is necessary to solve the dispersion equation (6) in combination with the binary cubic. A detailed analysis of the dispersion equation roots of symmetric lossless oscillations for the piezoelectric layer is given in [9], considering losses – in [10]. It is the sum of the particular and homogeneous solutions that will allow satisfying the boundary conditions both at the ends and on the lateral surfaces of the disk.

With an arbitrary ratio of disk sizes, the inverse problem of its forced oscillations (1–4) is very difficult to analyze and has a finite analytical solution only in some special cases (for example, oscillations of a thin disk or without considering its thickness when $\varepsilon \ll 1$). Therefore, when determining the modules of ceramics, it is more convenient to

solve the inverse boundary problem using approximate methods with allowance for thickness corrections for low-frequency radial oscillations of the disk. In this case, we can get an analytical solution in the form of finite formulas. In this paper, we seek the solution in the form of expansion with respect to ε small parameter:

$$\alpha^2 = \varepsilon^2\Omega_a^2 + \gamma\varepsilon^4\Omega_a^4 + \eta\varepsilon^6\Omega_a^6 \ldots \quad U = U_0 + \varepsilon^2\Omega_a^2 U_2 + \varepsilon^4\Omega_a^4 U_4 + \ldots \tag{7}$$

Here, $\boldsymbol{U_n}$ is vector function with $\boldsymbol{U}(U, W, \varphi)$ components; n is the order of the constructed approximate theory of symmetric disk oscillations considered in the paper; γ, η are unknown constants which depend on the modules of piezoelectric ceramics, they are determined from (1, 2) and satisfy the homogeneous (zero) boundary conditions (3).

Omit the cumbersome manipulations. We confine ourselves to the terms with ε^6 to determine α^2 wave number, the terms with ε^2 for $\boldsymbol{U}$ vector function in (7), and we give the final result of the considered boundary value problem with the boundary conditions (3) at the ends [11]:

$$\gamma = \frac{c_{13}^2}{3c_{33}^2}; \quad \nu = -\frac{s_{12}}{s_{11}}; \quad k_p^2 = \frac{2d_{31}^2}{\varepsilon_{33}^T(s_{11}+s_{12})}; \; t = \frac{c_{13}}{c_{33}} = \frac{-s_{13}}{s_{11}+s_{12}};$$

$$\eta = \gamma\left(\frac{2}{15}t + \frac{2c_{11}^p}{5c_{33}} + \gamma\right) + piezo;$$

$$piezo = \frac{t^2}{45c_{11}^p\varepsilon_{33}^T(1-k_p^2)}\left[\frac{d_{31}}{s_{11}+s_{12}} - c_{11}^p(2td_{31} + d_{33})\right]^2.$$

Here, S_{mn} are flexibility modules with E constant; d_{31} is piezo-module; k_p is planar coupling coefficient; ν is planar Poisson ratio; ε_{33}^T is free dielectric constant of the disk.

Next, we introduce the following definitions and notation: $\alpha_0^2 = \varepsilon^2\Omega_a^2$ is approximate zero-order wave number; $\alpha_2^2 = \varepsilon^2\Omega_a^2 + \gamma\varepsilon^4\Omega_a^4$ is approximate wave quadratic number; $\alpha_4^2 = \varepsilon^2{\Omega_a}^2 + \gamma\varepsilon^4{\Omega_a}^4 + \eta\varepsilon^6{\Omega_a}^6$ is approximate quartic wave number; C is disk capacity.

Table 1 presents the results of the exact solution of the wave number (α) of the PZT4 ceramics depending on the frequency from the dispersion equation (6) and an approximate calculation from (7) at ε = 0.033 for various approximations of α_m.

Table 1

An example of calculating wave number (α) at various frequencies for the piezoceramic disk under study

f, kHz	Ω	α from (6)	α_0	α_2	α_4 с *piezo* = 0	α_4
50	0.085	0.045055	0.045049	0.045055	0.045055	0.045055
250	0.425	0.2262	0.2252	0.22603	0.22605	0.2261
500	0.85	0.4578	0.4505	0.4568	0.4574	0.4575
700	1.1903	0.6522	0.6307	0.64777	0.6514	0.6518

The results given in Table 1 show that for the disk 1 mm thick and with frequencies up to 700 KHz, the calculation of the wave numbers from the dispersion equation (6) and the approximate calculation for α_4 almost coincide, and the *piezo* correction can be neglected. In this case, the decomposition (7) for α^2 depends only on the disk geometry, density, and moduli of flexibility – s_{11}, s_{12}, s_{13}.

Omitting the relatively cumbersome manipulations, we give the expression of Y conductivity for the piezoelectric disk. It is obtained from the approximate solution (7) for various ε^2.

$Y000$ is zero approximation of ε = 0, or the known equation of radial oscillations of a zero-thickness disk:

$$x = \frac{\alpha_0}{\varepsilon}; \quad Y000 = \omega C\left(1 - k_p^2 + k_p^2(1+\nu)\frac{J_1(x)}{xJ_0(x) - (1-\nu)J_1(x)}\right).$$

$Y040$ is approximate quartic wave number:

$$x = \frac{\alpha_4}{\varepsilon}; \quad Y040 = \omega C\left(1 - k_p^2 + k_p^2(1+\nu)\frac{J_1(x)}{xJ_0(x) - (1-\nu)J_1(x)}\right). \tag{8}$$

$Y042$ is approximate quartic wave number, quadratic particular solution:

$$Y042 = \omega C\left(1 - k_p^2 + c_{44}\frac{\Omega^2 e_{33}^2}{3\varepsilon_{33}^T c_{33}^2} + k_p^2(1+\nu)\frac{J_1(x)}{xJ_0(x) - (1-\nu)J_1(x)}\right).$$

$Y242$ is approximate quartic wave number, quadratic homogeneous and particular solution:

$$Y242 = \omega C\left(1 - k_p^2 + c_{44}\frac{\Omega^2 e_{33}^2}{3\varepsilon_{33}^T c_{33}^2} + k_p^2(1+\nu)\frac{J_1(x)}{zn}\left(1 - c_{44}\frac{\Omega^2 e_{33}c_{13}}{3e_{31}^p c_{33}^2}\right)\right);$$

$$zn = [xJ_0(x) - (1-\nu)J_1(x)]\left[1 + \varepsilon^2\alpha_0^2 t\left(\frac{1}{3} + \frac{t}{6}\right)\right] - \varepsilon^2\alpha_0^2\gamma\, xJ_0(x); \quad (9)$$

$$e_{31}^p = e_{31} + \frac{\varepsilon_{33}c_{13}}{e_{33}} = \frac{d_{31}}{s_{11}+s_{12}}.$$

Table 2 shows the numerical analytic calculation results. The conductivities of the exact solution (5, 6) and approximate solutions (8, 9) with respect to ε^2 were found using the MATLAB program [12]. For the disk made of PZT4 [13] with the thickness of 1 mm and the diameter of 30 mm, numerical calculations were carried out in the ANSYS and ACELAN systems [14]. The latter software package was developed by the employees of the Southern Federal University (SFU) and focused on the calculations of piezoelectric devices.

Table 2

Conductance calculation for various frequencies

Frequency, kHz	ANSYS, Cm/m	Solution (5,6), Cm/m	*Y*000, Cm/m	*Y*040, Cm/m	*Y*042, Cm/m	*Y*242, Cm/m
350	5.03	5.032	4.9688	5.014	5.0457	5.028
554.4	8.74169	8.741029	8.478	8.5864	8.73237	8.735
700	10.98	10.97	10.376	10.682	10.957	10.96

Table 2 shows that in the construction of approximate theories of the type (8, 9), it is required to use the decomposition (7) to calculate the wave number at least of the second order.

Research Results

1. Study of the dependence of the elastic ceramic moduli on frequency. For a sufficiently well-studied PZT piezoceramics, we will investigate the frequency dependence of the following modules: piezoelectric d_{31}, dielectric ε_{33}^T and flexibility modules - s_{11}, s_{12}, s_{13}. Consider low-frequency radial oscillations of a disc-shaped sample with electrodes on the ends. The sample thickness is 1 mm, the diameter is 40 mm, and the oscillation range is up to 700 KHz.

First, we study the frequency dependence for elastic modules. To do this, according to [15], we precheck the first three resonant low frequencies f_r (the major resonance and its two overtones). Elastic constants are determined from the solution of the frequency equation (9) of the radial oscillations of the disk considering ε relative thickness: three equations for three unknown variables. It is ε relative thickness that distinguishes the above frequency equation (9) for radial oscillations of the finite thickness disk from the known frequency equation for radial oscillations of the disk with "zero thickness" [15]:

$$R\,J_0(R) = (1-\nu)\,J_1(R).$$

The introduction of ε thickness correction into the solution of the known equation of radial oscillations of a disc-shaped sample improves the accuracy and measurement informativeness of the elastic modules.

The elastic compliances determined by [11, 15] through the technique of three resonances for the considered ceramics turned out to be equal:

$$s_{11} = 12.29\text{e}-12,\ s_{12} = -4.05\text{e}-12,\ s_{13} = -5.28\text{e}-12.$$

Table 3 shows the first ten resonant frequencies for the PZT19 ceramics. In the "Experiment" stock, the frequencies measured on the *WK* 6500B conductivity measuring device at the Institute of High Technologies and Piezotechnics at the Southern Federal University are given. In the "Analysis" line there are s_{11}, s_{12}, s_{13}, calculated by the formula (9) for the frequency-independent elastic modules defined by [11, 15]. Measurement errors did not exceed the values recommended by the standard [4].

Table 3

First ten resonant frequencies for PZT19 ceramics

	Resonant frequencies f_r, KHz									
Experiment	50.8	132.8	211	2884	364.6	439.4	513.2	585.4	654.4	722.8
Analysis	50.8	132.8	210.95	288.1	364.8	440.7	516	590.4	663	735.4

Table 3 shows that in the frequency range up to 600 KHz, the difference between the calculated and experimental data with constant elastic moduli does not exceed 1%, therefore the following conclusion can be made: "For the ceramics considered, s_{11}, s_{12}, s_{13} elastic modules with *E* superscript (it is omitted) or measured at a constant electric field are practically independent of the frequency in the range up to 650 kHz."

2. Study of the dependence on the frequency of d_{31} and ε_{33}^T modules. We use the expression (8) for *Y*040 conductance from the solution of the radial disk oscillations considering its thickness, as well as the values of imaginary parts of the complex conductivity of the piezoceramics under study measured at room temperature. In this case, it is possible to investigate the dependence of d_{31} and ε_{33}^T modules on the frequency in the range from 10 KHz to 600 KHz. To determine two unknown d_{31} and ε_{33}^T, measure *Y* at two frequencies – f_1, f_2. The difference between d_{31} and ε_{33}^T is selected so that we can neglect the dependence of d_{31} and ε_{33}^T modules on the frequency in f_1–f_2 range.

In this paper, two conditions are introduced:

1) $f_2 - f_1 = 200$ Hz;

2) the conductivities are calculated for an ideal piezoelectric body or without considering losses, therefore the frequencies of resonances or in the neighborhood of resonances are not taken into account.

As a result, we obtain an easily solvable system of two linear equations with respect to two unknown неизвестных k_p^2 and ε_{33}^T.

Fig. 1 shows k_p^2, d_{31} and $\varepsilon_{33}^T/\varepsilon_0$ dependences on 10-650 kHz frequencies.

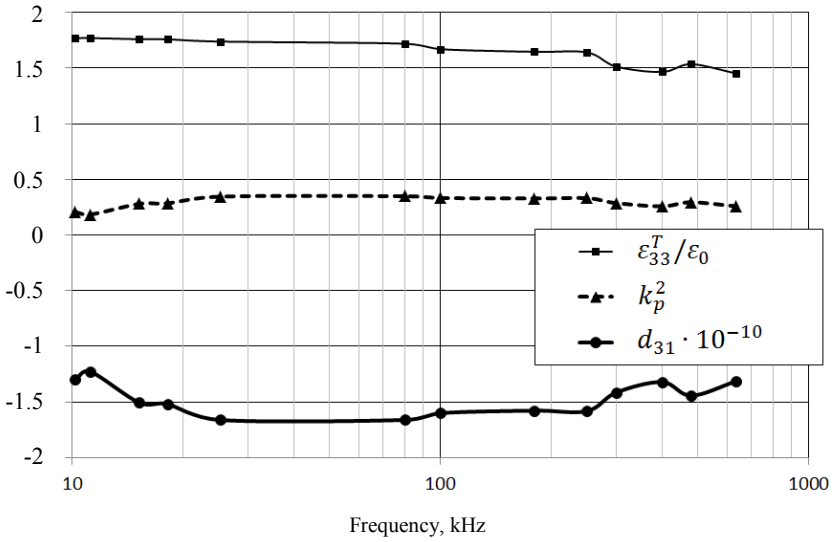

Fig. 1. Piezoelectric parameters – frequency dependences

Here, ε_0 is the dielectric constant of the vacuum. In the range from 15 to 650 KHz, k_p^2 coupling coefficient first increases with frequency growth from 0.28 to 0.34, and then decreases to 0.26. d_{31} piezo-module has a similar frequency dependence: at 15 KHz, from –1.50e $^{-10}$ to maximum of 1.661e $^{-10}$, and then decreases to 1.31e $^{-10}$. The relative dielectric constant decreases monotonically with increasing frequency from 1766 to 1455.

Fig. 2 shows frequency dependences in the range of 1–10 KHz measured and calculated from the formula (9) of the ceramics capacity with the constant modules defined according to OST [4, 15].

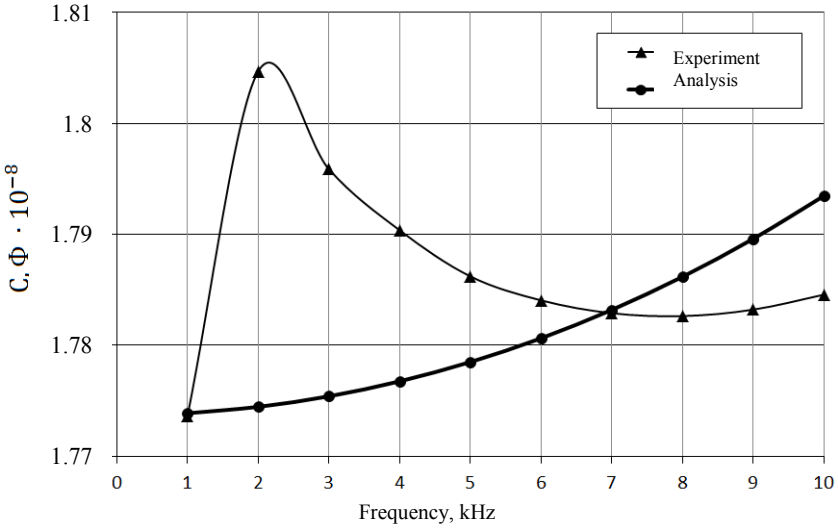

Fig. 2. Piezoceramics capacity – frequency dependence

There is sharp difference between two PZT ceramics capacities for low frequencies. This probably explains the dependence of the ceramics parameters on the frequency below 15 KHz (see Fig. 1). This implies a higher degree of dispersion — first of all, of d_{31} piezo-module d31. This issue will be considered in greater detail in the next paper (ε_{33}^T, d_{31}, k_p constants are investigated in the low-frequency range).

Discussion and Conclusions. A technique has been developed for determining frequency dependence of the PZT piezoelectric ceramic modules. The disk-shaped sample was studied within the frequency range of 15–700 KHz. It is shown that in the range up to 650 KHz, s_{11}, s_{12}, s_{13} elastic modules with E superscript (it is omitted) or measured at

a constant electric field are practically independent of frequency. In the indicated range, ε_{33}^{T}, d_{31}, k_p constants for the radial oscillations considered have an insignificant frequency dependence.

Only the frequency dependence of real part of the ceramic modules was studied, the losses were not considered. Therefore, the experimentally obtained frequency dependences of the imaginary part of the ceramics conductivities were measured far from resonances, where the effect of losses was absolutely null. Even so, in the future, both the real and imaginary parts of the modules must be considered. This means that losses are included. This problem is supposed to be studied considering the frequency dependence of the complex modules of the ceramics under study.

In the present paper, the radial oscillations of the sample are considered to obtain more complete information when measuring a larger set of constants (except for the piezoelectric and dielectric modules, s_{11}, s_{12}, s_{13} elastic modules are measured). This technique can be extended to other forms of samples (rods, plates, etc.), since in these one-dimensional problems, there is a simple replacement of Bessel functions by trigonometric functions.

References

1. Selvamani, R. Free vibration analysis of rotating piezoelectric bar of circular cross section immersed in fluid. Materials Physics and Mechanics, 2015, no. 24, pp. 24–34.

2. Bessonov, L.A. Teoreticheskie osnovy elektrotekhniki. Elektricheskie tsepi. [Theoretical foundations of electrical engineering. Electrical circuits.] Moscow: Yurayt, 2014, 701 p. (in Russian).

3. Sherrit, S., Wiederick, H.D., Mukherjee, B.K. Accurate Equivalent Circuits for Unloaded Piezoelectric Resonators. IEEE Ultrasonics Symposium Proceedings, 1997, vol. 2, pp. 931–935.

4. Materialy p'yezokeramicheskie. Tekhnicheskie usloviya. OST 11.0444-87 [Piezoceramic materials. Specifications. OST 11.0444-87] Standartinform. Moscow: Elektrostandart, 1987, 140 p. (in Russian).

5. IRE Standards on Piezoelectric Crystals: Measurements of Piezoelectric Ceramics. IEEE Proceedings of the IRE, 1961, vol. 49, iss. 7, pp. 1161–1169.

6. Advanced materials. National Physical Laboratory. Available at: http://www.npl.co.uk/science-technology/advanced-materials/materials-areas/functional/standards-for-piezoelectric-ceramic-materials (accessed: 18.09.18).

7. Tickoo, S. ANSYS Workbench 14.0: A tutorial Approach. Schererville: CADCINI Technologies, 2012, 416 p.

8. Bessonov, L.A. Teoreticheskie osnovy elektrotekhniki. Elektromagnitnoe pole. [Theoretical foundations of electrical engineering. Electromagnetic field.] Moscow: Yurayt, 2018, 317 p. (in Russian).

9. Madorsky, V.V., Ustinov, Yu.A. Simmetrichnye kolebaniya p'yezoelektricheskikh plastin. [Symmetric vibrations of piezoelectric plates.] Proceedings of the NAS RA, 1976, vol. 29, no. 5, pp. 51–58 (in Russian).

10. Madorsky, V.V., Mitko, V.N. Simmetrichnye kolebaniya p'yezoelektricheskikh tel s uchetom dissipatsii energii. [Symmetric vibrations in lossy piezoelectrics.] Akusticheskiy zhurnal, 1996, vol. 42, no. 2, pp. 282–285 (in Russian).

11. Madorsky, V.V. Issledovanie metodik opredelenie konstant polyarizovannoy p'yezokeramiki (chast' II). [Study on polarized piezoceramics constant techniques definition (Part 2).] Vestnik of DSTU, 2017, vol. 17, no. 4, pp. 14–21. 10.12737-1992-5980-2017-17-4-14-21 (in Russian).

12. Vasilyev, A.N. MATLAB. Prakticheskiy podkhod. [MATLAB. Practical approach.] mOSCOW: Nauka i tekhnika, 2015, 448 P. (in Russian).

13 Mason, W., ed. Fizicheskaya akustika. Ch. A. Metody i pribory zvukovykh issledovaniy. [Physical Acoustics. Part A. Acoustic Emission methods and equipment]. Moscow: Mir, 1966, pp. 204–324 (in Russian).

14. Soloviev, A.N., Oganesyan, P.A., Skaliukh, A.S. Modeling of Piezoelectric Elements with Inhomogeneous Polarization by Using ACELAN. Advanced materials — studies and applications. Hauppauge: Nova Science Publishers, 2015, pp. 169–192. DOI: 10.12737/16035.

15. Madorsky, V.V., Mitko, V.N. Issledovanie metodik opredeleniya konstant polyarizovannoy p'yezokeramiki. [Investigating constant determination techniques of polarized piezoceramics.]Vestnik of DSTU, 2014, vol. 14, no. 2, pp. 36–45. DOI: 10.12737/4469 (in Russian).

Submitted 11.01.2019
Scheduled in the issue 15.04.2019

Authors:

Madorsky, Victor V.,
associate professor of the Electrical Engineering and Electronics Department, Don State Technical University (1, Gagarin sq., Rostov-on-Don, 344000, RF), Cand.Sci. (Phys.-Math.), associate professor,
ORCID: http://orcid.org/0000-0002-0320-5074
epohrbats@Gmail.com

Rogov, Igor E.,
associate professor of the Electrical Engineering and Electronics Department, Don State Technical University (1, Gagarin sq., Rostov-on-Don, 344000, RF), Cand.Sci. (Eng.),
ORCID: https://orcid.org/0000-0003-1454-1660
igorro@rambler.ru

Kruglov, Alexander K.,
head of the laboratory, Institute for Advanced Technologies and Piezotechnics, Southern Federal University (10, Milchakov St., Rostov-on-Don, 344090, RF),
ORCID: https://orcid.org/0000-0003-0412-9445
kruglov@sfedu.ru

МАШИНОСТРОЕНИЕ И МАШИНОВЕДЕНИЕ
MACHINE BUILDING AND MACHINE SCIENCE

UDC 621.793 https://doi.org/10.23947/1992-5980-2019-19-2-151-157

Comparative characteristics of sterically hindered phenols and nitroxide radicals as stabilizers of polyethylene photodegradation *

I. Yu. Zhukova[1], I. I. Kashparov[2], S. V. Kucherenko[3], E. Sh. Kagan[4]**
[1,2,3] Don State Technical University, Rostov-on-Don, Russian Federation
[2,4] Platov South-Russian State Polytechnic University (NPI), Novocherkassk, Russian Federation

Сравнительная характеристика пространственно-затрудненных фенолов и нитроксильных радикалов как стабилизаторов фотодеструкции полиэтилена***

И. Ю. Жукова[1], И. И. Кашпаров [2], С. В. Кучеренко[3], Е. Ш. Каган[4]**
[1,2,3] Донской государственный технический университет, г. Ростов-на-Дону, Российская Федерация
[2,4] Южно-Российский государственный политехнический университет (НПИ) им. М. И. Платова, г. Новочеркасск, Российская Федерация

Introduction. Polymeric materials (PM) are increasingly used in various industries and agriculture. Under the action of UV light, PM are destroyed. UV stabilizers are used to protect PM from photodegradation. Their action is based on the absorption of the photoactive sunlight component or on the deactivation of excited molecules that have already absorbed a light quantum, as well as on the inhibition of dark light-induced reactions. The work objective is to provide a comparative analysis of compounds of the sterically hindered phenols (SHP) series and nitroxide radicals (NR) as the PM photodegradation inhibitors.

Materials and Methods. Reagents of the "purum" grade, LDPE premium grade 15803-020 polyethylene film were used for the investigations. The stabilizer was applied to the film by dipping. Carbonyl groups in polyethylene were determined by IR spectroscopy. IR spectra were recorded on Varian-640 instrument.

Research Results. 2,4,6-tri-tert-amylphenol (1), 2-methyl-4,6-di-tert-butylphenol (2), 4-acetylamino-2,2,6,6-tetramethylpiperidin-1-oxyl (3), 3-carboxamido-2,2,5,5-tetramethylpyrrolin-1-oxyl (4) were tested as stabilizers for photo-oxidative degradation of polyethylene. It is known that the accumulation of carbonyl and hydroxyl groups is recorded in PM samples under irradiation in the process of photodegradation through the IR spectroscopy. The absorption band of the carbonyl group at 1720 cm^{-1} appears in the IR spectra of oxidized polyethylene. The IR spectra analysis shows that the content of carbonyl groups in the check samples is significantly higher than in the samples treated by stabilizer solutions.

Введение. Полимерные материалы (ПМ) все шире используются в различных отраслях промышленности и сельского хозяйства. Под действием УФ-света ПМ разрушаются. Для защиты ПМ от фотодеструкции применяются УФ-стабилизаторы. Их действие основано на поглощении фотохимически активной компоненты солнечного света или на деактивации возбужденных молекул, уже поглотивших квант света, а также на торможении темновых реакций, индуцированных светом. Цель работы — сравнительный анализ соединений из ряда пространственно-затрудненных фенолов (ПЗФ) и нитроксильных радикалов (НР) в качестве ингибиторов фотодеструкции ПМ.

Материалы и методы. Для исследования использовали реактивы квалификации «ч», полиэтиленовую пленку ПЭВД в/с 15803-020. Стабилизатор наносили на пленки методом окунания. Карбонильные группы в полиэтилене определяли методом ИК-спектроскопии. ИК-спектры регистрировали на приборе Varian-640.

Результаты исследования. В качестве стабилизаторов фотоокислительной деструкции полиэтилена испытаны 2,4,6-три-трет-амилфенола (1), 2-метил-4,6-ди-трет-бутилфенола (2), 4-ацетиламино-2,2,6,6-тетраметилпиперидин-1-оксила (3), 3-карбоксамидо-2,2,5,5-тетраметилпирролин-1-оксила (4).

Известно, что при облучении в образцах ПМ в процессе фотодеструкции методом ИК-спектроскопии фиксируется накопление карбонильных и гидроксильных групп. В ИК-спектрах окисленного полиэтилена появляется полоса поглощения карбонильной группой при 1720 $см^{-1}$. Анализ ИК-спектров показывает, что содержание карбонильных групп в контрольных образцах значительно выше, чем в образцах, обработанных растворами стабилизаторов.

* The research is done within the frame of the independent R&D.
** E-mail: iyuzh@mail.ru, ivan-kashparov@yandex.ru, Kuh-sv82@mail.ru, kagan29@mail.ru
*** Работа выполнена в рамках инициативной НИР

Discussion and Conclusions. The experiments show that nitroxide radicals of 3-carboxamido-2,2,5,5-tetramethylpyrrolin-1-oxyl series and 4-acetylamino-2,2,6,6-tetramethylpiperidin-1-oxyl are the best photostabilizers of polyethylene. Moreover, there is no significant difference between the radicals of the 2,2,6,6-tetramethylpiperidine and 2,2,5,5-tetramethylpyrroline series. Sterically hindered phenols, under photodegradation, have a far smaller stabilizing effect, falling short of nitroxide radicals.

Keywords: polyethylene, photostabilizers, phenols, nitroxide radicals.

For citation: I.Yu. Zhukova, et al. Comparative characteristics of sterically hindered phenols and nitroxide radicals as stabilizers of polyethylene photodegradation. Vestnik of DSTU, 2019, vol. 19, no. 2, pp. 151−157. https://doi.org/10.23947/1992-5980-2019-19-2-151-157

Обсуждение и заключения. Эксперименты показали, что лучшими фотостабилизаторами полиэтилена являются нитроксильные радикалы 3-карбоксамидо-2,2,5,5-тетраметилпирролин-1-оксил и 4-ацетиламино-2,2,6,6-тетраметилпиперидин-1-оксил. Причем нет существенной разницы между радикалами ряда 2,2,6,6-тетраметилпиперидина и 2,2,5,5-тетраметилпирролина. Пространственно-затрудненные фенолы в условиях фотодеструкции оказывают значительно меньшее стабилизирующее действие, уступая нитроксильным радикалам.

Ключевые слова: полиэтилен, фотостабилизаторы, фенолы, нитроксильные радикалы.

Образец для цитирования: Сравнительная характеристика пространственно-затрудненных фенолов и нитроксильных радикалов как стабилизаторов фотодеструкции полиэтилена / И. Ю. Жукова [и др.] // Вестник Дон. гос. техн. ун-та. — 2019. — Т. 19, № 2. — С. 151−157. https://doi.org/10.23947/1992-5980-2019-19-2-151-157

Introduction. Polymeric materials (PM) are increasingly used in various industries and agriculture. With a sufficiently high resistance to climatic factors, the PM performance decreases when affected by humidity and temperature, as well as the ultraviolet (UV) component of the solar spectrum: in this case, radical particles are generated in the polymer, and transformations that cause material destruction occur [1, 2]. If in a PM there are products of its oxidation, for example, ketones, then they are photoinitiators of the decomposition process of the polymer. To protect the PM, it is required to ensure the interaction of radicals and highly efficient light stabilizers [3]. For this purpose, UV stabilizers are used which can act as follows:

- they absorb photoactive components of the sunlight;
- they deactivate excited molecules that have already absorbed a quantum of light;
- they inhibit dark light-induced reactions;
- they destroy or deactivate photoactive impurities and photoreaction products [4, 5].

Sterically hindered phenols (SHP), sterically hindered amines (SHA), and nitroxide radicals (NR) are widely used as UV stabilizers for polymers [6, 7]. The SHP act as chain terminators. Since the addition of mobile hydrogen to the primary radicals of the polymer photolysis is an oxidative reaction, the stabilizers themselves are easily oxidized [3]. Under photodegradation, the SHA form stable NR interacting with the alkyls of polymers which causes the photodegradation chain breaking [2].

The work objective is to provide a comparative analysis of compounds from the SHP and NR series as the PM photodegradation inhibitors.

Materials and Methods. Reagents of the “purum” grade of the Aldrich company, and high-pressure polyethylene film (LDPE 15803-020, GOST 16.337-77) 0.2 mm thick were used for the investigations. Photo-oxidative degradation stabilizers of the compound:

- from the NR series – 3-carboxamido-2,2,5,5-tetramethylpyrrolin-1-oxyl (1), 4-acetylamino-2,2,6,6-tetramethylpiperidine-1-oxyl (2);
- from the SHP series – 2-methyl-4,6-di-tert-butylphenol (3) and 2,4,6-tri-tert-amyl-phenol (4).

The surface treatment of the film for applying stabilizer solutions was carried out as follows: samples of 5×5 cm were fixed in a cassette without damaging the working part of the sample, washed in warm water, blotted with cotton cloth, degreased in acetone and dried for three minutes in air at 20 –25^{0}C.

To prepare stabilizer solutions, 50 ml of toluene were poured in each of twelve 100 ml capacity measuring flasks, and the stabilizers (1–4) were added in a volume of 0.01; 0.005; 0.0025 mol. Then, the contents of the flasks were made up to the mark with a solvent. The resulting solutions were used to process film samples.

The prepared film was dipped into a beaker with the solution of a UV stabilizer [8, 9] of the desired concentration for 30–40 min. Then, the sample was removed from the solution and kept over the beaker for 3–5 minutes so that the excess solution drained from the treated surface. The sample was completely dried being suspended.

For each stabilizer solution concentration, 5 film samples were tested. 120 samples were tested in total: 60 pieces – under the natural conditions and as many – under the simulated conditions. 10 check samples (CS) were not treated with stabilizers.

After testing, the IR spectra of the check and experimental samples were taken. IR spectroscopy determined the content of carbonyl groups in the samples [10, 11]. IR spectra were recorded on Varian 640 instrument.

Research Results. Field tests are the most reliable method for determining the PM resistance to UV exposure. To reduce the experiment time, quick tests in a lab environment are used. The samples were subjected to photodegradation with a UV stabilizer ((1–4) compounds) and without it. In this case, the samples were affected by:

- the sun, a natural source of UV rays – within 365 days (field tests according to GOST 9.708-83);
- a xenon lamp, an artificial source of UV rays (flux density of UV radiation of 68 W/m^2 in the range of wavelengths of 300–400 nm, GOST 9.708-83) – for 504 hours.

It is known that in the process of photodegradation through IR-spectroscopy, the carbonyl and hydroxyl groups are accumulated in the PM samples [1, 12]. But the yield of hydroxyl groups is a few dozen times less than carbonyl groups[12], therefore, the rate and degree of the polymer degradation is determined by the concentration of carbonyl groups according to the respective absorption bands in the IR spectrum [10].

The analytical IR-spectroscopy application to the determination of the film oxidation rate is based on the difference in the spectra of the processed and not processed (check) samples. After UV irradiation, the absorption band of the carbonyl group at 1720 cm^{-1} (stretch vibrations of the carbonyl group are C = O) appears in the IR spectra of polyethylene (PE). This band is analytical for the quantitative analysis. At the maximum of the absorption band at 1720 cm^{-1}, the optical density value was determined by the baseline method. Calculations of the content of carbonyl groups in the samples were carried out by the well-known methods [10]. The research results are shown in Tables 1 and 2.

Table 1

Carbonyl groups content in polyethylene samples * treated with stabilizer solutions, under irradiation of xenon lamp, artificial ultraviolet source

No	Stabilizer solution concentration mol/l / Stabilizer name	0.1 M	0.05 M	0.025 M
		Content of C = O groups, %		
1	3-carboxamido-2,2,5,5-tetramethyl-pyrrolin-1-oxyl (1)	—	—	0.02
2	4-acetylamino-2,2,6,6-tetramethyl-piperidine-1-oxyl (2)	—	—	0.025
3	2-methyl-4,6-di-tert-butylphenol (3)	0.10	0.25	0.40
4	2,4,6-tri-tert-amylphenol (4)	0.10	0.30	0.45
5	Check sample**	2.50	2.50	2.50

* No carbonyl groups were found in the sample before testing.

** Not treated with stabilizer solution.

Table 2

Carbonyl groups content in polyethylene samples* treated with stabilizer solutions, under irradiation of the sun, natural ultraviolet source (exposure period was 365 days)

No	Stabilizer solution concentration mol/l / Stabilizer name	0.1 M	0.05 M	0.025 M
		Content of C = O groups, %		
1	3-carboxamido-2,2,5,5-tetramethyl-pyrrolin-1-oxyl (1)	—	—	0.016
2	4-acetylamino-2,2,6,6-tetramethyl-piperidine-1-oxyl (2)	—	—	0.021
3	2-methyl-4,6-di-tert-butylphenol (3)	0.07	0.095	0.16
4	2,4,6-tri-tert-amylphenol (4)	0.06	0.09	0.17
5	Check sample**	0.35	0.35	0.35

* No carbonyl groups were found in the sample before testing.

** Not treated with stabilizer solution.

The IR spectra analysis showed that the content of carbonyl groups in the check samples was significantly higher than in the treated samples. Fig. 1 shows the IR spectra of CS and the samples treated with 0.025 M solutions of stabilizers (2) and (4) after irradiation with an artificial ultraviolet source.

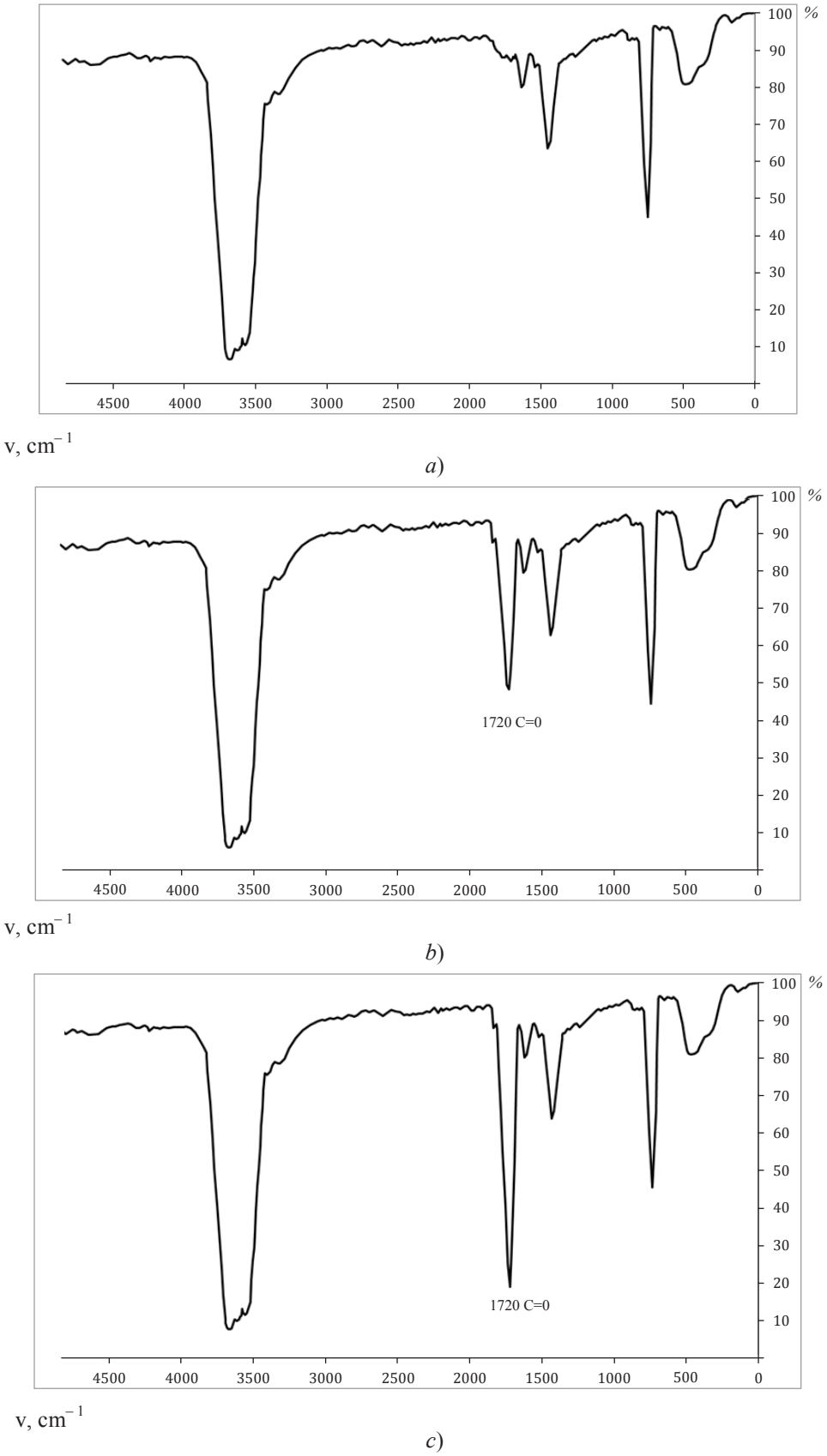

Fig. 1. IR spectra of PE-film samples: treated with 0.025 M solution of 4-acetylamino-2,2,6,6-tetramethylpiperidine-1-oxyl (2) (*a*); treated with 0.025 M solution of 2,4,6-tri-tert-amylphenol (4) (*b*); check sample (*c*). Absorption level is shown on the right vertical scale.

The onset of the degradation process in the sample treated with SHP (4) is characterized by the appearance of a low-intensity absorption band at 1720 cm^{-1} in the IR spectrum (Fig. 1, *b*). Such a band is practically absent in the sample treated with the stabilizer (2) from the NR series (Fig. 1, *a*). Consequently, the contribution of NR to the deceleration of photodecomposition processes is much higher than of the SHP.

UV radiation destroyed the CS. This is evidenced by the effect of accumulation of carbonyl groups in the sample manifested in an increase in the intensity of the absorption band at 1720 cm^{-1} (Fig. 1, *c)*.

Using IR spectroscopy, it was shown that UV-irradiation of PE films causes the accumulation of carbonyl groups associated with photodecomposition of PE carbon chains. Fig. 2 shows the kinetic curves of the accumulation of carbonyl groups during the simulated film photooxydation depending on the exposure time.

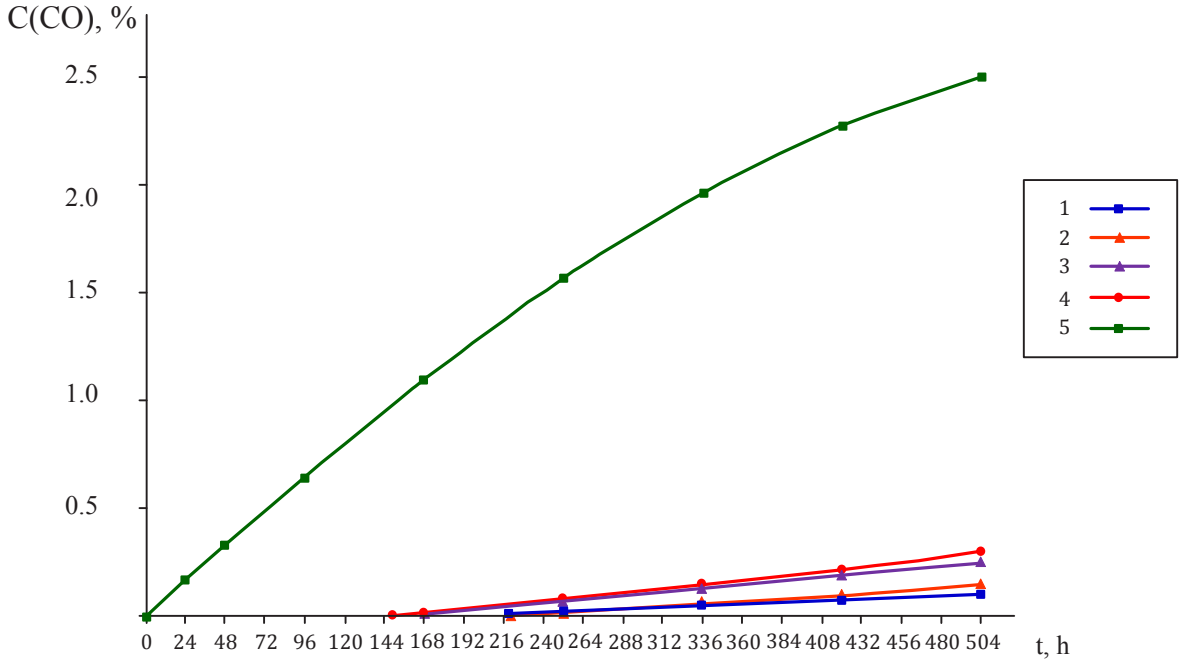

Fig. 2. Dependence of accumulation rate of carbonyl groups on time of simulated UV irradiation of samples treated with: 1 – 0.025 M solution of 3-carboxamido-2,2,5,5-tetramethylpyrrolin-1-oxyl; 2 – 0.025 M solution of 4-acetylamino-2,2,6,6-tetramethylpiperidine-1-oxyl; 3 – 0.025 M solution of 2-methyl-4,6-di-tert-butylphenol; 4 – 0.025 M solution of 2,4,6-tri-tert-amylphenol; 5 – check sample was not processed

The analysis of the data obtained shows that NR (1, 2) and SHP (3, 4) essentially slow down the photoinitiated oxidation destruction of PE and reduce the number of breaks of macromolecules. This is evidenced by the appearance of an induction period with an increase in the exposure time (see Fig. 2).

At the initial stage of the experiment, changes in CS are observed. Gradually, the concentration of carbonyl groups in the film not treated with a stabilizer increases. This is associated with an increase in the rate of oxidation processes causing the structure destruction of the PE carbon chains and the formation of low molecular weight active components (radical particles). In the PE samples treated with stabilizers (1-4), no changes are observed.

After about 150 hours, carbonyl groups are recorded in the samples treated with SHP (3, 4) solutions; after 220 hours – in the samples treated with NR solutions (1, 2). The accumulation rate of carbonyl groups increases linearly within 150–200 hours. Further, the dependence is maintained during the whole process of photo-oxidation (up to 504 hours).

The induction period in the presence of NR and SHP can be explained by the ability of stabilizers (1–4) to capture radicals quantitatively from the first moment; as a result, the process of destruction is inhibited at this stage. In this case, NR quickly interact with alkyl radicals, and, involving the polymer, they are converted into hydroxylamines capable of restoring radical particles [6, 7, 12]. SHP can turn into quinones or mono- and diesters of hydroquinones [6], which are also traps for radical particles.

The samples treated and not treated with stabilizers were also irradiated by a natural ultraviolet source according to GOST 9.708-83 for 365 days (see Table 2). The indicator of natural photo-oxidation of PE films was monitored after 1, 3, 6, 9, and 12 months (Fig. 3).

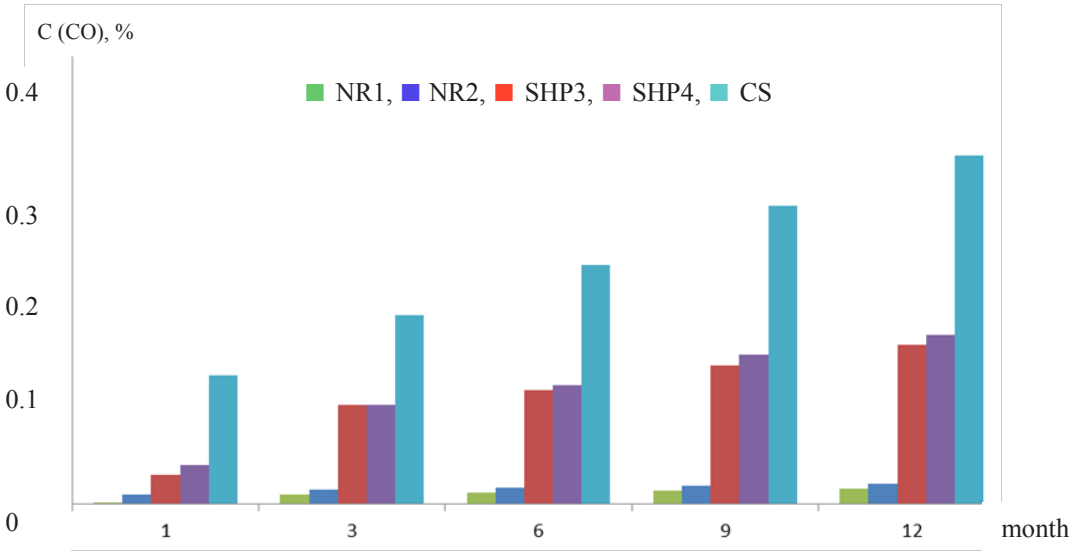

Fig. 3. Monitoring of indicator of concentration of carbonyl groups in PE film samples treated with 0.025 M stabilizer solution (1–4) and check sample (5)

Comparison of samples treated with NR (1, 2) and SHP (3, 4) shows the following: in the first case, the concentration of carbonyl groups increases insignificantly, in the second case, the content of carbonyl groups is sequence higher. In CS, a significant increase in the concentration of carbonyl groups was recorded after 1 month.

It should be also noted that in the course of testing of CS, PE films became brittle, and at the end of the experiment, they broke down, in contrast to the samples treated with stabilizer solutions.

Discussion and Conclusions. It is established that the best photo stabilizers of polyethylene are nitroxide radicals. Significant difference between the radicals of the 2,2,6,6-tetramethylpiperidine and 2,2,5,5-tetramethylpyrroline was not detected. Under the conditions of photodegradation, the SHP have a less stabilizing effect, yielding to nitroxide radicals.

The inhibitory effect of NR and SHP is associated with their ability to interact with radical particles formed as a result of the polymer photodegradation.

The tested compounds from NR class effectively slow down the process of photo-oxidation degradation and can be recommended for application as polymer stabilizers.

References

1. Kuleznev, V.N., Shershnev, V.N. Khimiya i fizika polimerov. [Chemistry and physics of polymers.] Moscow: KolosS, 2007, 367 p. (in Russian).

2. Emanuel, N.M., Zaikov, G.E., Kritsman, V.A. Khimicheskaya kinetika i tsepnye reaktsii. [Chemical kinetics and chain reactions.] Moscow: Nauka, 1989, 312 p. (in Russian).

3. Gorbunov, B.N., Gurvich, Ya.A., Maslova, I.P. Khimiya i tekhnologii stabilizatorov polimernykh materialov. [Chemistry and technologies of stabilizers of polymeric materials.] Moscow: Khimiya, 1981, 368 p. (in Russian).

4. Arkhireev, V.P. Starenie i stabilizatsiya polimerov. [Aging and Stabilization of Polymers.] Moscow: Nauka, 1984, 365 p. (in Russian).

5. Plate, N.A., Litmanovich, A.D., Kudruavtsev, Ya.V. Makromolekulyarnye reaktsii v rasplavakh i smesyakh polimerov. Teoriya i eksperiment. [Macromolecular reactions in melts and mixtures of polymers. Theory and experiment.] Moscow: Nauka, 2008, 380 p. (in Russian).

6. Yershov, V.V., Nikiforov, G.A., Volodkin, A.A. Prostranstvenno-zatrudnennye fenoly. [Sterically hindered phenols.] Moscow: Khimiya, 1972, 351 p. (in Russian).

7. Rozantsev, E.G., Goldfeinb, M.D. Organic Paramagnetics as Antioxidants . Oxidation Communications, 2009, no. 3 (32), pp. 485–506.

8. Shalkauskas, M.I. Metallizatsiya plastmass. [Metallization of plastics.] Chemistry and Chemists, 2008, no. 2, pp. 16–49 (in Russian).

9. Zernin, E.A., Tomas, K.I. Avtomatizirovannyy metod issledovaniya protsessa naneseniya pokrytiy. [An automated method for studying the process of coating.] Engineering Journal of Don, 2015, no. 2 (36), pp. 70 (in Russian).

10. Rabek, Ya. Eksperimental'nye metody v khimii polimerov. [Experimental methods in polymer chemistry.] Moscow: Mir, 1983, 384 p. (in Russian).

11. Averko-Antonovich, I.Yu., Bikmullin, R.T. Metody issledovaniya struktury i svoystv polimerov. [Methods for studying the structure and properties of polymers.] Kazan: Izd-vo KSTU, 2002, 604 p. (in Russian).

12. Shibryaeva, L.S., Gorbunova, I.Yu., Kerber, M.L. Termookislitel'naya destruktsiya kompozitsii na osnove epoksidnogo oligomera. [Thermal-oxidative degradation of the composition based on epoxide oligomer.] Chemical Physics, 2014, vol. 33, no. 9, pp. 65–77 (in Russian).

Submitted 17.05.2019
Scheduled in the issue 03.06.2019

Authors:

Zhukova, Irina Y.,
Head of the Chemical Technologies of Oil and Gas Complex Department, Don State Technical University (1, Gagarin sq., Rostov-on-Don, 344000, RF), Dr.Sci. (Eng.), professor,
ORCID: https://orcid.org/0000-0002-2781-4528
iyuzh@mail.ru

Kashparov, Ivan I.,
associate professor of the Chemical Technologies of Oil and Gas Complex Department, Don State Technical University (1, Gagarin sq., Rostov-on-Don, 344000, RF), Platov South-Russian State Polytechnic University (NPI) (132, ul. Prosveshcheniya, Novocherkassk, Rostov Region, 346428, RF), Cand.Sci. (Eng.),
ORCID: https://orcid.org/0000-0001-9926-1902
ivan-kashparov@yandex.ru

Kucherenko, Svetlana V.,
associate professor of the Chemical Technologies of Oil and Gas Complex Department, Don State Technical University (1, Gagarin sq., Rostov-on-Don, 344000, RF), Cand.Sci.(Chemistry),
ORCID: https://orcid.org/0000-0002-0731-6513
Kuh-sv82@mail.ru

Kagan, Efim Sh.,
Professor of the Chemical Technologies Department, Platov South-Russian State Polytechnic University (NPI) (1, ul. Prosveshcheniya, Novocherkassk, Rostov Region, RF), Dr.Sci.(Chemistry), professor,
ORCID: https://orcid.org/0000-0002-8339-1910
kagan29@mail.ru

МАШИНОСТРОЕНИЕ И МАШИНОВЕДЕНИЕ
MACHINE BUILDING AND MACHINE SCIENCE

UDC 621.825.54 https://doi.org/10.23947/1992-5980-2019-19-2-158-163

Study of the working body mechanism in forging-and-stamping equipment*

K. O. Kobzev[1**]
[1] Don State Technical University, Rostov-on-Don, Russian Federation

Изучение механизма рабочего органа в кузнечно-штамповочном оборудовании***

К. О. Кобзев[1**]
[1] Донской государственный технический университет, г. Ростов-на-Дону, Российская Федерация

Введение. Статья посвящена исследованию синтезированной принципиальной схемы фрикционного контакта твердых тел в кузнечно-штамповочных машинах. Установлена возможность получения максимума нагрузочной характеристики фрикционного контакта внутри интервала изменения коэффициента трения. Выявлены две следующие возможности сил трения фрикционного контакта: на границах указанного интервала они будут равны при наличии максимума равенства; при данных условиях они достигают наибольшей стабильности.

Материалы и методы. При изменении величины угла меняется положение точки максимума. Это приводит к нарушению равенства сил трения на границах интервала изменения коэффициента трения. В таком случае коэффициент точности должен определяться отношением максимума функции к наименьшему граничному значению. Для этого необходимо установить тенденции изменения граничных значений функции, связанные с варьированием величины угла. Для решения этой задачи новую величину тангенса угла давления представили в виде произведения коэффициента варьирования на базовое значение тангенса угла.

Результаты исследования. Полученные результаты показывают высокую стабильность силы трения при проскальзывании тел фрикционного контакта (ФК). Однако при больших величинах угла давления чувствительных элементов датчика-преобразователя максимальная сила трения кратковременно может быть пропорциональна текущему значению коэффициента трения.

Обсуждение и заключения. Модернизированная принципиальная схема ФК позволяет теоретически получить очень высокую стабильность силы трения. ФК не должен обращаться в ноль в интервале изменения коэффициента трения выходного параметра основной фрикционной группы (ОФГ) и при наличии максимума функции нагрузочной способности ФК. Необходимым условием этого является передача чувствительными элементами дополнительной фрикционной группы (ДФГ) ее полной нагрузки.

Introduction. The synthesized basic diagram of the frictional contact of solids in forging-and-stamping machines is considered. The possibility of obtaining the maximum load characteristics of the frictional contact within the variation interval of the friction factor is determined. The following two possibilities of frictional contact forces are indicated: they will be equal at the boundaries of the specified interval if there is maximum balance; they achieve the greatest stability under these conditions.

Materials and Methods. When the angle value changes, the position of the maximum point changes. This causes violation of the friction forces balance at the boundaries of the variation interval of the friction factor. In this case, the accuracy coefficient should be determined by the ratio of the maximum of function to the least boundary value. Doing this requires establishing trends of changing the boundary function values associated with the angle variation. To solve this problem, a new value of the pressure angle tangent was presented as a product of the coefficient of variation by the base value of the angle tangent.

Research Results. The results show high stability of the friction force under slipping of the frictional contact (FC) bodies. However, at large values of the pressure angle of sensing elements of the transducer, the maximum friction force can be for a short moment proportional to the current value of the friction factor.

Discussion and Conclusions. The upgraded FC basic diagram enables to theoretically obtain very high stability of the friction force. The FC should not vanish within the variation interval of the friction factor of the output parameter of the basic friction group (BFG) and at the maximum of function of the FC load capacity. A necessary condition for that is the transfer of full capacity of the additional friction group (AFG) by the sensing elements.

* The research is done within the frame of the independent R&D.
** E-mail: 5976765@mail.ru
*** Работа выполнена в рамках инициативной НИР.

Keywords: forging-and-stamping machines, friction factor, working mechanism, gain constant, overload, accuracy.

Ключевые слова: кузнечно-штамповочное оборудование, коэффициент трения, рабочий механизм, коэффициент усиления, перегрузка, точность.

For citation: K.O. Kobzev. Study of the working body mechanism in forging-and-stamping equipment. Vestnik of DSTU, 2019, vol. 19, no. 2, pp. 158–163. https://doi.org/10.23947/1992-5980-2019-19-2-158-163

Образец для цитирования: Кобзев, К. О. Изучение механизма рабочего органа в кузнечно-штамповочном оборудовании / К. О. Кобзев // Вестник Дон. гос. техн. ун-та. — 2019. — Т. 19, № 2. — С. 158–163. https://doi.org/10.23947/1992-5980-2019-19-2-158-163

Introduction. The synthesized schematic diagram of frictional contact (FC) of solids in forging-and-stamping machines is considered. The analysis shows the possibility of obtaining maximum load FC characteristics within the variation interval of the friction factor. The following two possibilities of frictional contact forces are identified: they will be equal at the boundaries of the specified interval if there is maximum balance; they achieve the greatest stability under these conditions. The results obtained show high stability of the friction force during slipping of FC bodies. However, at large values of the pressure angle of the sensitive elements of the transducer sensor, the maximum friction force can be briefly proportional to the current value of the friction factor.

Materials and Methods. The FC scheme shown in Fig. 1 is free from this disadvantage.

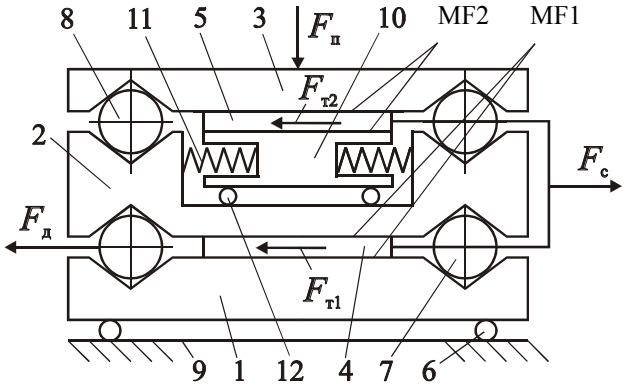

Fig. 1. Basic diagram of frictional contact

The master friction group (MF1) includes bodies 1, 2 and 4; the additional friction group (MF2) contains bodies 3, 5 and 10. Between 1 and 2, 2 and 3 bodies, sensitive elements in the form of rolling bodies 7 and 8 are placed in the profiled sockets.

The difference of the considered scheme is the division of body 2 into two parts, due to which the connection between bodies 2 and 5 is carried out using body 10 interacting with body 2 through the springs 11. This allows transferring half of the total load of MF2 from body 2 directly to the rolling elements 8 making them a leading element in the MF2. The second half of the total load of MF2 is transmitted through the springs 11 from body 2 to body 10, and further through friction – to body 5. In addition, the place of $F_д$ moving force is transferred from body 1 to the rolling elements 7. These differences allow excluding the impact of the pressure rolling 7 on the load distribution between the friction surfaces in MF1 and MF2 when the friction factor value changes [1].

To restrict to the linear nature of the friction between the bodies 1 and the supporting surface 9, as well as between the bodies 2 and 10, the rollers 6 and 12 are installed.

The formula for determining the value of the FC friction force depending on the disturbance input is as follows (at the same values of the feedback gain factor of MF1 and MF2]:

$$\sum F_т = \frac{4F_п f}{(1+f\text{tg}\alpha)^2}, \quad (1)$$

where $\sum F_т$ is total ultimate friction force between bodies 1, 2, 4 and 3, 5, 10; ; $F_п$ is initial clamp force of friction couples; f is current value of the friction factor between the mentioned bodies; α is pressure angle between rolling elements 7, 8 and the socket.

It was also established that the function (1) within $f_{\min}...f_{\max}$ range of values does not have a maximum since the friction force of MF1 vanishes at the value of the friction factor of $f_o = 1/\text{tg}\alpha$. (Here, $f_{\min}$ and $f_{\max}$ are, respectively, the smallest and largest values that the friction factor can take in actual FC operating conditions for the adopted combination of materials of friction couples.) The same value corresponds to the imaginary maximum of the function

(1) since in $f_0 \ldots f_{max}$ interval, the FC load is transferred through MF2friction group, the friction force of which increases with f growth. This does not ensure the FC friction force stability despite the fact that it is somewhat higher than that of the first-generation FC (at values $f_{min} = 0.1$, $f_{max} = 0.8$ and $\mathrm{tg}\alpha = 1.125$, the accuracy coefficient is equal to $K_т = 2.5$ and $K_т = 3.67$).

The real maximum of the FC load characteristics within the variation interval of the disturbance input is possible through modifying MF2 according to the scheme (see Fig. 1). This modification is to reduce the number of friction couples. To this end, it is necessary to exclude elements 10, 11 from the scheme and to rest body 5 directly upon body 2 through the rollers 12.

In accordance with this, we find:

$$F_{т2} = (F_п - F_{р2}) f ,$$

where $F_{т2}$ is friction force of MF2; $F_{р2}$ is control action of MF2 (expansion force on the rolling elements 8).

But

$$F_{р2} = F_{т2}\mathrm{tg}\alpha ,$$

hence,

$$F_{т2} = \frac{F_п f}{1+f\mathrm{tg}\alpha} . \quad (2)$$

Friction force between MF1 pairs is equal to:

$$F_{т1} = 2\left[F_п - \left(\frac{F_{т1}}{2} + F_{т2} \right) \mathrm{tg}\alpha \right] f .$$

Considering the relation (2), we find

$$F_{т1} = 2F_п \frac{f}{(1+f\mathrm{tg}\alpha)^2} . \quad (3)$$

The relation (3) does not contain the difference in the numerator; therefore, this function does not vanish on any conditions. It only asymptotically approaches zero under the following conditions:

- theoretically unlimited increase in friction factor;
- a maximum at the point corresponding to $f_к = 1/\mathrm{tg}\alpha$ value [2–5].

Summing up the friction forces in the relations (2) and (3), we obtain

$$\sum F_т = F_п f \frac{3 + f\mathrm{tg}\alpha}{(1+f\mathrm{tg}\alpha)^2} . \quad (4)$$

Differentiating the function (4) by f argument and equating the derivative to zero, we find the value of the friction factor corresponding to a maximum of the function:

$$f_к' = \frac{3}{\mathrm{tg}\alpha} . \quad (5)$$

Substituting in sequence f_{min}, f_{max} values in the expression (4), and equating the obtained relations to each other, we find:

$$\mathrm{tg}\alpha = \frac{(m+1)+\sqrt{(m+1)^2+12m}}{2f_{max}} . \quad (6)$$

Here, m is relative width of the friction factor interval: $m = f_{max} / f_{min}$.

At the found $\mathrm{tg}\alpha$ value, the function (6), having a maximum at the point corresponding to the value (5), takes the same values at the boundaries of the variation interval of the friction factor.

In this case, the coefficient of accuracy is determined by the ratio of a maximum of the function (4) to its any boundary value (for f_{min} or f_{max} values). Based on this, we get:

$$K_т = \frac{9(1+f_{max}\mathrm{tg}\alpha)^2}{8f_{max}\mathrm{tg}\alpha(3+f_{max}\mathrm{tg}\alpha)} . \quad (7)$$

Set the value of parameter ($\mathrm{tg}\alpha$) at which $K_т$ value is minimal. When $\mathrm{tg}\alpha$ value changes, the position of the maximum point ($f_к'$) changes as well. Only the relation (6) establishes the equality of the friction forces on the boundaries of the variation interval, therefore, changing the position of the maximum point of the function (4) violates the

above equality.

In this case, the accuracy coefficient should be determined by the ratio of a maximum of the function (4) to the smallest boundary value. To do this, it is required to establish trends in the boundary values of the function (4) associated with $\mathrm{tg}\alpha$ value variation [6 –10].

To solve this problem, let us present a new value of the pressure tangent as a product of K variation coefficient and the base value of the tangent angle in accordance with the expression (6), i.e.:

$$\mathrm{tg}\alpha_i = K\mathrm{tg}\alpha\,. \tag{8}$$

Based on this, we can write considering (4):

$$\frac{(3m + Kf_{\max}\mathrm{tg}\alpha)f_{\max}}{(m+Kf_{\max}\mathrm{tg}\alpha)^2} > \frac{(3+Kf_{\max}\mathrm{tg}\alpha)f_{\max}}{(1+Kf_{\max}\mathrm{tg}\alpha)^2}\,.$$

Here, the left side corresponds to the FC friction force at $f = f_{\min}$, and the right side – to the friction force at $f = f_{\max}$. The solution to the latter inequality with respect to the coefficient of variation is:

$$K \in \left(-\infty;\ \frac{(m+1)-\sqrt{(m+1)^2+12m}}{2f_{\max}\mathrm{tg}\alpha}\right)\cup(1;\ +\infty)\,.$$

Since $\mathrm{tg}\alpha > 0$, the fraction in parentheses of the left side of the solution is negative, therefore, for $K > 1$, the resulting inequality is undoubtedly fulfilled, i.e. when f'_{κ} maximum point is shifted to smaller values, to calculate the accuracy coefficient, it is necessary to use the value of the FC friction force corresponding to $f_{\max}$ value and conversely, when $1 > K > 0$, it is necessary to take the friction force value corresponding to $f_{\min}$ value [11–13].

Using this conclusion, we make the inequality of $K_{\mathrm{T}1} > K_{\mathrm{T}}$ form where $K_{\mathrm{T}1}$ is the accuracy coefficient calculated with consideration of the equality (8). We have:

$$\frac{(1+Kf_{\max}\mathrm{tg}\alpha)^2}{K(3+Kf_{\max}\mathrm{tg}\alpha)} > \frac{(1+f_{\max}\mathrm{tg}\alpha)^2}{3+f_{\max}\mathrm{tg}\alpha}\,.$$

The inequality is set up given that $K > 1$.

Transformation of the resulting inequality to the form

$$3+(1+K)f_{\max}\mathrm{tg}\alpha + Kf^2{}_{\max}\mathrm{tg}^2\alpha > 0$$

shows the validity of the assumption that $K_{\mathrm{T}1} > K_{\mathrm{T}}$.

We investigate the ratio of the values of the coefficients of accuracy when the maximum point of the function (4) is shifted to the region of large values, that is, at $K < 1$. Then, $K_{\mathrm{T}2} > K_{\mathrm{T}}$ or

$$\frac{(m+Kf_{\max}\mathrm{tg}\alpha)^2}{K(3m+Kf_{\max}\mathrm{tg}\alpha)} > \frac{(1+f_{\max}\mathrm{tg}\alpha)^2}{3+f_{\max}\mathrm{tg}\alpha}\,.$$

Transformation of the resulting inequality to the form

$$3m+(m+K)f_{\max}\mathrm{tg}\alpha - Kf^2{}_{\max}\mathrm{tg}^2\alpha > 0$$

and the solution of the latter give

$$K < \frac{m(3+f_{\max}\mathrm{tg}\alpha)}{(f_{\max}\mathrm{tg}\alpha-1)f_{\max}\mathrm{tg}\alpha}\,.$$

The fraction on the right side of the obtained solution is equal to one at the value

$$\mathrm{tg}\alpha = \frac{(m+1)+\sqrt{(m+1)^2+12m}}{2f_{\max}}\,,$$

which fully corresponds to the solution (6). Therefore, the inequality $K_{\mathrm{T}2} > K_{\mathrm{T}}$ is performed if $K < 1$.

Research Results. Let us take the final judgment on the stability of the FC friction force for various forms of load characteristics. For this purpose, we determine the FC accuracy coefficient when the function (4) has a maximum at $f = f_{\max}$. In this case, the function monotonically increases in the range of the friction factor variation. At that, $f_{\max} = 3/\mathrm{tg}\alpha$ equality is true. We will get:

$$K_{\mathrm{T}3} = \frac{\sum F_{\mathrm{T}(f_{\max})}}{\sum F_{\mathrm{T}(f_{\min})}} = \frac{(m+3)^2}{8(m+1)}\,.$$

Considering $K_{T3} > K_T$, we will find:

$$3m(3 - mf_{max}\,\mathrm{tg}\alpha) + m(3-m)f^2{}_{max}\,\mathrm{tg}^2\alpha + 9(1 - f_{max}\,\mathrm{tg}\alpha) < 0.$$

For all friction materials used as FC friction couples, $m > 3$. According to (6), $f_{max}\,\mathrm{tg}\alpha > 1$, therefore, it is obvious that the differences in the brackets of the obtained inequality are negative and the above assumption is true.

Thus, the analysis performed shows that the greatest stability of the FC output parameter is in the case when the function (4) has a maximum within the interval of the friction factor variation and takes the same values at its boundaries.

When $m = 8$ and $f_{max} = 0.8$, we get $\mathrm{tg}\alpha \approx 14$. Then, $f'_к \approx 0.214$. In this case, maximum of the function (3) will be at $f_к \approx 0.071$ which is almost identical to the lower boundary of the interval $f = f_{min} = 0.1$. The function (3) decreases within the interval of the friction factor variation. With such initial parameters, $K_T \approx 1.04$ and $K_{T3} \approx 1.68$.

Discussion and Conclusions. As is obvious, the modified FC block diagram enables theoretically to obtain very high stability of the friction force. However, due to the relatively large value of $\mathrm{tg}\alpha$ parameter, $F_П$ force is used inefficiently. The FC should not vanish in the variation interval of the friction factor of the output parameter of the master friction group (MFG) and in the presence of maximum of the function of the FC load capacity.

A necessary condition for this is the transfer of full load of the MFG by the sensitive elements of the additional friction group (FGD). An additional condition for the existence of a maximum can be formulated as follows: with an equal number of friction couples of both friction groups, the MFG sensitive elements transfer part of its full load; with a smaller number of friction couples than in the AFG, the sensitive elements transfer the full load of the MFG.

References

1. Braude, V.I., Ter-Mkhitarov, M.S. Sistemnye metody rascheta gruzopod"emnykh mashin. [System methods for calculating lifting machines.] Leningrad: Mashinostroenie, 1985, pp. 181–205 (in Russian).

2. Serensen, S.V. Prochnost' elementov konstruktsiy v statisticheskom aspekte i otsenka ikh ekspluatatsionnoy nadezhnosti. [Strength of structural elements in the statistical aspect and evaluation of their operational reliability.] Nadezhnost' i dolgovechnost' mashin i oborudovaniya. [Reliability and durability of machinery and equipment.] Moscow: Izd-vo standartov, 1972, pp. 136–146 (in Russian).

3. Kochaev, V.P., Makhutov, N.A., Gusenkov, A.P. Raschety detaley mashin konstruktsiy na prochnost' i dolgovechnost'. [Calculations of machine parts structures for strength and durability.] Moscow: Mashinostroenie, 1985, 224 p. (in Russian).

4. Afanasyev, M.K. Issledovanie friktsionnykh muft povyshennoy tochnosti ogranicheniya nagruzki: avtoref. dis. … kand. tekhn. nauk. [Study on friction clutches with increased accuracy of load limiting: Cand.Sci. (Eng.), diss., author's abstract.] Rostov-on-Don, 1971, 21 p. (in Russian).

5. Yesipenko, Ya.I., Palamarenko, A.Z., Afanasyev, M.K. Mufty povyshennoy tochnosti ogranicheniya nagruzki. [Enhanced load limiting couplings.] Kiev: Tekhnika, 1972, pp. 168–175 (in Russian).

6. Zaporozhchenko, R.M. O kharakteristikakh predokhranitel'nykh friktsionnykh muft povyshennoy tochnosti srabatyvaniya. [On the characteristics of safety friction clutches of high accuracy.] Proceedings of Higher Educational Institutions. Machine Building, 1971, no. 1, pp. 48–52 (in Russian).

7. Zaporozhchenko, R.M K voprosu ob effektivnosti friktsionnykh predokhranitel'nykh muft s tochki zreniya snizheniya vesa privodov. [On the efficiency of friction safety clutches in terms of weight reduction of drives.] Bulletin of NTU KhPI, 1971, iss. I.XIV, no. 58, pp. 16–19 (in Russian).

8. Tepinkichiev, V.K. Predokhranitel'nye ustroystva ot peregruzki stankov. [Machine overload protectors.] 2nd revised and enlarged ed. Moscow: Mashinostroenie, 1968, pp. 112–118 (in Russian).

9. Shishkarev, M.P., Kobzev, K.O. Issledovanie tochnosti srabatyvaniya adaptivnykh friktsionnykh muft s kombinirovannoy obratnoy svyaz'yu (chast' 2). [Research of response accuracy of adaptive friction clutch with combined feedback (part 2).] Naukovedenie, 2013, no. 4 (17). Available at: http://naukovedenie.ru/PDF/03tvn413.pdf (accessed 27.03.19) (in Russian).

10. Shishkarev, M.P., Kobzev, K.O. Sintez printsipial'noy skhemy modernizirovannogo varianta adaptivnoy friktsionnoy mufty s kombinirovannoy obratnoy svyaz'yu. [The synthesis of the concept of the upgraded version of the adaptive friction clutch with combined feedback.] Engineering Journal of Don, 2013, no. 2. Available at: http://www.ivdon.ru/magazine/archive/n2y2013/1738 (accessed 27.03.19) (in Russian).

11. Shishkarev, M.P., Kobzev, K.O. Elementy teorii otritsatel'no-nulevoy obratnoy svyazi v adaptivnykh friktsionnykh muftakh. [Theory elements of zero-negative feedback in adaptive friction clutches.] Vestnik of DSTU, 2014, no. 1, pp. 180—191 (in Russian).

12. Shishkarev, M.P., et al. Osnovy metodologii rascheta i proektirovaniya adaptivnykh friktsionnykh muft s razdel'nym silovym zamykaniem. [Methodological bases of calculation and design of adaptive friction clutch.] Naukovedenie, 2013, no. 5. Available at: http://www.naukovedenie.ru/PDF/17tvn513.pdf (accessed 27.03.19) (in Russian).

13. Shishkarev, M.P., et al. Spetsifika metodik rascheta i proektirovaniya adaptivnykh friktsionnykh muft s razdel'nym silovym zamykaniem. [Features procedure and designing of adaptive friction clutch with separate force closure.] Naukovedenie, 2013, no. 5. Available at: http://www.naukovedenie.ru/PDF/18tvn513.pdf (accessed 27.03.19) (in Russian).

Submitted 24.04.2019
Scheduled in the issue 08.05.2019

Author:

Kobzev, Kirill O.,
associate professor of the Transport Systems Operation and Logistics Department, Don State Technical University (1, Gagarin sq., Rostov-on-Don, 344000, RF), Cand. Sci. (Eng.),
ORCID: https://orcid.org/0000-0002-5633-3352
5976765@mail.ru

МАШИНОСТРОЕНИЕ И МАШИНОВЕДЕНИЕ
MACHINE BUILDING AND MACHINE SCIENCE

UDC 622.323; 629.3.064.3 https://doi.org/10.23947/1992-5980-2019-19-2-164-169

Effectiveness analysis of external heating system of gauge tank of pumping unit using exhaust piping of the IC engine *

S. O. Kireev[1], V. N. Stepanov[2], M. V Korchagina[3], A. V. Yefimov[4]**
[1, 2, 3, 4] Don State Technical University, Rostov-on-Don, Russian Federation

Анализ эффективности системы внешнего обогрева мерной емкости насосной установки от выхлопной системы двигателя внутреннего сгорания***

С. О. Киреев[1], В. Н. Степанов[2], М. В. Корчагина[3], А. В. Ефимов[4]**
[1, 2, 3, 4] Донской государственный технический университет, г. Ростов-на-Дону, Российская Федерация

Introduction. The heating efficiency or regulation of the operating temperature of the fluid located in the gauge tank of a mobile pumping unit (PU) using the exhaust system of the internal combustion engine (ICE) is studied. The paper objective is to improve the design process and to reduce costs of field experiments.

Materials and Methods. To solve this problem, numerical analysis methods were used when calculating the heating systems of the gauge tank with the external location of the pipeline from the ICE exhaust system by the example of the widely used installations (TsA-320, UNB, AChF, etc.). Siemens STAR-CCM+, a non-stationary non-linear solver of gas-dynamic processes, was used, which evaluates the correctness of the problem statement and reduces significantly the costs of full-scale field tests.

Research Results. The study was conducted for the operating conditions of the cementing unit on the Kamaz-43118 chassis with the SIN-32 pump and a drive from the power take-off attachment on the gearbox of the chassis engine. In the calculation model, a convection-type heat transfer was applied between the body of the gauge tank and the surrounding air; between the body of the gauge tank and the liquid; between the chassis exhaust system duct and ambient air; between the exhaust system duct and exhaust gases. The following study results were obtained: characteristic curves of the temperature variation of the gauge tank liquid at the watch points; the distribution of the temperature field of the liquid in the gauge tank; the distribution of the ambient air temperature field; lines of flows and ambient air speed field and of the ICE exhaust gases.

Введение. Статья посвящена исследованию эффективности обогрева или поддержания рабочей температуры жидкости, находящейся в мерной емкости передвижной насосной установки, от выхлопной системы двигателя внутреннего сгорания. Цель работы — совершенствование процесса проектирования и снижение затрат на натурные эксперименты.

Материалы и методы. Для решения поставленной задачи были использованы методы численного анализа при расчете систем обогрева мерной емкости с внешним расположением трубопровода от выхлопной системы двигателя внутреннего сгорания (ДВС) на примере широко распространенных установок ЦА-320, УНБ, АЧФ и др. Применен нестационарный нелинейный решатель газодинамических процессов (Siemens STAR-CCM+), позволяющий оценить правильность постановки задачи и значительно сокращающий затраты на полномасштабные натурные испытания.

Результаты исследования. Исследование проводилось для условий работы цементировочного агрегата на шасси «Камаз-43118» с насосом «СИН-32» и приводом от коробки отбора мощности на коробке переключения передач двигателя шасси.

В расчетной модели применен конвекционный тип теплопередачи между корпусом мерной емкости и окружающим воздухом; между корпусом мерной емкости и жидкостью; между трубопроводом выхлопной системы шасси и воздухом окружающей среды; между трубопроводом выхлопной системы и выхлопными газами.

В результате исследования получены графические зависимости изменения температуры жидкости мерной емкости в контрольных точках; распределение поля температур жидкости в мерном баке; распределение поля температур окружающего воздуха; линии потоков и поля скоростей окружающего воздуха и выхлопных газов ДВС.

* The research is done within the frame of the independent R&D no. AAAA-A18-118120390043-0 of 03.12.2018.
**E-mail: kireevso@yandex.ru, st_fem@bk.ru , ms.korchaginamv@mail.ru, spu-45.2@donstu.ru
*** Работа выполнена в рамках инициативной НИР № AAAA-A18-118120390043-0 от 03.12.2018 г.

Discussion and Conclusions. The study has revealed poor effectiveness of the considered structure. The data analysis allows us to offer an improved design of the gauge tank heating. The results obtained in the work can be used in the calculations of such devices used in the hydraulic fracturing units and grout machines.

Обсуждение и заключения. В ходе исследования выяснилась недостаточная эффективность рассматриваемой конструкции. Анализ данных позволяет предложить усовершенствованную конструкцию обогрева мерной емкости. Результаты, полученные в работе, могут быть использованы при расчетах подобных устройств, применяемых в установках гидроразрыва пласта и цементирования скважин.

Keywords: mobile pump unit, gauge tank, water feeding pump, high pressure pump, internal combustion engine (ICE).

Ключевые слова: передвижная насосная установка, мерная емкость, водоподающий насос, насос высокого давления, двигатель внутреннего сгорания (ДВС).

For citation: S.O. Kireev, et al. Effectiveness analysis of external heating system of gauge tank of pumping unit using exhaust piping of the IC engine. Vestnik of DSTU, 2019, vol. 19, no. 2, pp. 164−169. https://doi.org/10.23947/1992-5980-2019-19-2-164-169

Образец для цитирования: Анализ эффективности системы внешнего обогрева мерной емкости насосной установки от выхлопной системы двигателя внутреннего сгорания / С. О. Киреев [и др.] // Вестник Дон. гос. техн. ун-та. — 2019. — Т. 19, № 2. — С. 164−169. https://doi.org/10.23947/1992-5980-2019-19-2-164-169

Introduction. The deposits of hard-to-recover hydrocarbons in the northern latitudes of Russia are confined to low-permeable, low-drained, heterogeneous and segregated reservoirs. Whereas it is necessary to develop such oil and gas areas, need arises for a guaranteed the above-zero temperature of the liquid that is in the gauge tank of the installation. This problem remains relevant in the construction and workover of wells.

The quality of hydraulic fracturing (HF) fluid, drilling fluid and cement slurry is affected by the following factors:

- types of rocks that interact with these systems;
- well depth (pressure);
- bottomhole temperature.

We will accept two statements of the TNK-BP standard “Quality and Compliance under HF”:

1) liquid chemicals specific for mixing at the well pad should be stored or transported above 15ºC;

2) storage, transportation, testing and injection of all liquid reagents should be carried out above 15ºC, regardless of weather conditions [1].

The temperature of the system should not be lower than 8–10° C for all types of work on the preparation of the tempering fluid, pressurizing systems and systems of drilling and flushing solutions [2].

The 1979 oil and gas equipment literature mentions the use of a chassis or deck engine (TsA-320A cementing unit) for heating the exhaust gas system of the engine [3]. There are references to the vent dehumidifying system of the booster pulser hydraulic unit in two operating manuals: “Pumping units UNB-1000, UNB-800, UNB-630” and “Cementing hydraulic fracturing unit ACF-1050. UPETROM”. In the operating manuals of “Two-pump mobile unit UNP-320 × 40” and “Pumping unit UNB-125-50 SO”, the items on operating the drying and heating systems are highlighted.

In the present paper, the effectiveness of external heating system of gauge tank of pumping unit using exhaust piping of the IC engine is analyzed.

Materials and Methods. Methods of numerical simulation were used. As examples, the widespread installations of the TsA-320, UNB, AChF, and others were considered.

The application of numerical methods permits to assess the correctness of the problem statement (with an error of an idealized model selection), reduces significantly the cost of full-scale field tests or fully proves the design-engineering inefficiency of the problem. In the absence of statistical data on the problem under study, the results of numerical methods narrow the spectrum of the field problems to be solved. The non-stationary nonlinear solver of gas-dynamic processes (Siemens STAR-CCM +) [4] was applied as a numerical method tool.

For the numerical study, the problem of heating a two- compartment gauge tank was selected. For this purpose, the cementing unit on the Kamaz-43118 chassis with the SIN-32 pump and a drive from the power take-off attachment on the gearbox of the chassis engine were used. In the rear zone of the chassis truck, capacity of 2 × 2 m^3 was installed. It is an all-welded sheet-metal construction which has two compartments with a sloping bottom and bottom valves. In the scheme proposed for calculation and analysis, the exhaust pipe (heating pipe) passes under the bottom of the gauge tank and rises upwards along the wall of the left tank (Fig. 1).

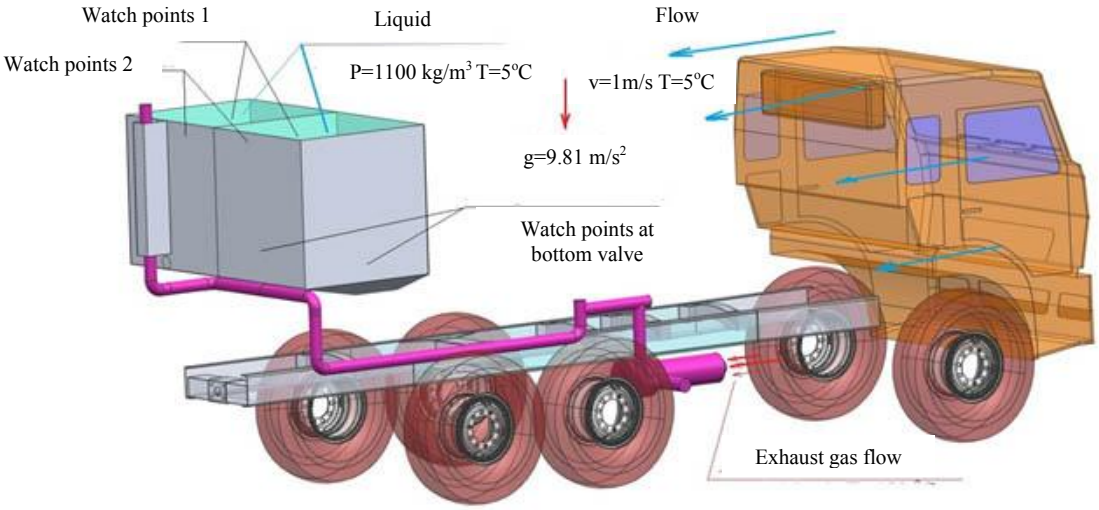

Fig. 1. Idealized design model of cementing unit on "Kamaz-43118" chassis with "SIN-32" pump

Research Results. The study was conducted for the following operating conditions of the unit at the field:
- pump unit is fixed;
- ambient temperature (air) is 5°C above zero;
- wind speed is 1.0 m/s;
- liquid density in both sections of the gauge tank is 1100 kg / m3;
- liquid temperature in gauge tank is 5°C above zero.

In the calculation model, a convection-type heat transfer was applied between the following media was used:
- body of the gauge tank and the surrounding air;
- body of the gauge tank and liquid;
- chassis exhaust system duct and ambient air;
- exhaust system duct and exhaust gases.

To simplify the task, air was used as exhaust gases to eliminate the application of a multiphase solver.

Air parameters were as follows: density was 1.184 kg m^3; thermal conductivity was 0.026 W/m·K; specific heat capacity was 1003.6 J/kg·K.

The parameters of the liquid in the gauge tank were as follows: density was 1100 kg/m^3; thermal conductivity was 0.569 W/ m·K; specific heat capacity was 4217 J / kg·K.

The material parameters of the steel body of the gauge tank and the exhaust system duct were as follows: density was 7832 kg/m^3; thermal conductivity was 63.9 W/m·K; specific heat capacity was 434.0 J/kg·K; thickness of the body sheet of the gauge tank was 4 mm; exhaust pipe thickness was 3 mm [5].

The exhaust gas outlet temperature of the ICE manifold was 450° C [5, 6]; the exhaust outlet flow of the engine manifold was 35 m/s [5].

The calculation (see Fig. 1) was made from the ICE working condition for 1800 seconds (30 minutes). The test points of the liquid temperature were obtained for the left and right compartments of the gauge tank at the bottom valves at a distance of 200 mm from the bottom, at a distance of 1000 mm from the bottom (T1), and at a distance of 1000 mm from the bottom and 200 mm from the back wall (T2). The liquid temperature lines during the ICE operation for 30 minutes are shown in Fig. 2. The temperature fields and current lines are shown in Fig. 3–6.

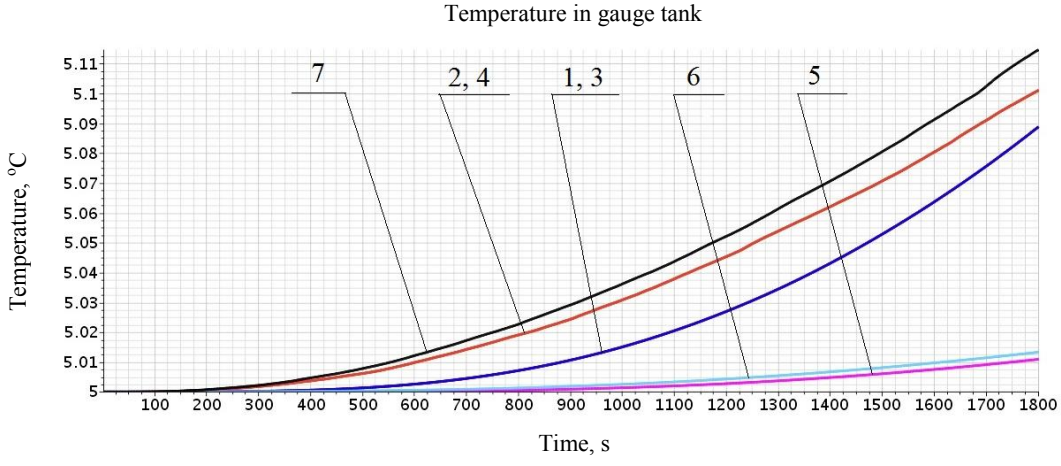

Fig. 2. Liquid temperature lines of gauge tank at watch points: 1 is temperature at top point of left gauge-tank compartment; 2 is temperature in left compartment (point 1); 3 is temperature in left compartment (point 2); 4 is temperature in left gauge-tank compartment at bottom valve; 5 is temperature in right compartment (point 1); 6 is temperature in right compartment (point 2); 7 is temperature in right gauge-tank compartment at bottom valve.

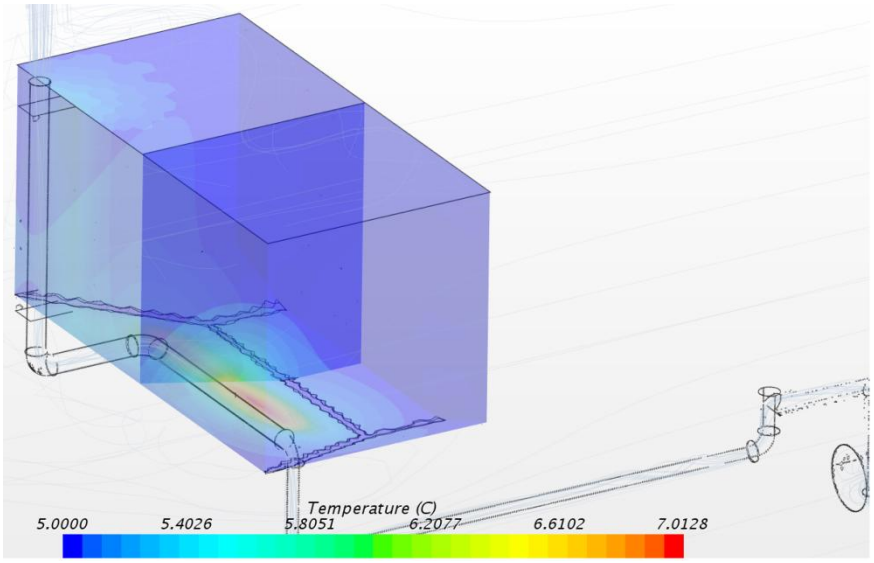

Fig. 3. Distribution of liquid temperature field in gauge tank (left view)

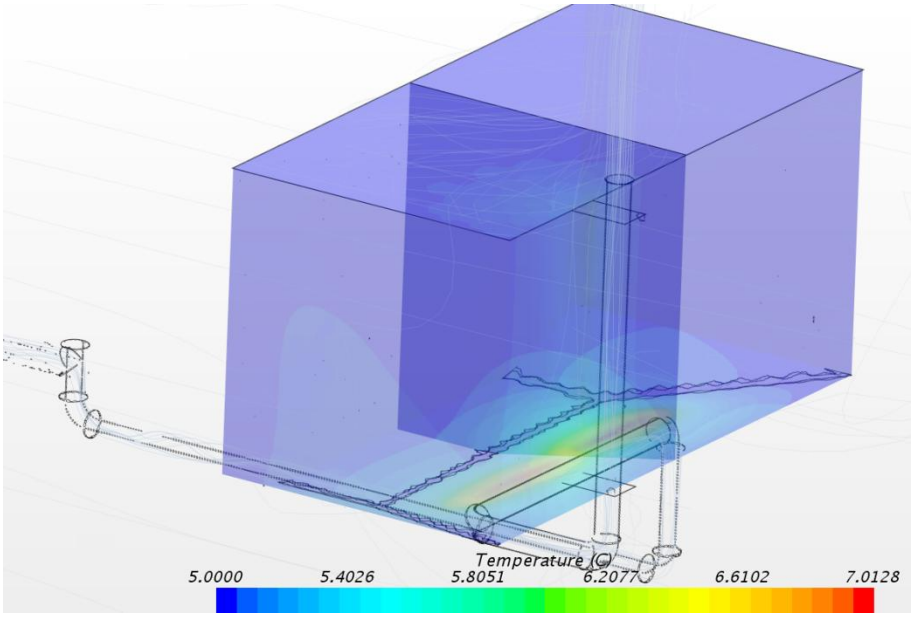

Fig. 4. Distribution of liquid temperature field in gauge tank (right view)

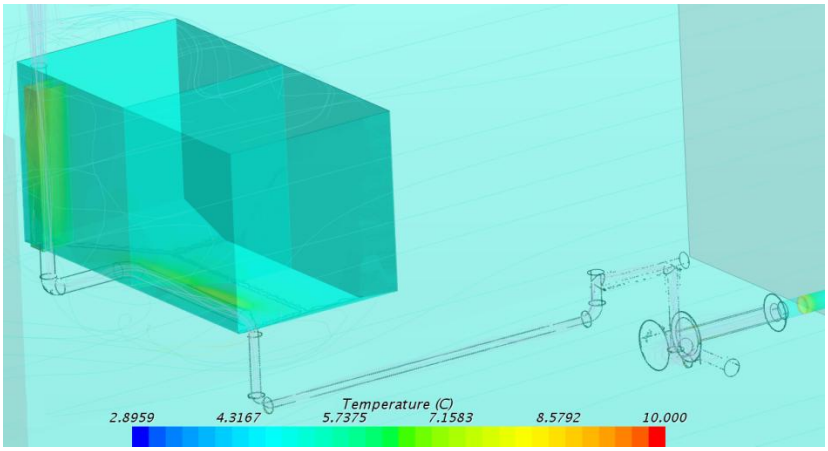

Fig. 5. Distribution of ambient air and gauge-tank body temperature field

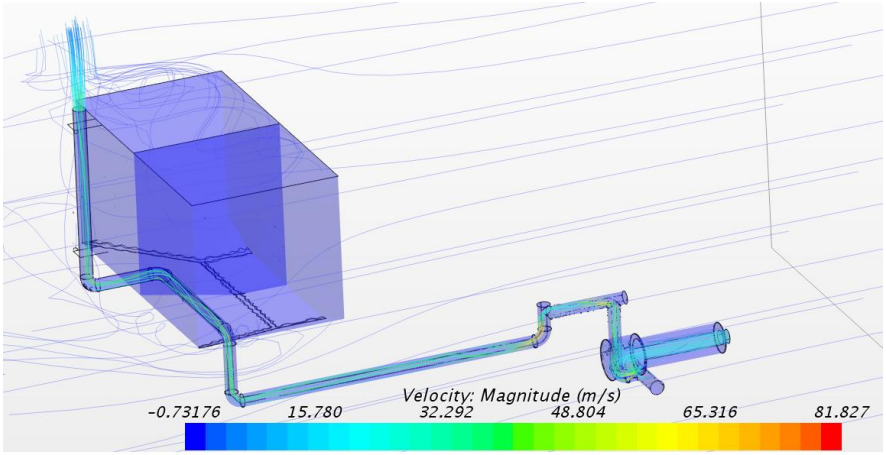

Fig. 6. Flow line and speed field of ambient air and ICE exhaust gases

Discussion and Conclusions. The calculation results obviously demonstrate that for 30 minutes of the ICE operation and convection heat exchange between the hot exhaust pipe, air and liquid in the gauge tank at the test points at the bottom valves, the liquid is heated up to 0.1° C in the left compartment and to 0.1 ° C in right compartment.

This brings us to the following conclusion: at the considered variant of the constructive solution, most of the thermal energy is directed to the operator's cabin heating. This is a positive factor, but not a solution to the problem. The studies and graphical dependences show that it is required to place the exhaust tube directly in the gauge tank for a more efficient distribution of heat flows inside the gauge tank and in the environment. Given the design features, it is advisable to place the pipe inlet at the bottom of the right side of the tank and, passing through the left side, direct it along the tank up to the relief passage.

In order to determine the possibility of heating the gauge tank, it is necessary to carry out calculations for a new schematic construction.

References

1. Ob"edinennye standarty TNK-VR po soblyudeniyu kontrolya kachestva pri provedenii GRP i kislotnykh obrabotok. Iyun' 2008. Version 11.1 [TNK-BP combined standards for the observance of quality control during hydraulic fracturing and acid treatments. June, 2008. Version 11.1] TNK-BP. Available at: https://www.petroleumengineers.ru/sites/default/files/qaqc_version_11.1_final.pdf (accessed 20.01.18) (in Russian).

2. RD 39-00147001-2000. Instruktsiya po krepleniyu neftyanykh i gazovykh skvazhin. [RD 39-00147001-2000. Instructions for fixing oil and gas wells.] Directorate for drilling gas and gas condensate wells of OAO Gazprom; NGO "Burenie". Library of regulatory documentation. Available at: https://files.stroyinf.ru/Data2/1/4293809/4293809149.htm (accessed 27.03.19) (in Russian).

3. Bezborodny, I.O., et al. Spravochnoe rukovodstvo po tsementirovochnomu oborudovaniyu. [Cementing Equipment Reference Guide.] Moscow: Nedra, 1979, 202 p. (in Russian).

4. Siemens STAR-CCM+ Multidiscipliary Design Exploration. Siemens. Available at: www.siemens.com/mdx (accessed 11.05.18).

5. MAN Diesel & Turbo. Exhaust Gas System. MAN Energy Solutions. Available at: https://marine.man-es.com/applications/projectguides/4stroke/manualcontent/PG_M-II_L1624.pdf (accessed 16.02.18).

6. Donaldson. Engine Horsepower & Exhaust Flow Guide. Donaldson Company. Available at: https://www.donaldson.com/content/dam/donaldson/engine-hydraulics-bulk/catalogs/Exhaust/North-America/F110028-ENG/Exhaust-Product-Guide.pdf (accessed 20.05.18).

Submitted 28.03.2019
Scheduled in the issue 15.04.2019

Authors:

Kireev, Sergey O.,
Head of the Oil and Gas Complex Machinery and Equipment Department, Don State Technical University (1, Gagarin sq., Rostov-on-Don, 344000, RF), Dr.Sci. (Eng.), professor,
ORCID: http://orcid.org/0000-0001-9352-3852
kireevso@yandex.ru

Stepanov, Valentin N.,
senior lecturer of the Oil and Gas Complex Machinery and Equipment Department, Don State technical University (1, Gagarin sq., Rostov-on-Don, 344000, RF),
ORCID: https://orcid.org/0000-0002-1425-9174
st_fem@bk.ru

Korchagina, Marina V.,
associate professor of the Oil and Gas Complex Machinery and Equipment Department, Don State Technical University (1, Gagarin sq., Rostov-on-Don, 344000, RF), Cand.Sci. (Eng.),
ORCID:http://orcid.org/0000-0001-7092-7176
ms.korchaginamv@mail.ru

Yefimov, Andrey V.,
associate professor of the Oil and Gas Complex Machinery and Equipment Department, Don State technical University (1, Gagarin sq., Rostov-on-Don, 344000, RF), Cand.Sci. (Eng.), associate professor,
ORCID: https://orcid.org/0000-0001-9940-9030
spu-45.2@donstu.ru

МАШИНОСТРОЕНИЕ И МАШИНОВЕДЕНИЕ
MACHINE BUILDING AND MACHINE SCIENCE

UDC 621.792.8 https://doi.org/10.23947/1992-5980-2019-19-2-170-178

On ensuring joint tightness on the basis of technological induction*

G. A. Pilyushina[1], P. G. Pyrikov[2], E. A. Pamfilov[3], V. V. Kapustin[4]**
[1,2,3,4]Bryansk State Technical University, Bryansk, Russian Federation

К вопросу обеспечения герметичности соединений на основе технологического индуцирования***

Г. А. Пилюшина[1], П. Г. Пыриков[2], Е. А. Памфилов[3], В. В. Капустин[4]**
[1,2,3,4]Брянский государственный технический университет, г. Брянск, Российская Федерация

Introduction. Some theoretical and engineering aspects of sealing joints through magnetostriction, as well as the polarization of the sealed medium under the external induction are considered. Control of surface roughness of joined parts to increase the joint density when induced by an external magnetic field is studied. The creation of electromagnetic barriers for the migration of molecules of the sealed medium through a sealer is considered. The work objective is to validate the technological conditions for sealing movable joints in the cases described above.

Materials and Methods. The conditions for ensuring the joint density are shown as a result of the contact problem solution and as a factor determined by the molecular-mechanical friction theory. Geometric, operational and tribological conditions of joint tightness are accepted. Damping properties of the fixed friction contact are determined by the molecular component. The theoretical and calculated analysis of the factors affecting the joint density is presented. Decrease in the smoothing depth, reduction of the ratio of transverse and longitudinal roughness steps, and increase in the contact area are indicated as the target results of the process preparation of the surfaces of the joint parts. Loss of tightness is defined as a specific transfer of molecules. They are transferred to the area of the joined surfaces or migrate freely through the sealer at the stages of sorption, diffusion and desorption. The predominance of any stage occurs when the entropy changes, and it is due to temperature and pressure. The schemes of sealing joints in the controlled magnetic field and of the dependence of magnetostriction and magnetostrictive stresses on the magnetic field strength are visualized.

Research Results. The stability of sealers in highly volatile and gaseous media during their polarization and magnetization in an external field is experimentally investigated. In the former case, the magnetic induction vector was first oriented perpendicular to the longitudinal axis of the joint. A drop in the magnitude of the magnetic flux was observed when the

Введение. Статья посвящена некоторым теоретическим и технологическим аспектам обеспечения герметичности соединений на основе магнитострикции, а также поляризации герметизируемой среды в состоянии внешнего индуцирования. Исследовано управление шероховатостью поверхностей стыкуемых деталей для повышения плотности стыка при их индуцировании внешним магнитным полем. Рассмотрено создание электромагнитных барьеров для перемещения молекул герметизируемой среды через герметизатор. Цель работы — обоснование технологических условий обеспечения герметичности подвижных соединений в описанных выше случаях.

Материалы и методы. Условия обеспечения плотности стыка показаны как результат решения контактной задачи и как фактор, определяемый положениями молекулярно-механической теории трения. Приняты геометрические, эксплуатационные и трибологические условия герметичности соединений. Демпфирующие свойства неподвижного фрикционного контакта определены молекулярной составляющей. Представлено теоретическое и расчетное обоснование факторов, влияющих на плотность стыка. В качестве целевых результатов технологической подготовки поверхностей деталей соединения указаны уменьшение глубины сглаживания, уменьшение отношения шагов поперечной и продольной шероховатости и увеличение площади контакта. Потеря герметичности определена как специфический трансфер молекул. Они переносятся в зону стыкуемых поверхностей или свободно перемещаются через герметизатор на стадиях сорбционного поглощения, диффузии и десорбции. Преобладание какой-либо стадии происходит при изменении энтропии и обусловлено температурой и давлением. Визуализированы схемы герметизации соединений в управляемом магнитном поле, зависимости магнитострикции и магнитострикционных напряжений от напряженности магнитного поля.

Результаты исследования. Экспериментально исследована устойчивость герметизаторов в легколетучих и газовых средах при их поляризации и намагничивании во внешнем поле. В первом случае сначала вектор магнитной индукции ориентировался перпендикулярно продольной оси

* The research is done within the frame of Contract No. 9.10677.2018/11.12.
** E-mail: gal-pi2009@yandex.ru, pyrikovpg@mail.ru, epamfilov@yandex.ru, vovakapustin1990@mail.ru
*** Работа выполнена по договору 9.10677.2018/11.12.

compound was under the on-load operation for 268 hours. The total operating time of the joint was 1070 hours. If the magnetic induction vector was oriented longitudinally to the shaft axis, the operating time to the correction of the field strength was 87 hours. In the gas environment, the operating time of the connection to the adjustment of the tension was 187 hours with a total operating time of 935 hours.

Discussion and Conclusions. The penetrating ability of pressurized media decreases in the "gas – vapor – liquid" series. It depends on the temperature at the joint contact. Depressurization can be traced through changes in the magnetic flux determined by the intrinsic magnetic permeability of the molecules of the sealed medium as they penetrate the interface surface.

To increase tightness, it is required to suppress the activity of molecules. For this purpose, ionization and induction in the constant and alternating magnetic field with the intensity of <60 kA/m are used.

Keywords: tightness, joint, machine parts, induction, density,magnetic field, crystallographic ordering, contact rigidity, anisotropic effects.

For citation: G.A. Pilyushina, et al. On ensuring joint tightness on the basis of technological induction. Vestnik of DSTU, 2019, vol. 19, no. 2, pp. 170−178. https://doi.org/10.23947/1992-5980-2019-19-2-170-178

соединения. Установлено падение величины магнитного потока при работе соединения под нагрузкой в течение 268 часов. Общая наработка соединения составила 1070 часов. Если же вектор магнитной индукции ориентировался продольно оси вала, наработка до момента коррекции величины напряженности поля составила 87 часов. В газовой среде продолжительность работы соединения до момента корректировки напряженности составила 187 часов при общей наработке 935 часов.

Обсуждение и заключения. Проникающая способность герметизируемых сред уменьшается в ряду «газ — пар — жидкость». Она зависит от температуры на контакте соединения. Разгерметизацию можно отследить по изменениям магнитного потока, определяемого собственной магнитной проницаемостью молекул герметизируемой среды при их проникновении на поверхность стыка. Чтобы повысить герметичность, необходимо подавить активность молекул. Для этого применяются ионизация и индуцирование в постоянном и переменном магнитном поле напряженностью <60 кА/м.

Ключевые слова: герметичность, соединение, детали машин, индуцирование, плотность, магнитное поле, кристаллографическое упорядочение, контактная жесткость, анизотропные эффекты.

Образец для цитирования: К вопросу обеспечения герметичности соединений на основе технологического индуцирования / Г. А. Пилюшина [и др.] // Вестник Дон. гос. техн. ун-та. — 2019. — Т. 19, № 2. — С. 170−178. https://doi.org/10.23947/1992-5980-2019-19-2-170-178

Introduction. The theoretical basis of hermetology is presented in the works of G.A. Golubev, A.V. Chichinadze, V.P. Tikhomirov, L.A. Kondakova, G.V. Makarova, H.H. Wachter, E.Mayer, R.H.Waring, etc. It is known that tightness is mostly due to two factors:

- stability of the processing density of abutting rough surfaces of the sealer parts;

- stability of the sealer material properties and the sealed medium excluding the penetration and migration of molecules through its sealer beyond the interface.

The conditions for ensuring the joint consistency are justified through solving the contact problem and are largely determined by the principles of the molecular-mechanical friction theory [1, 2, 3]. The mentioned approach remains one of the fundamental in hermiticity engineering.

Penetration of sealed media (liquids, gases) through the sealer is described by the physical model of S. Slichter, I. Kozeni, T. Carman and D.K. Kollerov (for porous polymers). From its analysis, it follows that the volume flow of the medium through the seal is determined by the length of the free path of the molecules [4, 5, 6] and depends on the following:

- microroughness height of solid surface - R_{max},
- joint density - P,
- relative approximation - ε,
- geometrical dimensions of seal.

Specifically, the fretting operation is initiated by boundary structures which are different polymer seals, liquids and films on the interfaces at the amplitudes of contact vibrations less than 0.05 mm. These media can act as catalysts; that causes a decrease in the technologically secured design value of the specific pressure on the seal and increases leakage.

The amplitude and frequency of the relative displacements of the joint parts can be reduced through controlling the joint density, for example, through increasing the nominal pressure on the seal. The studies performed on polymers in the friction units [7] show that the joint density and contact rigidity depend largely on the compressive force of surfaces and on their intermolecular activation:

$$F_{mp} = aS + bP_y,$$

where F_{mp} is friction force; a is average intensity of the molecular component of the friction force; S is true contact area; b is coefficient of the mechanical component of the friction force; P_y is surface compression force.

Consequently, the molecular component aS is proportional to:

- the true contact area,
- the intensity of mutual adhesion of contacted materials.

Both of these indicators can be increased through plastic saturation along the interface plane, as well as during the alignment of the joint parts. Similar conditions can be created on the basis of magnetostrictive effects, which are pronounced to a greater degree for textured materials. Such conditions are applicable also in cases when reloading of joint parts is hindered or not provided for by the engineering performance standards.

A decrease in the penetrating power of sealed media is predicted when a mobile spherulitic structure of the sealer is formed or modified by sealing with low-modulus materials [8]. However, the conditions that develop at drastically negative temperatures and under cracking of the polymer sealer require special consideration. In these cases, differences in the temperature linear expansion coefficients with metals are observed; therefore, to control the permeability of the sealed medium molecules through creating electromagnetic barriers for them is of interest.

Now then, this work objective is to study the technological conditions for ensuring the joint tightness based on the induction effects created in the materials of the joint parts and in a sealed environment.

Materials and Methods. The conditions for joint tightness follow from the conclusions of the Lame problem, in which the boundary factors are:

- geometric (for example, l - length of the contact of surfaces and d - diameter of the mating parts);
- operational (R_{oc} - longitudinal axial force or $M_{кр}$ - torque tending to move one part relative to another);
- tribological (f - friction factor) determining the moment of pressing or turning.

Friction locking is provided while minimizing the amplitude of the relative displacements of the surfaces, at contact stresses not exceeding the region of the damping capacity of materials [7].

Damping properties of the fixed friction contact are determined, in particular, by the molecular component. Moreover, the interface with the textured (anisotropic) structure in the direction of ensuring high damping capacity allows for a higher value of the critical vibration loads in a wide frequency range [8].

In addition, when an external induction changes R_a roughness parameter due to the magnetostrictive effect, they can affect the joint density. This is explained by the comparability of magnetostriction values and the sizes of blocks of structural components (about 10^{-4}–10^{-5} m). Moreover, the technological texturing in crystallographic directions with pronounced maxima of the elastic or plastic properties of materials causes a maximum magnetostriction effect at the unidirectional position of the magnetic induction vector. This causes an increase of the nominal pressure value in the preloaded demountable joints since part of the stresses spending on the parts' compliance is compensated by magnetostrictive stresses within the elastic properties. In permanent joints, on the contrary, part of the stresses can be spent on the plastic saturation of the contact. For the same reason, the actual preload is greater than the calculated one.

P is joint density coefficient with magnetostrictive effect:

$$P = (V_{1m(hkl)} + V_{2m(hkl)})k_{(hkl)} / V_{общ}. \quad (1)$$

Here, $V_{1м(hkl)}$ is the material volume of the rough layer with hkl texture; $V_{2м(hkl)}$ is the material volume of an incompressible seal extruded into the gaps; k is the magnetostriction coefficient; $V_{общ}$ is the total volume of the rough layer.

It is known that the presence of waves causes a decrease in the bearing contact area by a factor of 5–10 [9]. Therefore, the solution to the contact problem in the aspect of ensuring the joint tightness requires consideration of the waviness of the surfaces.

The height and step parameters of roughness are interrelated; therefore the technological preparation of the surfaces of the joint parts should be aimed at the following results:

- reducing the depth of smoothing (R_p);
- reducing the ratio of steps of transverse and longitudinal roughness;
- increasing the contact area and R_p / R_a ratio.

As a rule, there is no direct relationship between the tolerance value and the height of irregularities; however, it should be noted that the depressions on the surface profilogram turn out to be reservoirs in which by-products accumulate, which initiate surface weakening.

While ensuring the joint density due to the preload, S_N compliance of the compound is represented as:

$$S_N = x(t) + (\xi_{(hkl)}(B)k^{`}) / N^*, \quad (2)$$

where x (t) is normal contact displacement in the function of time; $\xi_{(hkl)}(B)$ is the magnetostriction tensor at a regulated crystallographic ordering considering plastic deformations in the coating and changing with magnetic induction; $k`$ is coefficient of crystallographic ordering; N*is dynamic load.

When the compounds operate under the hydrostatic pressure of the sealed medium (liquid or gas), loss of tightness is expressed in a certain form of transfer of molecules. They are transferred to the area of the joined surfaces or migrate freely through the sealer at the stages of sorption, diffusion and desorption. The predominance of any stage occurs when the entropy changes, and it is due to temperature and pressure.

The simplest case of phase transfer in seals is the flow of a viscous incompressible fluid in a porous medium. The determination of the leakage value follows from the Darcy law. However, in this case, it is not considered that the sealing joint, in contrast to the porous solid body, is formed as a result of the contact of two surfaces. Therefore, under the load increase and the alignment of the surfaces, individual contact spots can form isolated volumes (effective channels). Their number decreases with increasing load until the formation of a hydrodynamic film along the seal perimeter [10–11]. Thus, considering the conductive capacity of most sealed media, it is advisable to investigate tightness from the standpoint of polarization and external induction.

According to [12], when a medium passes through an electric current source or ionizer, molecules obtain q charge. If a charged particle with an initial velocity v moves in a uniform magnetic field along the magnetic induction lines B of the external field, then the angle α between the vectors of v and B is equal to zero. The magnetic field does not affect the particle (the Lorentz force is also zero), and it moves uniformly and rectilinearly.

If a charged particle moves with velocity v in a magnetic field perpendicular to vector B, then the Lorentz force $F = q[\nu B]$ is constant in magnitude and perpendicular to the particle trajectory, which prevents its displacement (Fig. 1, *a*).

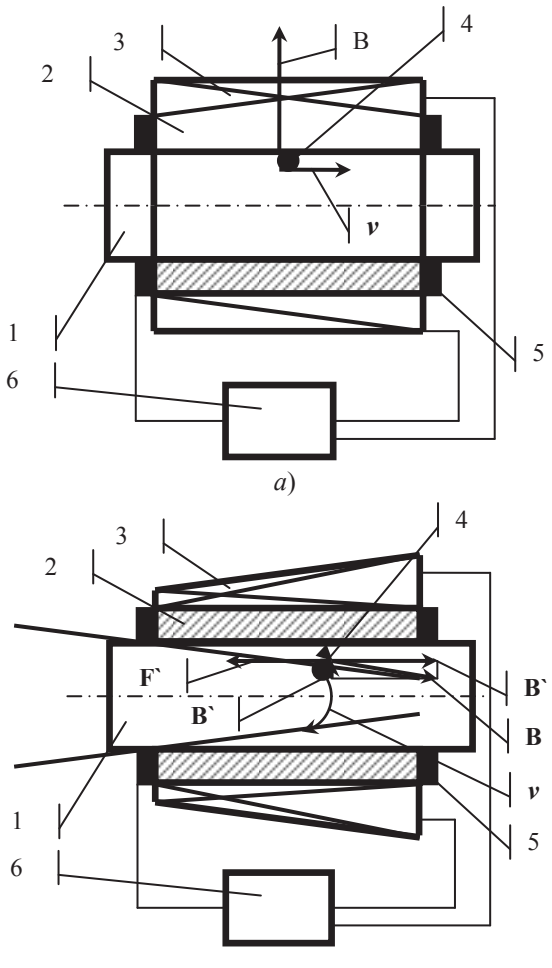

Fig. 1. Schemes for sealing joints in controlled magnetic field: in uniform field of toroidal inductor (*a*); in inhomogeneous field solenoid (*b*); 1 is shaft; 2 is sleeve; 3 is magnet; 4 is charged medium particle; 5 is source of electric current (or ionizer); 6 is automatic solenoid control unit with voltage generator); v is orbit of positively charged medium particle

Assuming the direction of medium motion, knowing its electric potential, viscosity, density, penetrating ability, and changing the field strength and the position of the magnetic induction vector, it is possible to provide the Lorentz force in quantities sufficient to completely suppress the motion. Thus, the effect reactive to the hydrostatic pressure is realized.

Similarly, in an inhomogeneous magnetic field, the component of magnetic induction $B`$ creates force F', which pushes the particle into the region of a weak field (see Fig. 1, *b*). Initially, the particle moves along the radius of constant magnitude with velocity *v*. However, its own magnetic field counteracts the externally induced one, and this explains the extreme instability of its state. As a result, the particle is pushed into the field region with a reduced voltage.

The sealing effect is based on creating – by the magnetic field – the reactive repulsion of pre-charged medium molecules penetrating the interface. Whereby, the degree of sealing depends on the magnetic inductance, the value of which is set through the strength of the current considering the relative magnetic permeability and form factor of the inductor.

It can be assumed that the conditions of joint vacuumization are created when the surfaces of the mating parts come closer to the appearance of molecular (adhesive) interaction. In this case, the magnetic permeability of the materials of the joint components is represented by the ratio of the magnetic fluxes in the material Φ and in vacuum $\Phi 0$ ($\mu = \Phi/\Phi_0$). Under the assumption of $\Phi = \Phi_0$, the magnetic permeability of vacuum can be taken as a unit ($\mu = 1$).

In the medium with constant magnetic permeability, the magnetic field induction is proportional to its density. Consequently, the magnetic flux from the external field, initially defined for vacuum, depends on the magnetic permeability of the medium. Its presence at the interface, due to its own magnetic permeability, either increases the magnetic flux (in paramagnetic media), or decreases it (in diamagnetic media).

Thus, it is possible to evaluate and correct the performance of the sealer in the induction state through changing the magnetic flux and, accordingly, magnetic induction.

Research Results. The crystallographic areas described below can be taken as regulated directions under the process part texturing.

1. For detachable joints without a polymer sealer: [110] (for structures with body-centered cubic (bcc) lattice), [111] (with face-centered cubic (fcc) lattice), [1000] (with hexagonal close-packed (hcp) lattice).

2. For permanent joints and connections with a sealer: [100] - [111] (with bcc lattice), [100] - [110] (with fcc lattice), [0001] - [2110] (with hcp lattice).

When the magnetic induction vector is established in the indicated directions, the magnetostriction λ in the crystals turns out to be field oriented. This is because its magnitude is non-linear to the field strength and is determined mainly by the position of the easiest magnetic axis [13, 14].

In the absence of preliminary texturing, a mean change in roughness for structures with cubic lattices is represented as:

$$0 \le \Delta\overline{R}_a < \left(\frac{2}{5}\lambda_{100} + \frac{3}{5}\lambda_{111}\right)d`, \tag{3}$$

where λ_{100}, λ_{111} are magnetostriction constants along the [100] and [111] crystallographic directions; $d`$ is an average size of the dispersed structural components.

In the case of texturing in the directions [100] or [111], when the field is oriented along the normal to the surface (Fig. 2), the changes in roughness (R_a) will be:

$$0 \le \Delta\overline{R}_a < \lambda_{100}\overline{d} / k, \tag{4}$$

$$0 \le \Delta\overline{R}_a < \frac{3}{4}\lambda_{111}\overline{d} / k, \tag{5}$$

where *k* is demagnetization loss factor.

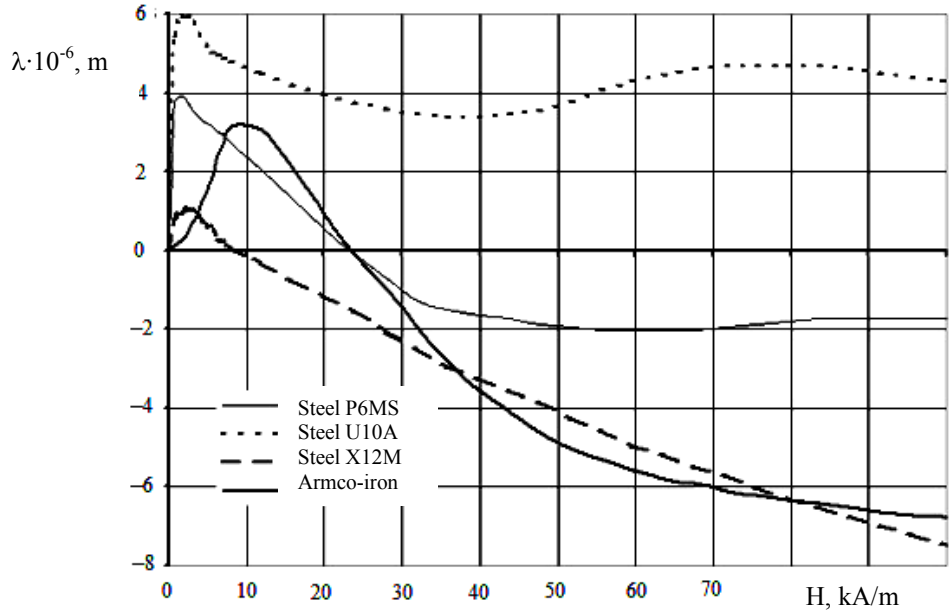

Fig. 2. Magnetostriction λ – magnetic field intensity *H* dependence

Valves with a seat made of X12M steel with a coating in the direction [111] of $CoFe_2O_4$ cobalt ferrite coating with thickness of 20×10^{-5} m (R_{max} 2.4 μm, $r_1 = 52\times10^{-3}$ and $r_2 = 50\times10^{-3}$ m) and a brass valve by the amount of leakage flow of Q, μPa • m^3/s of helium (T = 77 K) are tested. It is established that, during the compound magnetization in the field of 60 kA/m, this value is 780–10240. The number of shutter cycles is 200–5000, respectively. Under similar test conditions for a saddle-valve pair in the absence of a magnetic field and prior texturing of saddles, the Q value was 960–15340 μPa • m^3/s, respectively.

With an increase in the magnetic field strength, no major changes in the connection health are established. Apparently, this is due to the fact that effective magnetostriction stresses are formed in fields <40 kA/m (Fig. 3). This conclusion is consistent with the results of the magnetostriction study.

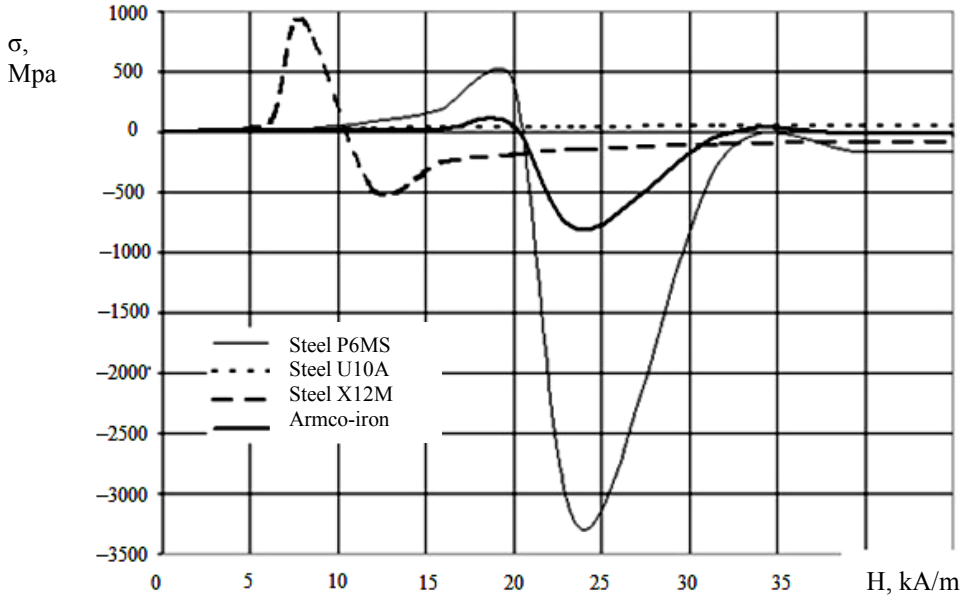

Fig. 3. Magnitude of magnetostriction stresses σ – magnetic field intensity *H* dependence

Changes in the properties of the sealed medium, the materials of the sealer and the temperature affect the penetrating ability and tightness in general. The permeability of media decreases in the "gas - vapor - liquid" series. With that in mind, the performance of sealers in volatile and gaseous media during their polarization and magnetization in an external field was investigated.

At the end of a rigid detachable shaft – copper hub connection, a source of electrical current was attached, one of the poles of which was fixed to the ends of the hub. At that, the second pole had a minimum clearance with the shaft generatrix.

The joint was placed between the poles of a toroidal electromagnet connected to the automatic control unit with a voltage generator, a voltmeter and a webermeter. The magnetic induction vector was oriented perpendicular to the longitudinal axis of the joint. The joint was installed in a chamber filled with diamagnetic benzene. Pressure of 30–35 kPa was developed in it. The sleeve was rigidly fixed, after which the source of electric current and the inductor were turned on, and the magnetic field strength was set at 60 kA/m. The shaft was mechanically loaded in the radial and axial direction relative to the sleeve in a symmetrical alternating cycle with the load of 1.5 N with the frequency of 50 Hz. The tests were performed until the reduction of the magnetic flux recorded upon the webermeter indication. This moment characterized the violation of tightness expressed in the penetration of benzene to the joint surface. The inductor automatic control unit corrected the voltage in the toroid, due to what the magnetic field strength was set equal to the initially predetermined one.

A drop in the magnitude of the magnetic flow was observed when the joint was under the on-load operation for 268 hours. The total operating time of the joint was 1070 hours. The criterion for the completion of the tests was the reduction of the interval of operating time until the moment of correction of the magnitude of the magnetic force. It should exceed 60 kA/m. This is due to the need to increase the operating time to the value corresponding to the previous cycles.

With the orientation of the magnetic induction vector longwise the axis of the shaft under similar test conditions, the operating time until the correction of the field strength was 87 hours.

The simulation of the operating conditions of the joints in the gas environment was carried out in a similar way. An ionizer was mounted on the shaft which was attached to the ends of the sleeve. The joint was placed in a solenoidal inductor, the density of the turns of which increased from the end of the sleeve. As a result, a non-uniform magnetic field was generated, the intensity of which increased from the end of the solenoid.

The joint was placed in a chamber under the pressure of 30–35 kPa with paramagnetic nitrogen, after which the ionizer and inductor were switched on. The shaft was loaded in the modes described above with periodic recording of the magnetic flow. The moment of changing its initial value characterized the violation of tightness and the penetration of nitrogen to the interface. In this case, the inductor automatic control unit provided a reduction in voltage in the solenoid winding to the value corresponding to the magnetic field strength of 60 kA/m.

The operating period of the joint until the adjustment of H value of was 187 hours with a total operating time of 935 hours. The long duration of the tests caused the correction of the magnetic field strength with the time interval of less than 187 hours.

Discussion and Conclusions. Reduction of leakage through the seals is provided by the joint density (specific pressure p_a) management while reducing the amplitude and frequency of the relative displacements of the joint parts. The latter is obtained through increasing the true contact area and the intensity of mutual adhesion of the contacted materials, in particular due to magnetostriction effects. In this case, the level of magnetostriction stresses should not cause plastic deformations of the sealer (ie, $p_a \approx 1.1\ \sigma_m$) and can be provided in the fields up to 40–50 kA/m. As the complex roughness parameter Δ changes due to magnetostriction, an increase in the contact bearing area is observed, mostly due to the material whose elastic modulus is lower and the magnetostriction is higher.

The impact of the bearing contact surface area, which increases with magnetostriction, grows with decreasing the smoothing depth R_p and the ratio of of transverse and longitudinal roughness steps. As a result, the nominal pressure in the joints grows due to the compensatory effect from the side of magnetostrictive voltages. Magnetostriction is stimulated by crystallographic magnetic anisotropy, in particular under technological texturing. In the “gas - vapor - liquid” series, the penetrating power of sealed media decreases. It is dependent on the temperature at the joint contact. Depressurization is detected through changes in the magnetic flux under the influence of the intrinsic magnetic permeability of the molecules of the sealed medium as they penetrate the interface surface. You can increase the tightness if you suppress the activity of molecules. For this purpose, ionization and induction in the constant and alternating magnetic field with the intensity of <60 kA/m are used.

References

1. Galin, L.A. Kontaktnye zadachi teorii uprugosti i vyazkouprugosti. [Contact problems of the elasticity and viscoelasticity theory.] Moscow: Fizmatgiz, 1980, 303 p. (in Russian).
2. Demkin, M.N., Izmailov, V.V. Zavisimost' ekspluatatsionnykh svoystv friktsionnogo kontakta ot mikrogeometrii kontaktiruyushchikh poverkhnostey. [The relation between the friction contact performance and the microgeometry of contacting surfaces.] Journal of Friction and Wear, 2010, vol. 31, no. 1, pp. 68–77 (in Russian).
3. Zharskiy, I.M., et al. Tekhnologicheskie metody obespecheniya nadezhnosti detaley mashin. [Technological methods to ensure the reliability of machine parts.] Minsk: Vysshaya shkola, 2005, 299 p. (in Russian).
4. Chistyakov, A.N., et al. Spravochnik po khimii i tekhnologii tverdykh goryuchikh iskopaemykh. [Handbook of Chemistry and Technology of Solid Fuels.] St.Petersburg: Sintez, 1996, 362 p. (in Russian).
5. Ren, X., et al. A Relation of Hydraulic Conductivity — Void Ratio for Soils Based on Kozeny-Carman Equation. Engineering Geology, 2016, vol. 213, pp. 89–97.
6. Tang, T., McDonough, J.M. A Theoretical Model for the Porosity — Permeability Relationship. International Journal of Heat and Mass Transfer, 2016, vol. 103, pp. 984–996.
7. Makushkin, A.P. Polimery v uzlakh treniya i uplotneniyakh pri nizkikh temperaturakh. [Polymers in friction units and seals at low temperatures.] Moscow: Mashinostroenie, 1993, 288 p. (in Russian).
8. Okhlopkova, T.A., et al. Mikroskopicheskie issledovaniya deformatsii rastyazheniya sferolitnykh struktur v polimernykh kompozitsionnykh materialakh. [Microscopic investigations of spherulitic structures tensile strain in polymeric composite materials.] Vestnik of North-Eastern Federal University, 2015, no. 3 (47), pp. 75–86 (in Russian).
9. Bukanova, I.S., Tatarkin, E.Yu., Yatlo, I.I. Tekhnologicheskoe obespechenie povyshennoy nesushchey sposobnosti nepodvizhnykh soedineniy tipa «korpus — vtulka». [Technological support of the increased bearing capacity of fixed joints of the “body - sleeve” type.] Polzunovsky Vestnik, 2009, no. 1, pp. 46–50 (in Russian).
10. Heifez, L.I., Neumark, A.V. Mnogofaznye protsessy v poristykh sredakh. [Multiphase processes in porous media.]. Moscow: Khimiya, 1982, 319 p. (in Russian).
11. Mukutadze, M.A., Garmonina A.N., Prikhodko, V.M. Raschetnaya model' upornogo podshipnika s poristym pokrytiem na poverkhnosti napravlyayushchey. [Design model of thrust bearing with porous coating on the way surface.] Vestnik of DSTU, 2017, no. 3 (90), pp. 70–77 (in Russian).
12. Pamfilov, E.A., Pyrikov, P.G. Sposob formirovaniya pokrytiy na poverkhnostyakh metallicheskikh materialov: patent 2240360 Ros. Federatsiya: C21D10/00, C23C26/00, C23C16/56. [Method of forming coatings on the surfaces of metallic materials.] RF Patent, no. 2240360, 2004 (in Russian).
13. Pustovoyt, V.N. Termodinamika, mekhanizm i kinetika fazovykh perekhodov v stali v usloviyakh deystviya vneshnego magnitnogo polya. [Thermodynamics, mechanism and kinetics of phase transitions in steel under conditions of an external magnetic field.] Vestnik of DSTU, 2005, vol. 5, no. 3, pp. 427–447 (in Russian).
14. Pyrikov, P. The tribotechnical properties control of metallic materials by magnetic fields. BALTRIB 2007: International Conf. 21–23 November. Kaunas: Lithuanian University oh Agriculture, 2007, pp. 211–217.

Submitted 25.04.2019
Scheduled in the issue 07.05.2019

Authors:

Pilyuschina, Galina A.,
associate professor of the Tribotechnical Materials Science and Engineering Department, Bryansk State Technical University (7, 50 let Oktyabrya Blvd., Bryansk, 241035, RF) Cand.Sci. (Eng.), associate professor,
ORCID: http://orcid.org/0000-0002-2422-0919
gal-pi2009@yandex.ru

Pyrikov, Pavel G.,
research scholar of the Laboratory of Materials Engineering and Adaptive Technological Systems, associate professor of the Tribotechnical Materials Science and Engineering Department, Bryansk State Technical University (7, 50 let Oktyabrya Blvd., Bryansk, 241035, RF) Dr.Sci. (Eng.), associate professor,
ORCID: http://orcid.org/0000-0003-2338-7458
pyrikovpg@mail.ru

Pamfilov, Evgeny A.,
research scholar of the Laboratory of Materials Engineering and Adaptive Technological Systems, Head of the Tribotechnical Materials Science and Engineering Department, Bryansk State Technical University
(7, 50 let Oktyabrya Blvd., Bryansk, 241035, RF) Dr.Sci. (Eng.), professor,
ORCID: http://orcid.org/0000-0002-1522-7246
epamfilov@yandex.ru

Kapustin, Vladimir V.,
research scholar of the Laboratory of Materials Engineering and Adaptive Technological Systems, postgraduate of the Tribotechnical Materials Science and Engineering Department, Bryansk State Technical University
(7, 50 let Oktyabrya Blvd., Bryansk, 241035, RF),
ORCID:http://orcid.org/0000-0002-5207-172X
vovakapustin1990@mail.ru

ИНФОРМАТИКА, ВЫЧИСЛИТЕЛЬНАЯ ТЕХНИКА И УПРАВЛЕНИЕ
INFORMATION TECHNOLOGY, COMPUTER SCIENCE, AND MANAGEMENT

UDC 004.94 https://doi.org/10.23947/1992-5980-2019-19-2-179-184

Formation of similarity criteria for physical objects and processes based on NonDimCritFormer 1.0 computer program *

I. M. Tsibirova[1]**
[1]North Ossetian State University after K.L. Khetagurov, Vladikavkaz, Russian Federation

Формирование критериев подобия физических объектов и процессов на основе компьютерной программы NonDimCritFormer 1.0***

И. М. Цибирова[1]**
[1]Северо-Осетинский государственный университет им. К. Л. Хетагурова, Владикавказ, Российская Федерация

Introduction. The problem of adequate modeling of physical processes and objects is an urgent task of modern science. Automation of work in this area increases the accuracy of modeling and saves money on full-scale modeling of objects under study. The research objective was to create a computer program that would automatically form dimensionless similarity criteria based on the initial set of parameters.
Materials and Methods. The calculation algorithm is based on π-theorem of similarity theory and the basic provisions of the dimensional theory.
Research Results. The computer program is developed. It enables to get all the theoretically possible similarity criteria for the simulation of the physical process or object of interest.
Discussion and Conclusions. The results obtained can be used in the industrial and scientific modeling of physical objects of research, calculation of new similarity criteria, solving problems of describing complex processes, etc.

Keywords: similarity criterion, theory of similarity, dimensional theory, π-theorem, dimensionless complex, Kirpichev-Gukhman theorem.

For citation: I.M. Tsibirova. Formation of similarity criteria for physical objects and processes based on NonDimCritFormer 1.0 computer program. Vestnik of DSTU, 2019, vol. 19, no. 2, pp. 179−184. https://doi.org/10.23947/1992-5980-2019-19-2-179-184

Введение. Современная наука признает актуальной проблему адекватного моделирования физических процессов и объектов. Автоматизация работ в этой сфере повышает точность моделирования и экономит средства на натурном моделировании объектов изучения. Целью данного исследования было создание компьютерной программы, которая по исходному набору параметров автоматически формирует безразмерные критерии подобия.
Материалы и методы. В основе расчетного алгоритма лежит π-теорема теории подобия и основные положения теории размерностей.
Результаты исследования. Создана компьютерная программа, которая позволяет получить все теоретически возможные критерии подобия для моделирования изучаемого физического процесса или объекта.
Обсуждение и заключение. Полученные результаты могут быть использованы в промышленном и научном моделировании физических объектов исследования, расчете новых критериев подобия, решении задач описания сложных процессов и т. д.

Ключевые слова: критерий подобия, теория подобия, теория размерностей, π-теорема, безразмерный комплекс, теорема Кирпичева — Гухмана.

Образец для цитирования: Цибирова, И. М. Формирование критериев подобия физических объектов и процессов на основе компьютерной программы NonDimCritFormer 1.0 / И. М. Цибирова // Вестник Дон. гос. техн. ун-та. — 2019. — Т. 19, № 2. — С. 179−184. https://doi.org/10.23947/1992-5980-2019-19-2-179-184

Introduction. Similarity criteria are dependencies between dimensionless combinations of parameters describing an object or physical process. On the basis of similarity criteria, it is possible to create mathematical models of the objects of interest [1-4].

Similarity criteria enable to establish the correspondence of the model and the object under study. They become irreplaceable when the mathematical description of processes according to experiments or observations is not

* The research is done within the frame of the independent R&D.
** E-mail: 571334@mail.ru
*** Работа выполнена в рамках инициативной НИР.

formed. In fact, similarity criteria are dimensionless power complexes of sets of physical parameters describing objects and processes. They are identical in form and numerically equal for similar objects or processes.

The algorithm is based on the second theorem of similarity theory, the so-called π-theorem. In the source [5], it is formulated as follows*: any complete equation of the physical process, written in a certain system of units, can be represented by a functional dependence between the similarity criteria obtained from the parameters involved in the process.* From this, it follows that analyzing and combining with each other the physical parameters describing the object of study, it is possible to make the similarity criteria of the object or physical process [5, 6].

When modeling objects of research on the basis of similarity theory, the analysis of the dimensions of the physical parameters describing the object at its primary points [6, 7] is most frequently used.

Researchers select the determining physical parameters that describe the object of interest, in particular, pressure, viscosity, density, speed, temperature, resistance, current, and, working with their dimensions, obtain a theoretically possible number of similarity criteria [8]. These criteria can then be used as the basis for mathematical or full-scale modeling.

In the case when the initial object under study and the model have similarity criteria that are numerically equal in the critically important zones, then, according to the third similarity theorem (Kirpichev -Gukhman theorem) [9], it implies their physical similarity [6]. Therefore, to create, for example, a model of flow along the contour of pipes, it is necessary to find the appearance and numerical value of the similarity criteria describing the real object, and then to build a model or laboratory installation so that the values of the similarity criteria in it are numerically equal to the values of the same criteria on the real object.

The NonDimCritFormer 1.0 program presented in this paper enables a person who studies a physical object or process to select significant physical parameters (see Fig. 1), which determine its basic parameters and calculate automatically all theoretically possible similarity criteria and dimensionless complexes (see Fig. 2) formed on their basis. The basis of this algorithm is the methods of analysis of dimensions of the selected physical parameters.

2. Description of the program algorithm

The basis of the algorithm implemented in the program of formation of similarity criteria based on the dimensions of the selected physical parameters is a technique that includes five steps.

Step 1. Determination of physical parameters that affect significantly the physical properties of the object under study. The accuracy of the results depends on the correct choice of parameters, neglecting nonessential ones. A large number of selected parameters causes an increase in the number of obtained dimensionless complexes, but does not increase the accuracy of the model formed on their basis.

Step 2. Compiling a matrix of dimensions for the selected physical parameters. In it, the dimensions of the selected parameters in the corresponding degrees are arranged in rows. The dimension of the matrix corresponds to the number of parameters and their units of measurement, that is, in the matrix there are as many rows as the selected parameters, and there are as many columns as the units of measurement. For example, a string corresponding to the physical parameter “electrical resistance, R”, which has a dimension of four units $\frac{m^2 kg}{s^3 A^2}$, в матрице размерностей будет иметь вид (2 1 -3 -2).

Step 3. Determination of the number of independent parameters. The number of independent parameters *k* corresponds to the rank of the dimension matrix, i.e. the largest order of the non-zero determinant which is based on the rows of the matrix under study.

Step 4. Formation of groups of independent parameters. At this step, combinations of *k* pieces of *m* parameters that make up a dimensionless complex are formed. That is, the units that are included in the dimension of the selected parameters are mutually reduced, which leads to the fact that this combination of the selected physical parameters has no dimension. Generally speaking, the complex consists of such parameters, the partial matrix of dimensions of which has at least one determinant of *k-th* order unequal to zero.

According to the combinatorial placement formula, the theoretically possible number of such complexes can be [1]

$$C_m^k = \frac{m!}{k! \cdot (m-k)!},$$

where *m* is the total number of parameters, *k* is the rank of the complete matrix of dimensions.

Not all obtained complexes of the selected parameters make up a complex with a matrix of *k-th* order, therefore, very often the number of groups after the test is less than C_m^k.

Step 5. Determination of expressions for similarity criteria based on calculated groups of independent parameters. Expressions are formed by the following algorithm.

1. Take another group of parameters. For example, set #1- $P_1 \ldots P_k$.

2. We begin the calculation of similarity criteria with dividing the parameters of the next group by the parameters of the current group. In particular, the following criteria can be drawn up for the set #1

$$\pi_1 = \frac{P_{k+1}}{P_1^{x_{1.1}} \cdot \ldots \cdot P_k^{x_{1.k}}}, \quad \ldots \quad \pi_{m-k} = \frac{P_m}{P_1^{x_{m-k.1}} \cdot \ldots \cdot P_k^{x_{m-k.k}}}.$$

Ordinary division of a parameter by a set does not produce a dimensionless expression. To do this, you need to calculate the values of powers $x_{i.1} \ldots x_{i.k}$ for each of the criterion expression.

3. Considering that the dimensions of the parameters in the numerators and denominators of the criterion complexes should be equal, we form and solve a system of linear equations. Obtaining such a system is due to the equalization of degrees at the same units of measurement in the numerators and denominators of the criteria, which are the products of combinations of dimensions selected at the beginning of the calculation of physical parameters. As a result, we obtain a system of q equations with $k = q$ unknowns.

We obtain sets of m-k criteria for each group of parameters. The maximum possible number of dimensionless complexes, which can be calculated on the basis of m parameters, is

$$\pi_s = C_m^k \cdot (m-k).$$

This value can be quite large. For example, for $m = 7$ and $k = 3$, the total number is $\pi_s = 140$. But, due to the fact that the list of calculated criteria has a lot of the similar and reciprocal ones, the total number of selected criteria is less than π_s. The proportion of criteria which failed verification depends on the initial set of physical parameters selected for study.

3. Program interface and functionality

The program NonDimCritFormer 1.0 is written in the language VisualBasic.Net. It has an intuitive Windows interface and is easy to operate.

The user chooses physical parameters, which are essential, in his opinion, for the simulated object or process (see Fig. 1), then, by clicking the mouse on the button “Generate all criteria” and “Remove repetitions of criteria”, all similarity criteria (dimensionless complexes), which can be made on the basis of the selected physical parameters (see Fig. 2) are displayed.

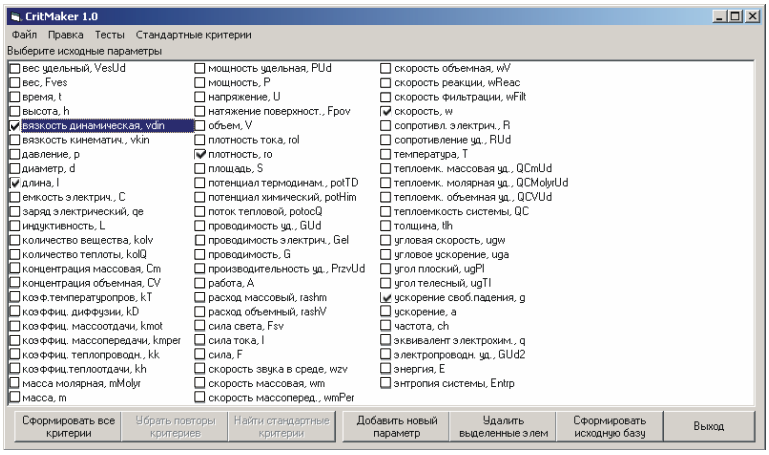

Fig. 1. Selection of initial physical parameters

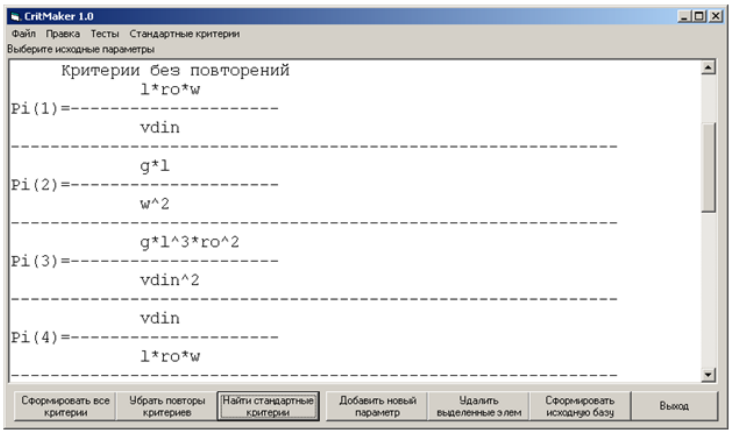

Fig. 2. Calculated similarity criteria

Using the "Find standard criteria" button, you can detect the existing (named) similarity criteria in the list. NonDimCritFormer 1.0 also enables to print the entire list of criteria or part of it, to save the list as a separate file, to edit the base of standard criteria.

4. Examples of using the program

Calculation example 1. Under constant voltage conditions, we find similarity criteria describing the current flow in a resistor, choke, and capacitor connected in series [8].

Step 1. Select the physical parameters essential for the simulated object. They include: current, I, A ; *inductance, L,* $\frac{\text{kg}\cdot m^2}{s^2\cdot A^2}$; capacitance, C, $\frac{\text{s}^4\cdot A^2}{kg\cdot m^2}$; resistance, R,; $\frac{\text{kg}\cdot m^2}{s^3\cdot A^2}$; voltage U, $\frac{\text{kg}\cdot m^2}{s^3\cdot A}$ and time t, s. Total parameters are $m = 6$ and base unit are $q = 4$.

Step 2. The matrix of dimensions of the specified parameters has the form:

$$\begin{array}{c|cccc} & m & kg & s & A \\ t & 0 & 0 & 1 & 0 \\ C & -2 & -1 & 4 & 2 \\ L & 2 & 1 & -2 & -2 \\ U & 2 & 1 & -3 & -1 \\ I & 0 & 0 & 0 & 1 \\ R & 2 & 1 & -3 & -2 \end{array}$$

Step 3. The rank of this matrix is $k = 3$. It follows that the number of independent parameters in the group will be three, and the number of criteria for each independent group will be $m - k = 3$.

Step 4. The total number of groups of independent parameters can be: $C_m^k = C_6^3 = 20$. Combinations of parameters are made automatically with the help of the described program. The algorithm checks the rank of the partial matrix for each composed combination.

For example, for an ILU combination, a partial matrix would look like this:

$$ILU = \begin{vmatrix} 0 & 0 & 0 & 1 \\ 2 & 1 & -2 & -2 \\ 2 & 1 & -3 & -1 \end{vmatrix}$$

The rank of this matrix is 3, therefore, this combination forms a group of independent parameters. Not all of the possible 20 combinations are dimensionless similarity criteria. For example, *tCL* combination is not a criterion because the rank of the matrix is not equal to k. In the context of the initial set of physical parameters under consideration, only 15 can be considered as similarity criteria.

Step 5. Drawing up similarity criteria passes through the solution of systems of linear equations, which are formed on the basis of criterion complexes. For example, for a combination of *ILU*:

$$\pi_1 = \frac{t^{x_{1.1}}}{I^{x_{1.2}}\cdot L^{x_{1.3}}\cdot U^{x_{1.4}}},\quad \pi_2 = \frac{C^{x_{2.1}}}{I^{x_{2.2}}\cdot L^{x_{2.3}}\cdot U^{x_{2.4}}},\quad \pi_3 = \frac{R^{x_{3.1}}}{I^{x_{3.2}}\cdot L^{x_{3.3}}\cdot U^{x_{3.4}}},$$

after solving the system, which will result in finding the values of powers of dimensions x, the following criteria will be obtained:

$$\pi_1 = \frac{t}{I\cdot L\cdot U^{-1}},\quad \pi_2 = \frac{C}{I^2\cdot L\cdot U^{-2}},\quad \pi_3 = \frac{R}{I^{-1}\cdot L^0\cdot U}.$$

For each of 15 possible combinations of initial physical parameters, 3 criteria will be obtained. Among these 45 criteria, there are often repetitive and reciprocal ones. For this example, NonDimCritFormer 1.0 gives 11 unique criteria:

$$\pi_1 = \frac{t}{C^{0,5}\cdot L^{0,5}};\quad \pi_2 = \frac{I\cdot L^{0,5}}{C^{0,5}\cdot U};\quad \pi_3 = \frac{C^{0,5}\cdot R}{L^{0,5}};$$

$$\pi_4 = \frac{C\cdot L}{t^2};\quad \pi_5 = \frac{I\cdot t}{C\cdot U};\quad \pi_6 = \frac{C\cdot R}{t};$$

$$\pi_7 = \frac{C \cdot U^2}{I^2 \cdot L}; \quad \pi_8 = \frac{R \cdot I}{U}; \quad \pi_9 = \frac{L}{C \cdot R^2};$$

$$\pi_{10} = \frac{U \cdot t}{I \cdot L}; \quad \pi_{11} = \frac{R \cdot t}{L}.$$

Calculation example 2. Consider the process of fluid motion in a horizontal pipe. To do this, we form similarity criteria that describe the pressure drop in this process [10]. The most important parameters that describe the pressure drop in the pipe during the passage of the liquid medium, the following values can be called:

$$\Delta p = f(\omega, \rho, \mu, L),$$

where Δp is the pressure, $\frac{\text{kg}}{\text{m} \cdot \text{s}^2}$; ω is the flow rate of the fluid, $\frac{\text{m}}{\text{s}}$; ρ is fluid density, $\frac{kg}{m^3}$; μ is the coefficient of dynamic viscosity, $\frac{kg}{m \cdot s}$.

Total parameters are $m = 5$, and the base units are $q = 3$. The complete matrix of dimensions of the selected parameters has the form:

	m	kg	s
μ	-1	1	-1
Δp	–1	1	–2
L	1	0	0
ρ	–3	1	0
ω	1	0	–1

The rank of the reduced matrix is $k = 3$. The number of independent parameters in group is three and the number of criteria for each independent group is $m - k = 2$. Total groups can be $C_m^k = C_5^2 = 10$.

According to the calculations of the program, in this example, out of ten possible combinations, only nine are independent groups. It follows that a total of 18 dimensionless complexes can be obtained. After removing the repetitive and reciprocal ones, the program gives 6 unique combinations.

$$\pi_1 = \frac{L \cdot \Delta p}{\mu \cdot \omega}; \quad \pi_2 = \frac{\Delta p}{\rho \cdot \omega^2}; \quad \pi_3 = \frac{L \cdot \Delta p^{0,5} \cdot \rho^{0,5}}{\mu};$$

$$\pi_4 = \frac{\rho^{0,5} \cdot \omega}{\Delta p^{0,5}}; \quad \pi_5 = \frac{L \cdot \rho \cdot \omega}{\mu}; \quad \pi_6 = \frac{L^2 \cdot \Delta p \cdot \rho}{\mu^2}.$$

It is important to note that the complexes π_2 and π_5 are expressions of the Euler and Reynolds criteria, respectively [3].

4. Conclusion

The computer program NonDimCritFormer 1.0 is proposed. With its help, on the basis of selected physical parameters that determine the characteristics of the object under study or the physical process in its characteristic spatial and temporal points, it is possible to form dimensionless complexes – similarity criteria describing the object of study.

References

1. Zarubin, V.S. Matematicheskoe modelirovanie v tekhnike. [Mathematical modeling in engineering.] Moscow: Vysshaya shkola, 2015, 474 p. (in Russian).

2. Batuner, L.M., Pozin, M.E. Matematicheskie metody v khimicheskoy tekhnike. [Mathematical methods in chemical engineering.] Leningrad: Khimiya, 1972, 724 p. (in Russian).

3. Buchanan, M. Dimensional Analysis. Nature Physics, 2010, vol. 6, pp. 555.

4. Zohuri, B. Dimensional Analysis and Self-Similarity Methods for Engineers and Scientists. Cham; Heidelberg; New York; Dordrecht; London: Springer, 2015, 372 p.

5. Venikov, V.A., Venikov, G.V. Teoriya podobiya i modelirovaniya (primenitel'no k zadacham elektroenergetiki). [Theory of similarity and modeling (as applied to the tasks of the power engineering).] Moscow: Vysshaya shkola, 1987, 454 p. (in Russian).

6. Gukhman, A.A. Primenenie teorii podobiya k issledovaniyu protsessov teplo-massoobmena. Protsessy perenosa v dvizhushcheysya srede. [Application of the theory of similarity to the study of heat-mass transfer processes. Transport processes in moving medium.] Moscow: URSS, 2018, 328 p. (in Russian).

7. Zohuri, B. Dimensional Analysis beyond the Pi Theorem. Cham: Springer, 2015, 372 p.

8. Frishter, L.U. Application of the Method of the Theory Similarity and Dimensional Analysis for Research the Local Stress-strain State in the Neighborhood of an Irregular Point of the Boundary. Procedia Engineering, 2016, vol. 153, pp. 151–156.

9. Bluman, G.W., Cole, J.D. Similarity Methods for Differential Equations. New York; Heidelberg; Berlin: Springer-Verlag, 1974, 333 p.

10. Ayala, L.F., Kouassi, J.P. The Similarity Theory Applied to the Analysis of Multiphase Flow in Gas-Condensate Reservoirs. Energy Fuels, 2017, no. 21 (3), pp. 1592–1600.

Submitted 15.04.19.
Scheduled in the issue 30.04.19.

Author:
Tsibirova, Ilvira M.,
senior lecturer of the Physics and Astronomy Department, K.L. Khetagurov North Ossetian State University
(44, Vatutin St., Vladikavkaz, 362025, RF), Cand.Sci. (Pedagogics),
ORCID: https://orcid.org/0000-0002-1744-6266
571334@mail.ru

ИНФОРМАТИКА, ВЫЧИСЛИТЕЛЬНАЯ ТЕХНИКА И УПРАВЛЕНИЕ
INFORMATION TECHNOLOGY, COMPUTER SCIENCE, AND MANAGEMENT

UDC 004.942 https://doi.org/10.23947/1992-5980-2019-19-2-185-194

Comparative analysis of NTRUEncrypt modified post-quantum cryptographic system and standard RSA cryptosystem*

P. V. Razumov[1], I. A. Smirnov[2], I. A. Pilipenko[3], A. V. Selyova[4], L. V. Cherkesova[5]**
[1,2,3,4,5] Don State Technical University, Rostov-on-Don, Russian Federation

Сравнительный анализ модифицированной постквантовой криптографической системы NTRUENcrypt и общепринятой криптосистемы RSA***

П. В. Разумов[1], И. А. Смирнов[2], И. А. Пилипенко[3], А. В. Селёва[4], Л. В. Черкесова[5]**
[1,2,3,4,5] Донской государственный технический университет, г. Ростов-на-Дону, Российская Федерация

Introduction. The NTRUEncrypt cryptographic system, the calculation of the algorithmic complexity of the development of the NTRUEncrypt cryptosystem and its modifications are considered. The study objectives are to develop NTRUEncrypt, an efficient post-quantum cryptographic algorithm, which has high cryptographic resistance to quantum computer attacks, to work out a modification of the proposed algorithm, to analyze and experimentally validate its advantages.

Materials and Methods. A description of the NTRUEncrypt encryption system is proposed. The modification of the considered algorithm is studied; the block diagram of the implementation of the software based on it is presented. An example of the software operation and its characteristic is given. The reliability of the results is proved using the Mann-Whitney U test. During the experiment, the third-party software implementation of the RSA cryptosystem was used. A Stopwatch class element was introduced in the source code of all three programs of NTRUEncrypt, RSA, and NTRUEncrypt modifications. This class provides a set of methods and properties that can be used for the precise measurement of the execution time. Thus, it became possible to record the results of the time spent on all three basic stages: key creation, encryption and decryption of the message.

Research Results. The advantages of the developed cryptosystems in terms of the performance characteristics are proved. An experimental comparison of the implemented NTRUEncrypt algorithm and its modification is performed. All advantages of the latter are indicated.

Discussion and Conclusions. The advantage of using the NTRUEncrypt algorithm modification is experimentally validated. The new application is 25% faster to perform general work on key generation, encryption and decryption. In

Введение. Статья посвящена исследованию криптографической системы NTRUEncrypt, расчету алгоритмической сложности разработки криптосистемы NTRUEncrypt и ее модификации. Цели исследования: разработка эффективного постквантового криптографического алгоритма NTRUEncrypt, обладающего высокой криптостойкостью к атакам с квантового компьютера, а также разработка модификации предложенного алгоритма, анализ и экспериментальное доказательство его преимуществ.

Материалы и методы. Предложено описание системы шифрования NTRUEncrypt. Изучена модификация рассматриваемого алгоритма, представлена блок-схема реализации основанного на нем программного средства. Приведен пример работы программного средства и дана его характеристика. Достоверность результатов обоснована с помощью *U*-критерия Манна — Уитни. При проведении эксперимента использована сторонняя программная реализация криптографической системы RSA. В исходный код всех трех программ NTRUEncrypt, RSA, модификации NTRUEncrypt был внедрен элемент класса Stopwatch. Данный класс предоставляет набор методов и свойств, которые можно использовать для точного измерения времени, затраченного на выполнение. Таким образом, появилась возможность фиксировать результаты затраченного времени на всех трех основных этапах: создание ключей, шифрование и расшифрование сообщения.

Результаты исследования. Доказаны преимущества разработанных криптосистем по характеристикам производительности. Выполнено экспериментальное сравнение реализованного алгоритма NTRUEncrypt и его модификации. При этом обозначены все преимущества последней.

Обсуждение и заключения. Экспериментально доказано преимущество использования модификации алгоритма NTRUEncrypt. Новое приложение на 25 % быстрее выполняет общую работу по генерации ключей, шифрованию и расшифрованию. Помимо этого оптимизируется использование внутренней памяти за счет уменьшения веса ис-

*The research is done within the frame of the independent R&D.
**E-mail: therazumov@gmail.com, terran.doatk@mail.ru, ipilipenko@donstu.ru, tone4ka.selyova@yandex.ru, chia2002@inbox.ru
*** Работа выполнена в рамках инициативной НИР.

addition, the internal memory usage is optimized through reducing the weight of the source program file and the size of the secret key. When attempting to crack a ciphertext, cryptographic robustness and complexity of using quantum algorithms are shown.

ходного файла программы и размера секретного ключа. При попытке взлома шифротекста проявляется криптографическая стойкость и сложность использования квантовых алгоритмов.

Keywords: cryptographic system, post-quantum cryptographic algorithm, cryptographic strength, Mann-Whitney U test, encryption.

For citation: P.V. Razumov, et al. Comparative analysis of NTRUEncrypt modified post-quantum cryptographic system and standard RSA cryptosystem. Vestnik of DSTU, 2019, vol. 19, no. 2, pp. 185−194. https://doi.org/10.23947/1992-5980-2019-19-2-185-194

Ключевые слова: криптографическая система, постквантовый криптографический алгоритм, криптостойкость, *U*-критерий Манна — Уитни, шифрование.

Образец для цитирования: Сравнительный анализ модифицированной постквантовой криптографической системы NTRUENcrypt и общепринятой криптосистемы RSA / П. В. Разумов [и др.] // Вестник Дон. гос. техн. ун-та. — 2019. — Т. 19, № 2. — С.185−194. https://doi.org/10.23947/1992-5980-2019-19-2-185-194

Introduction. The paper [1] gave an impulse to the development of a new cryptographic system. It shows that quantum computers potentially threaten to hack into all widely used cryptographic algorithms.

The software presented in this paper is cryptosecure versus possible quantum attacks and surpasses its counterparts (for example, RSA cryptosystem) in the algorithm speed characteristics and in the quantity of spendable resources [2]. This explains the urgency of the research.

The object of the study is the NTRUEncrypt cryptosystem.

The subject of the research is the algorithmic complexity of the development of the NTRUEncrypt cryptosystem and its modifications.

The work objectives are to develop an efficient post-quantum cryptographic NTRUEncrypt algorithm, which has high cryptographic resistance to quantum computer attacks, to work out modifications of the proposed algorithm, to analyze and experimentally validate its advantages.

To achieve the objective, the following tasks were defined.

1. To investigate the algorithm of the NTRUEncrypt cryptosystem.

2. To develop an algorithm for modifying NTRUEncrypt.

3. To implement the NTRUEncrypt cryptosystem software and its modifications.

4. To analyze and compare two programs with each other and with their counterpart - RSA cryptosystem.

Materials and Methods. Consider the description of the encryption NTRUEncrypt system. The cryptographic system with the public NTRUEncrypt key uses operations over the $Z[X] / (X^N - 1)$ ring of polynomials of degree not exceeding $N - 1$ [3]:

$$a = a_0 + a_1 * X^1 + a_0 * X^2 + \cdots + a_{N-1} * X^{N-1},$$

where $a_0, a_1, a_2 \ldots a_{N-1}$ are integers.

The operations of addition and multiplication are performed as usual, except that X^N is replaced by 1, X^{N+1} is replaced by X^1, X^{N+2}, so on.

The cryptosystem is determined by a number of parameters, the key parameters are: *N, p* and *q*. To maintain the algorithm strength, it is necessary for *p* and *q* parameters to be coprime.

To provide high resistance of the algorithm to various attacks, it is recommended to use the following parameters (Fig. 1):

Indication	N	q	p	df	dg	dr	Guaranteed resistance
NTRU167:3	167	128	3	61	20	18	Moderate level of resistance
NTRU251:3	251	128	3	50	24	16	Standard level of resistance
NTRU503:3	503	256	3	216	72	55	Highest level of resistance
NTRU167:2	167	127	2	45	35	18	Moderate level of resistance
NTRU251:2	251	127	2	35	35	22	Standard level of resistance
NTRU503:2	503	253	2	155	100	65	Highest level of resistance

Fig.1. Recommended parameters

Research Results

Key generation. Bob wants to send a message to Alice. For this, he needs public and private keys. Therefore, he chooses randomly two small polynomials *f* and *g* from the ring of truncated polynomials *R*. The smallness of polynomials means that the small polynomial will be much less than *q* with respect to the arbitrary polynomial modulo *q*, in which the coefficients are uniformly distributed [4]. To determine the smallness of polynomials, the numbers *df* and *dg* are used which Bob chooses independently.

The polynomial *f* will have *df* coefficients equal to one, (*df* – 1) coefficients equal to minus one, and the rest coefficients equal to zero.

The polynomial *g* will have *dg* coefficients equal to one, as many coefficients equal to minus one, and the rest coefficients equal to zero.

Bob should keep the selected polynomials in secret since anyone he learns them will be able to decrypt the message.

Further, Bob calculates the inverse polynomials f_p and f_q modulo *p* and *q*, respectively, such that:

$$f \times f_p = 1(mod\ p) \text{ и } f \times f_q = 1(mod\ q).$$

If by chance these inverse polynomials do not exist, then Bob goes back and re-selects the polynomial *f*.

The secret key is the pair (f, f_p), and the public key *h* is calculated using the formula:

$$h = p \times f_q \times g\ (mod\ q).$$

Encryption. Alice wants to send a message to Bob using the public key *h*. To do this, Alice needs to present her message as a polynomial *m* with the coefficients modulo *p* selected from the range (–*p*/2, *p*/2]. Then, Alice needs to choose another small polynomial *r* which is called “blinding”, and calculate the ciphertext:

$$e\ =\ (r \times h + m)(mod\ q).$$

Decryption. Bob receives an encrypted message *e* from Alice and wants to decrypt it. First, using his secret key, Bob calculates:

$$a = f \times e\ (mod\ q).$$

Since Bob calculates the value *a* modulo *q* number, he should choose its coefficients from the range (–*q*/2, *q*/2] and then calculate:

$$b = a\ (mod\ p).$$

Finally, Bob, using the second part of the secret key, receives the original message from Alice:

$$c = f_p \times b\ (mod\ p).$$

Modification of the NTRUEncrypt algorithm. As can be seen from the description of the algorithm, the polynomial *f* shall comply with the following requirements:

- the polynomial *f* is invertible modulo *p*,
- the polynomial *f* is invertible modulo *q*,
- the polynomial *f* is a small polynomial.

In the algorithm itself, the invertibility modulo *p* and *q* was guaranteed as follows. If the polynomial *f* being not invertible in one of the moduli was generated, then it was discarded and the next one was generated — and so on as long as the required polynomial was found.

The proposed modification is to replace the polynomial *f* by a polynomial of the form:

$$f = 1 + pF, \quad (1)$$

where *F* is a small polynomial.

This approach has the following advantages.

1. From the expression (1), it is clear that the polynomial *f* is always invertible modulo *p*. This fact accelerates the key generation since it is not necessary to additionally calculate f_p.

2. Since $f^{-1} = 1 \ mod \ p$, then decoding does not require additional multiplication by f^{-1}, which speeds up the decryption process itself. In this case, the private key will not be the pair (f, f_p), but (f).

Key generation. As in the original algorithm, Bob first selects the encryption parameters *N, p, q* and the numbers *df, dg*. Then, he selects randomly two small polynomials *F* and *g* from the ring of truncated polynomials *R*.

He calculates the modified polynomial *f* using the formula (1).

Next, Bob calculates the inverse polynomial f_q modulo *q:*

$$f \times f_q = 1(mod\ q).$$

If by chance an inverse polynomial is not found, Bob goes back and re-selects the polynomial *f*.

The secret key is the polynomial *f*, and the public key *h* is calculated as follows:

$$h = p \times f_q \times g\ (mod\ q).$$

Encryption. Encryption remains unchanged; all is quite as in the original NTRUEncrypt algorithm.

Alice wants to send a message to Bob using the public key *h*. To do this, Alice needs to present her message as the polynomial *m* with coefficients modulo *p* selected from the range (–*p*/2, *p*/2]. Then, Alice needs to choose another small polynomial *r*, which is called "blinding", and calculate the ciphertext:

$$e\ =\ (r \times h + m)(mod\ q).$$

Decryption. Bob receives the encrypted message *e* from Alice and wants to decrypt it. In the first place, using his secret key, Bob calculates:

$$a = f \times e\ (mod\ q).$$

Since Bob calculates the value *a* modulo *q* number, he should choose its coefficients from the range (–*q*/2, *q*/2], and then calculate:

$$b = a\ (mod\ p).$$

That is all, calculation is finished at that; we have received the original message from Alice: $b = m$ [5].

Proof of the modified algorithm. To prove the algorithm, consider the decryption process itself.

Alice's encrypted message looks like:

$$e\ =\ (r \times h + m)(mod\ q).$$

Bob uses his secret key — polynomial *f*:

$$a = f \times e\ (mod\ q)\ = (f\ \times\ (r\ \times\ h\ +\ m))(mod\ q)\ = (f\ \times\ (r\ \times\ pf_q \times g\ +\ +m))(mod\ q).$$

As a result:

$$a = (pr\ \times\ g\ +\ m\ \times\ f)(mod\ q).$$

Thereafter, Bob obtains the polynomial *b* through decreasing the coefficients of the polynomial *a* modulo *p*:

$$b = a(modp) = m \times f(modp) = (m\ +\ m\ \times\ p\ \times\ F)(mod\ p) = m\ (mod\ p).$$

Thus, we have checked and proved that the polynomial *b* is the original message *m* indeed.

Implementation of the algorithm. The programming language used is the object-oriented programming language *C#*, which belongs to the family of languages with a *C*-like syntax. Development framework was Microsoft Visual Studio 2015 Enterprise. The primary advantage of this software product is the application with a graphical interface that allows the user to make short work with the device and the operation scheme of this software product.

Fig. 2 shows a generalized block diagram of the software.

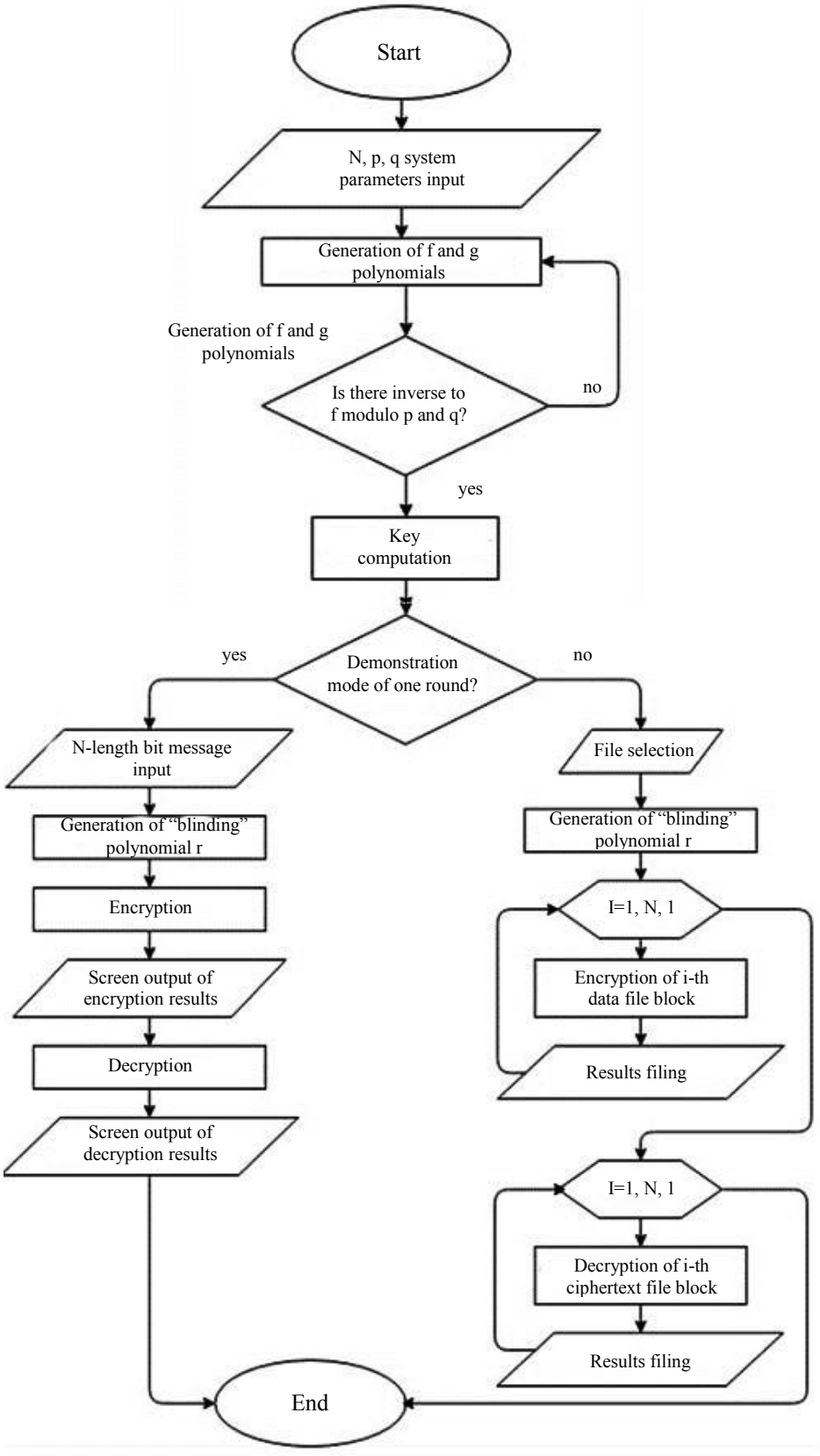

Fig. 2. Flowchart of software implementation

Example of the software. NTRUEncrypt uses three constant parameters: *N, p, q*. The user enters them in the *System Settings* panel.

Next, there is the *Key Generation* panel. The parameters entered by the user in the previous step are input. Then, two polynomials *f* and *g* are randomly formed, so that:

- the number of coefficients equal to one and zero to be equal to the number that was previously determined in the program;

- the degree of polynomials to be corresponded to the input parameter N.

Then, the Euclidean theorem on computing the greatest common divisor for polynomials and its backward course is used to calculate two polynomials inverse to f modulo p and q, respectively. The public key h is computed.

The user enters the binary message type m in the *Encryption* panel in the *Message* window. It should be mentioned that the original message should be divided into blocks of N bits, each of which will be processed separately and converted into a polynomial with the coefficients {–1, 0, 1} (in this program, instead of the value "–1", "2" is used).

For an encryption operation, the program needs to perform preliminary preparation — to generate one blinding polynomial. It is formed in the same way as f and g polynomials.

The resulting public key and the polynomial r make it possible to encrypt message m using the appropriate formula. Then, the result is checked on the membership to the ring of truncated polynomials of a degree not exceeding $N - 1$, and is displayed on the screen.

The next block implements the decryption mechanism. For this, actions are consistently performed considering the ring $Z[X]/(X^N - 1)$.

The operation result is shown in Fig. 3.

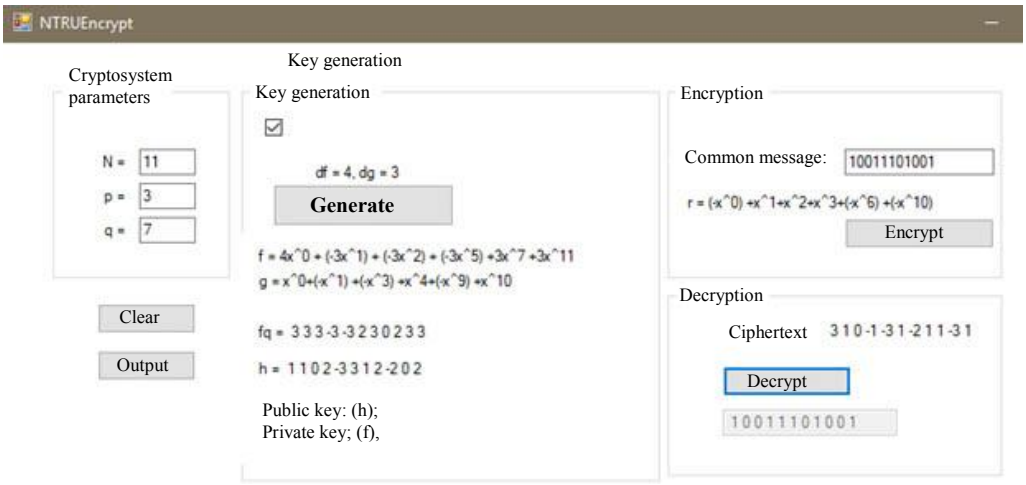

Fig. 3. Appearance of NTRUEncrypt program

Fig. 4 shows the software results in the form of source text, encrypted and decrypted.

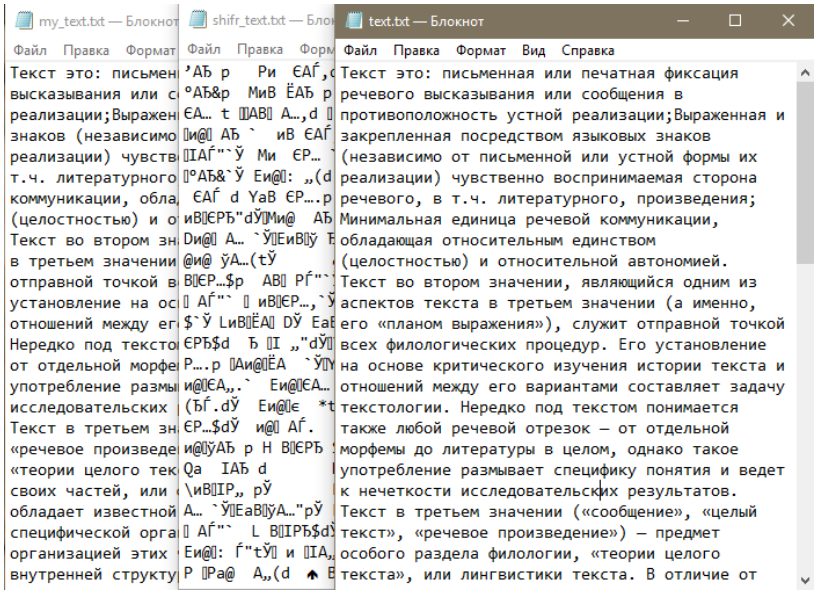

Fig. 4. Software result

Experiments. The experimental research objective is to show and prove the advantages in the performance characteristics of the developed cryptosystems in comparison with the analogue. (In this paper, an RSA public key cryptosystem was chosen as an alternative [6].) In addition, it was necessary to compare the implemented NTRUEncrypt algorithm and its modification in order to note the advantages of the latter and provide experimental evidence.

To verify the results, the statistical Mann – Whitney *U*-test was used, which is intended for comparing two independent samples by the level of any feature measured quantitatively. The criterion enables to determine the degree of difference between samples and is more powerful than the Rosenbaum criterion.

For the experiment, a third-party software implementation of the RSA cryptographic system was used. An element of the Stopwatch class was introduced in the source code of all three programs – NTRUEncrypt, RSA, and NTRUEncrypt modifications. This class provides a set of methods and properties that can be used to accurately measure the time spent on the execution. Thus, it became possible to record the results of the elapsed time at all three main stages: key creation, encryption and decryption of the message. The experiment results are shown in Table 1.

Table 1

Experiment results

№	NTRUEncrypt operate time, s	NTRUEncrypt modification operate time, s	RSA operate time, s
Key generation			
1	0.0239676	0.0190014	0.0964144
2	0.0149743	0.0109994	0.1023557
3	0.0129915	0.0099936	0.1372658
4	0.0170503	0.0099772	0.0491137
5	0.0139885	0.0099773	0.0869555
6	0.0139880	0.0099782	0.0587503
7	0.0129761	0.0099936	0.0986608
8	0.0139931	0.0109775	0.0707417
9	0.0139918	0.0099773	0.0595015
10	0.0169748	0.0099777	0.0517874
Encryption			
1	0.0069961	0.0069770	0.0453772
2	0.0049961	0.0059796	0.0598658
3	0.0059954	0.0049965	0.0265461
4	0.0049966	0.0069966	0.0402407
5	0.0069765	0.0060854	0.0783415
6	0.0049961	0.0069989	0.0097463
7	0.0059795	0.0059954	0.0247876
8	0.0069961	0.0059954	0.0272320
9	0.0089956	0.0049798	0.0494907
10	0.0059954	0.0049744	0.0100916
Decryption			
1	0.0009843	0.0009843	1.0624476
2	0.0010212	0.0010026	0.3692022
3	0.0010193	0.0009974	0.7651423
4	0.0009989	0.0009975	0.9922103
5	0.0030012	0.0009988	0.3056423
6	0.0010017	0.0009975	0.3757183
7	0.0009989	0.0009988	1.2844272
8	0.0010021	0.0009989	0.5902735
9	0.0010026	0.0009984	0.9932694
10	0.0009844	0.0009970	0.8740392

The Mann – Whitney *U*-test is applicable to the results given in Table 1. Compare the key generation rate of the NTRUEncrypt algorithm and its modifications.

Following the algorithm of the Mann-Whitney *U*-test, we criterion write the computation step by step.

1. Create a common ranked list of both samples assigning a lower value to a lower rank.
2. Divide the total ranked list into two consisting of the elements of the first and second samples.
3. Calculate the sum of ranks for the first and second samples separately, as shown in Fig. 5.

№	Sample 1	Rank 1	Sample 2	Rank 2
1	0.0239676	20	0.0190014	19
2	0.0149743	16	0.0109994	9
3	0.0129915	11	0.0099936	6.5
4	0.0170503	18	0.0099772	1
5	0.0139885	13	0.0099773	2.5
6	0.0139880	12	0.0099782	5
7	0.0129761	10	0.0099936	6.5
8	0.0139931	15	0.0109775	8
9	0.0139918	14	0.0099773	2.5
10	0.0169748	17	0.0099777	4
Sums		146		64

Fig. 5. The second step of calculating the Mann-Whitney *U*-test

4. Calculate the value of the Mann-Whitney *U*-test: $U = 9$. The critical value of the criterion for the data $n1$ and $n2$ should be determined from to the table of statistical significance level (Fig. 6).

U_{Kp}	
p≤0.01	p≤0.05
19	**27**

Fig. 6. The forth step of calculating Mann-Whitney *U*-test

Since the values of $n1$ and $n2$ are the same for all experiments, this table will be used in each calculation.

Hence it follows that the obtained empirical value $U = 9$ is in the zone of significance (Fig. 7). Consequently, there is a significant difference between the speed of the NTRUEncrypt program and its modification. If this fact is expressed percentagewise, it turns out that the NTRUEncrypt modification is 28% faster than the program itself.

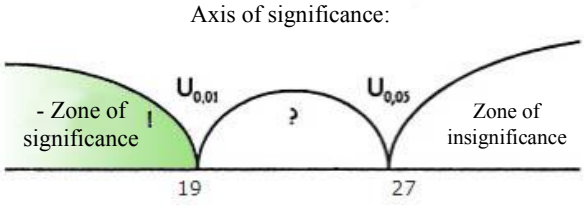

Fig. 7. Axis of significance

Similarly, in shorthand, we present the results of the Mann-Whitney *U*-test and the percentage superiority for the remaining cases.

Key generation

1. NTRUEncrypt modification is 28% faster than NTRUEncrypt. The obtained empirical value $U = 9$ is in the significance zone.

2. NTRUEncrypt program is faster than RSA by 80%. The obtained empirical value $U = 0$ is in the area of significance.

3. NTRUEncrypt modification is faster than RSA by 86%. The obtained empirical value $U = 0$ is in the area of significance.

Message encryption

1. The obtained empirical value $U = 47$ is in the zone of insignificance.

2. NTRUEncrypt program is f80%aster than RSA. The obtained empirical value $U = 0$ is in the area of significance.

3. NTRUEncrypt modification is faster than RSA by 84%. The obtained empirical value $U = 0$ is in the area of significance.

Decryption

1. NTRUEncrypt modification is 17% faster than NTRUEncrypt. The obtained empirical value $U = 24$ is in the zone of uncertainty.

2. NTRUEncrypt program is faster than RSA by 99%. The obtained empirical value $U = 0$ is in the area of significance.

3. NTRUEncrypt is99% faster than RSA. The obtained empirical value $U = 0$ is in the area of significance.

Discussion and Conclusions. In the framework of this research, the following is developed:

- software that implements the NTRUEncrypt cryptosystem operation;
- software that implements this cryptosystem modification.

One of the NTRUEncrypt advantages over its counterpart - the RSA cryptosystem, a higher speed of operation can be specified. Performing encryption and decryption operations requires $O(n^2)$ operations, unlike $O(n^3)$ in the same RSA. As for the experimental data, the NTRUEncrypt program wins significantly on the speed of the algorithm compared to RSA. In addition, there is a slight increase in durability with the same key length. The disadvantage of the system is the necessity for using the recommended parameters.

Regarding the NTRUEncrypt resistance, after the creation of quantum computers, the problems of fast factorization and discrete logarithmation will be solved [7]. In this case, RSA, DSA, and similar algorithms will become useless. The relevance of NTRUEncrypt will remain: it will be fully applicable in the “post-quantum” era since there is no algorithm that solves the problem of the shortest lattice vector.

The advantage of using the NTRUEncrypt algorithm modification is experimentally proven. The developed application performs the general work on key generation, encryption and decryption 25% faster. In addition, it optimizes the use of internal memory through reducing the weight of the original program file and the size of the private key. When attempting to crack a ciphertext, cryptographic robustness and the complexity of using quantum algorithms are manifested.

References

1. Shor, P. Algorithms for Quantum Computation: Discrete Log and Factoring. Murray Hill: AT&T Bell Labs, 1994, pp. 124–134.

2. Shakleina, T.A. «Mozgovye tsentry» i ikh rol' v formirovanii vneshney politiki SShA. [“Brain centers” and their role in making US foreign policy.] Vvedenie v prikladnoy analiz mezhdunarodnykh situatsiy. [Introduction to the applied analysis of international situations.] Moscow: Aspect press, 2014, p. 112 (in Russian).

3. Alferov, A.P., et al. Osnovy kriptografii. [Cryptography basics.] Moscow: Gelios ARV, 2002, pp. 209–220 (in Russian).

4. Laponina, O.R. Kriptograficheskie osnovy bezopasnosti. [Cryptographic Security Basics.] Moscow: National Open University INTUIT, 2016, pp. 118 (in Russian).

6. Ishmukhametov, Sh.T. Metody faktorizatsii natural'nykh chisel. [Methods of factorization of natural values.] Kazan: Kazan University Publ. House, 2011, pp. 74–82 (in Russian).

5. Bakhtiari, M., Maarof, M.A. Serious Security Weakness in RSA Cryptosystem. International Journal of Computer Science and Information Security, 2012, no. 3, pp. 175–178.

7. Vasilenko, O.N. Teoretiko-chislovye algoritmy v kriptografii. / [Number theoretic cryptoalgorithms.] Moscow: MTsNMO, 2003, pp. 73–74 (in Russian).

Submitted 23.10.2018
Scheduled in the issue 14.03.2019

Authors:

Razumov, Pavel V.,
student of the Cybersecurity of IT Systems Department, Don State Technical University
(1, Gagarin sq., Rostov-on-Don, 344000, RF),
ORCID: https://orcid.org/0000-0003-2454-3600
therazumov@gmail.com

Smirnov, Ivan A.,
student of the Cybersecurity of IT Systems Department, Don State Technical University
(1, Gagarin sq., Rostov-on-Don, 344000, RF),
ORCID: https://orcid.org/0000-0001-6533-4368
terran.doatk@mail.ru

Pilipenko, Irina A.,
postgraduate student of the Cybersecurity of IT Systems Department, Don State Technical University
(1, Gagarin sq., Rostov-on-Don, 344000, RF),
ORCID: https://orcid.org/0000-0003-3236-6069
ipilipenko@donstu.ru

Selyova, Antonina V.,
student of the Cybersecurity of IT Systems Department, Don State Technical University
(1, Gagarin sq., Rostov-on-Don, 344000, RF),
ORCID: https://orcid.org/0000-0003-0990-7429
tone4ka.selyova@yandex.ru

Cherkesova, Larisa V.,
professor of the Cybersecurity of IT Systems Department, Don State Technical University
(1, Gagarin sq., Rostov-on-Don, 344000, RF), Dr.Sci. (Eng.), professor,
ORCID: https://orcid.org/0000-0002-9392-3140
chia2002@inbox.ru

ИНФОРМАТИКА, ВЫЧИСЛИТЕЛЬНАЯ ТЕХНИКА И УПРАВЛЕНИЕ
INFORMATION TECHNOLOGY, COMPUTER SCIENCE, AND MANAGEMENT

UDC 51–76 https://doi.org/10.23947/1992-5980-2019-19-2-195-203

Optimization of two-stage methanogenesis regime based on the Pontryagin's maximum principle *

S. A. Korolev[1], D. V. Maykov[2]**

[1] Kalashnikov Izhevsk State Technical University, Izhevsk, Russian Federation
[2] Izhevsk Trade and Economics College, Izhevsk, Russian Federation

Оптимизация двухстадийного режима метаногенеза на основе принципа максимума Понтрягина***

С. А. Королев[1], Д. В. Майков[2]**

[1] Ижевский государственный технический университет им. М. Т. Калашникова, г. Ижевск, Российская Федерация
[2] Ижевский торгово-экономический техникум, г. Ижевск, Российская Федерация

Introduction. The solution to the problem of optimal control of the biogas process under its conversion in two digesters is considered. The work objectives are to propose a mathematical model of this process and to develop an optimal control algorithm.

Materials and Methods. The developed mathematical model describes the biomethanation from animal waste through the downstream processing of the substrate in two digesters. Cases of the same and different temperature media (mesophilic and thermophilic) are considered. An optimal control problem is defined as a Lagrange problem for this model. Its modifiers are the rates of substrate entry into the digesters. The algorithm for solving this problem is proposed; it is based on the numerical implementation of the Pontryagin maximum principle. When optimizing, a hybrid genetic algorithm was used with an additional search in the neighborhood of the best solution through the conjugate gradient method.

Research Results. A new mathematical model is developed. It describes the biomethanation during the downstream processing of the substrate in two digesters. A numerical algorithm for solving an optimal control problem is proposed and software-implemented. The numerical studies have shown that the biogas production rate is nearly twice as high for a thermophilic medium as for a mesophilic one. It is established that the downstream processing of the substrate in two digesters with the same temperature medium allows the biogas production rate to be doubled. If the temperature media in the digesters are different, then in the first of them, the mesophilic medium should be used, and in the second - the thermophilic medium. At this, the biogas formation rate is somewhat lower compared to the case when there is a mesophilic medium in each of the digesters; however, the degree of the substrate processing is by 10–15% higher.

Введение. Статья посвящена решению задачи оптимального управления процессом получения биогаза при непрерывном режиме его переработки в двух метантенках. Цели работы: представить математическую модель данного процесса и разработать алгоритм выбора оптимального управления.

Материалы и методы. Созданная математическая модель описывает получение биогаза из отходов животноводства при последовательной переработке субстрата в двух метантенках. Рассматриваются случаи одинаковых и различных температурных сред (мезофильной и термофильной). Для данной модели сформулирована задача оптимального управления в виде задачи Лагранжа. Ее управляющими параметрами являются скорости поступления субстрата в метантенки. Предложен алгоритм решения данной задачи, основанный на чис
ленной реализации принципа максимума Понтрягина. При оптимизации применялся гибридный генетический алгоритм с дополнительным поиском в окрестности лучшего решения методом сопряженных градиентов.

Результаты исследования. Разработана новая математическая модель, описывающая процесс получения биогаза при последовательной переработке субстрата в двух метантенках. Предложен и программно реализован численный алгоритм решения задачи оптимального управления.Численные исследования показали, что для термофильной среды скорость образования биогаза практически вдвое выше, чем для мезофильной. Установлено, что последовательная переработка субстрата в двух метантенках с одинаковыми температурными средами позволяет вдвое увеличить скорость образования биогаза. Если температурные среды в метантенках различны, то в первом из них следует использовать мезофильную среду, а во втором — термофильную. При этом скорость образования биогаза несколько ниже по сравнению со случаем, когда в каждом из метантенков мезофильная среда, однако степень переработки субстрата выше на 10–15 %.

* The research is done within the frame of the independent R&D.
** E-mail: stkj@mail.ru, MaykovD@yandex.ru
*** Работа выполнена в рамках инициативной НИР.

Discussion and Conclusions. The results obtained can be used for the calculation and design of biogas plants, as well as in the development of appropriate software.

Keywords: methanogenesis, biogas, digester, animal waste treatment, mathematical model, differential equation system, numerical solution, optimization methods, optimal control, Pontryagin's maximum principle.

For citation: S.A. Korolev, D.V. Maykov. Optimization of two-stage methanogenesis regime based on the Pontryagin's maximum principle. Vestnik of DSTU, 2019, vol. 19, no. 2, pp. 195–203. https://doi.org/10.23947/1992-5980-2019-19-2-195-203

Обсуждение и заключения. Полученные результаты могут быть использованы для расчета и конструирования биогазовых установок, а также при разработке соответствующего программного обеспечения.

Ключевые слова: метаногенез, биогаз, метантенк, переработка отходов животноводства, математическая модель, система дифференциальных уравнений, численное решение, методы оптимизации, оптимальное управление, принцип максимума Понтрягина.

Образец для цитирования: Королев, С. А. Оптимизация двухстадийного режима метаногенеза на основе принципа максимума Понтрягина / С. А. Королев, Д. В. Майков // Вестник Дон. гос. техн. ун-та. — 2019. — Т. 19, № 2. — С.195–203. https://doi.org/10.23947/1992-5980-2019-19-2-195-203

Introduction. When livestock enterprises, in particular, poultry farms, pig farms, cattle farms, are operated, a large amount of waste is generated. As a result of their fermentation in special tanks (digesters), fuel gas (biogas) and valuable organic fertilizers can be obtained [1]. This process is called methanogenesis. It can occur under the periodic and continuous delivery of the substrate. In the first case, the digester is filled once and emptied completely upon completion of the fermentation. In the second case, two processes occur simultaneously and continuously: the supply of the substrate and the removal of its processed portion.

Usually, mesophilic medium (at a temperature of 25–38° C) or thermophilic (45–60° C) is used for methanogenesis. The optimum temperature for the mesophilic medium is 37° C, for the thermophilic medium, it is 56° C. The fermentation time for these media is 25 and 12 days, respectively.

The economic efficiency of biogas production depends on various factors: type and quantity of raw materials, climatic conditions [2], etc. In addition, the rate of substrate input into the digester affects significantly the biomethanation. This parameter value depends on the volume of the digester and the type of raw materials. To find the optimal value of the specified magnitude, it is required to solve an optimal control problem.

Under the continuous mode of fermentation, the substrate does not have time to go through full processing. To increase the biogas production, it is necessary to use two digesters so that the substrate is sequentially processed in each of them. Various aspects of this process are studied in [3, 4], and its technical implementations are reflected in the patents [5–7].

In the papers on the mathematical simulation of methanogenesis, for example [8, 9], the search for optimal control is not presented or its asymptotic value is found [10–12]. An analytical solution to the optimal control problem is obtained in [13]. However, the mathematical model described there differs significantly from that presented in this paper. The numerical method proposed here for solving an optimal control problem is applicable to a wide class of models.

Materials and Methods. The scheme of downstream processing of the substrate is shown in Fig. 1.

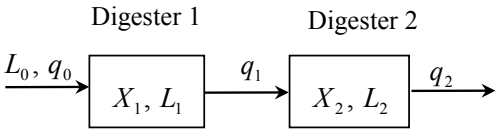

Fig. 1. Scheme of two-stage mode of methanogenesis

Assume L_0 is the concentration of nutrients in the substrate fed to the first digester (kg/m^3); L_1 and L_2 are the concentration of nutrients in the substrate for the first and second digesters, respectively (kg/m^3); X_1 and X_2 are the concentration of methane-producing bacteria in the first and second digesters (kg/m^3); Q_1 is the volume of the substrate in the first digester (m^3), Q_2 - in the second one; q_0 is the rate of the substrate input in the first digester (m^3/day), $q_1 = \frac{dQ_1}{dt}$ and $q_2 = \frac{dQ_2}{dt}$ are the rate of substrate delivery from the first and second digesters, respectively.

Losses of the substrate do not occur, therefore

$$q_0 = q_1 = q_2 = q\,.$$

The value of q_0 is determined by the volume of waste, the quantity and capacity of the biogas plants.

Relative rates of substrate input for the digesters are:

$$u_1 = \frac{1}{Q_1} \cdot \frac{dQ_1}{dt} = \frac{q_1}{Q_1} \text{ and } u_2 = \frac{1}{Q_2} \cdot \frac{dQ_2}{dt} = \frac{q_2}{Q_2}.$$

Substrate volumes in the digesters are equal to

$$Q_1 = \frac{q}{u_1} \text{ and } Q_2 = \frac{q}{u_2} = \frac{u_1 Q_1}{u_2}.$$

To describe methanogenesis during downstream processing of the substrate, a mathematical model based on the mathematical model of the population dynamics of methane-producing bacteria for a one-stage methanogenesis mode is used [11, 14]:

$$\begin{cases} \frac{dX_1}{dt} = \left(\frac{\mu_{mg1} L_1}{a_1 + L_1} - \frac{\mu_{md1} b_1}{b_1 + L_1} - u_1 \right) \cdot X_1, \\ \frac{dL_1}{dt} = u_1 \cdot (L_0 - L_1) - \frac{\beta_1 \mu_{mg1} L_1 X_1}{a_1 + L_1}, \\ \frac{dX_2}{dt} = \lambda u_2 X_1 + \left(\frac{\mu_{mg2} L_2}{a_2 + L_2} - \frac{\mu_{md2} b_2}{b_2 + L_2} - u_2 \right) \cdot X_2, \\ \frac{dL_2}{dt} = u_2 \cdot (L_1 - L_2) - \frac{\beta_2 \mu_{mg2} L_2 X_2}{a_2 + L_2}. \end{cases} \quad (1)$$

Here, the subscripts of the variables (X_i, L_i) and parameters ($\mu_{mg\,i}$, $\mu_{md\,i}$, a_i, b_i, β_i, u_i) correspond to the number of the digester $i \in \{1, 2\}$. The model parameters are $\mu_{mg\,i}$ and $\mu_{md\,i}$, the maximum possible relative rates of growth and dieoff of bacteria, respectively (day^{-1}); β_i is dimensionless coefficient of the substrate absorption; a_i and b_i are empirical coefficients (m^3/kg); λ is parameter equal to zero if the temperature media in the digesters are different, and equal to one if these media are the same.

Values of the model parameters are determined in accordance with the selected temperature regime of the methanogenesis (mesophilic or thermophilic). If temperature media in the digesters are the same, then $\mu_{mg1} = \mu_{mg2} = \mu_{mg}$, $\mu_{md1} = \mu_{md2} = \mu_{md}$, etc.

The initial conditions are:

$$X_1(0) = X_2(0) = X_0,\ L_1(0) = L_2(0) = L_0,$$

where X_0 is a natural concentration of methane-producing bacteria in the feedstock; L_0 is equal to the concentration of nutrients in the unprocessed substrate.

The model (1) is built on the assumption that the digesters maintain an optimal and constant process temperature. If the temperature media are different, then, when the substrate is fed from one digester to another, heating or cooling to the temperature in the second digester should occur.

The rate of biogas production (m^3/day) in the i-th digester is equal to

$$w_i = \frac{\gamma_i \mu_{mg\,i} L_i X_i}{a_i + L_i},$$

where γ_i is the coefficient characterizing the rate of conversion of substrate nutrients into biogas (m^3 • m^3/kg).

To obtain the optimal control problem, it is necessary to supplement the system of equations (1) with the criterion functional

$$V = \int_0^T \left(\frac{\gamma_1 \mu_{mg1} L_1 X_1}{a_1 + L_1} + \frac{\gamma_2 \mu_{mg2} L_2 X_2}{a_2 + L_2} \right) dt \to \max, \quad (2)$$

that determine the total biogas yield from 1 m^3 of the substrate in the first and second digesters over time T. The optimized parameters of the problem are relative rates of the substrate delivery into the digesters u_1 and u_2 in the system of equations (1).

The systems (1) - (2) are Lagrange problems. In general case of the optimal control problem, there is a system of differential equations of the form:

$$\frac{d\mathrm{x}}{dt} = \mathrm{f}(\mathrm{x}(t), \mathrm{u}(t), t),\ t \in [0, T],\ \mathrm{x} \in R^n,\ \mathrm{u} \in R^k, \quad (3)$$

its initial conditions are:

$$\mathrm{x}(0)=\mathrm{x}_0.$$

It is required to find the optimal control $\mathrm{u}(t)$ delivering a maximum to the criterion functional

$$J=\int_0^T F_0\left(\mathrm{x}(t),\,\mathrm{u}(t),\,t\right)\to\max. \tag{4}$$

For the numerical solution to the problem, a difference grid with nodes $t_0=0$, t_1, t_2, ..., t_i, t_{i+1}, ..., $t_q=T$ with the constant step $h=t_{i+1}-t_i$ is introduced on the interval $[0,\,T]$ [15].

The numerical solution to the system of differential equations (3) is carried out through the fourth-order Runge–Kutta method:

$$\begin{gathered}\mathrm{x}_{i+1}=\mathrm{x}_i+\frac{h}{6}\cdot\left(\mathrm{k}_1+2\mathrm{k}_2+2\mathrm{k}_3+\mathrm{k}_4\right),\ i=\overline{0,\,q-1},\\ \mathrm{k}_1=\mathrm{f}\left(\mathrm{x}_i,\,\mathrm{u}_i,\,t_i\right),\\ \mathrm{k}_2=\mathrm{f}\left(\mathrm{x}_i+\frac{h}{2}\cdot\mathrm{k}_1,\,\mathrm{u}_i,\,t_i+\frac{h}{2}\right),\\ \mathrm{k}_3=\mathrm{f}\left(\mathrm{x}_i+\frac{h}{2}\cdot\mathrm{k}_2,\,\mathrm{u}_i,\,t_i+\frac{h}{2}\right),\ \mathrm{k}_3=\mathrm{f}\left(\mathrm{x}_i+\frac{h}{2}\cdot\mathrm{k}_2,\,\mathrm{u}_i,\,t_i+\frac{h}{2}\right),\\ \mathrm{k}_4=\mathrm{f}\left(\mathrm{x}_i+h\cdot\mathrm{k}_3,\,\mathrm{u}_i,\,t_i+h\right).\end{gathered} \tag{5}$$

To solve the problem, it is convenient to introduce qk-dimensional full control vector $\mathrm{U}=\left(\mathrm{u}_i\right),\ i=\overline{1,\,q}$. In this case, the difference approximation of the criterion functional (4) is the expression:

$$J=J\left(\mathrm{U}\right)=\sum_{i=0}^{q}F_0\left(\mathrm{x}_i,\,\mathrm{u}_i,t_i\right)\cdot h\to\max. \tag{6}$$

The problem is solved in the sequence given below.

1) Set the full control vector U.

2) The initial system of differential equations (3) is solved numerically using the relations (5), and the value of the criterion functional (4) is calculated using the difference approximation (6).

3) The system of adjoint equations is numerically integrated (in the direction "from right to left") according to the relations:

$$\begin{gathered}\mathrm{p}_i=\mathrm{p}_{i+1}+h\cdot\frac{\partial F_0}{\partial\mathrm{x}_i}+G_i^T\cdot\mathrm{p}_{i+1}\cdot h,\ i=\overline{1,\,q-1},\\ \mathrm{p}_q=0.\end{gathered} \tag{7}$$

Here, $\mathrm{p}=\mathrm{p}(t)$ are dual variables of the Pontryagin maximum principle; $G_i=\left(\frac{\partial\mathrm{f}\left(\mathrm{x}_i,\mathrm{u}_i,t_i\right)}{\partial\mathrm{x}_i}\right)$ is Jacobi matrix composed for the system (3).

4) The optimization process is performed by vector U. In this paper, the genetic algorithm with real coding and an additional search in the neighborhood of the best solution through the conjugate gradient method was used as the optimization method.

For the considered problem of methanogenesis optimization, the vector of phase variables is equal to $\mathrm{x}=\mathrm{colon}\left(X_1,\,L_1,\,X_2,\,L_2\right)$, the control vector is equal to $\mathrm{u}=\mathrm{colon}\left(u_1,u_2\right)$, and the Jacobi matrix has the form:

$$G=\begin{pmatrix}\frac{\mu_{mg1}L_1}{a_1+L_1}-\frac{\mu_{md1}b_1}{b_1+L_1}-u_1 & \frac{a_1\mu_{mg1}X_1}{\left(a_1+L_1\right)^2}+\frac{b_1\mu_{md1}X_1}{\left(b_1+L_1\right)^2} & 0 & 0\\ -\frac{\beta_1\mu_{mg1}L_1}{a_1+L_1} & -u_1-\frac{\beta_1a_1\mu_{mg1}X_1}{\left(a_1+L_1\right)^2} & 0 & 0\\ \lambda u_2 & 0 & \frac{\mu_{mg2}L_2}{a_2+L_2}-\frac{\mu_{md2}b_2}{b_2+L_2}-u_2 & \frac{a_2\mu_{mg2}X_2}{\left(a_2+L_2\right)^2}+\frac{b_2\mu_{md2}X_2}{\left(b_2+L_2\right)^2}\\ 0 & u_2 & -\frac{\beta_2\mu_{mg2}L_2}{a_2+L_2} & -u_2-\frac{\beta_2a_2\mu_{mg2}X_2}{\left(a_2+L_2\right)^2}\end{pmatrix}.$$

Research Results. The theoretical values of the variables found as a result of the numerical solution to the system of differential equations of the mathematical model of methanogenesis are recorded. The deviations of the specified values from the experimental values with respect to the vector of parameters [10, 16] (Table 1) are considered. The parameter values of the methanogenesis model are estimated through minimizing the sum of squares of these deviations.

Table 1

Estimates of methanogenesis model parameters for mesophilic / thermophilic media

Coefficient	Source of raw materials		
	Poultry factories	Pig farms	Cattle farms
μ_{mg}	0.482 / 0.821	0.346 / 0.783	0.297 / 0.563
μ_{md}	0.353 / 0.528	0.291 / 0.423	0.254 / 0.351
a	34.781 / 43.875	7.242 / 21.653	5.013 / 8.733
b	116.457 / 14.674	37.347 / 9.278	18.722 / 5.455
β	2.344 / 3.189	1.495 / 2.084	1.413 / 1.983
γ	1.463 / 1.963	1.373 /1.907	1.299 / 1.813

The following methods for processing the substrate are considered.

I. A single digester is used.

II. Two digesters are used with the downstream processing of the substrate, in which temperature media coincide.

At this, two options of the medium are possible for each digester: mesophilic or thermophilic (Table 2).

Table 2

Optimal methanogenesis parameters

Characteristics	Source of raw materials		
	Poultry factories	Pig farms	Cattle farms
I. One digester with mesophilic / thermophilic medium			
u^*, day $^{-1}$	0.149 / 0.402	0.128 / 0.341	0.112 / 0.268
w^*, m^3/ day	7.25 / 24.51	3.58 / 10.76	1.81 / 5.42
L^* / L_0, %	56 / 43	51 / 38	52 / 41
II. Two digesters with mesophilic / thermophilic medium in each			
u_1^*, day $^{-1}$	0.168 / 0.432	0.144 / 0.362	0.117 / 0.287
u_2^*, day $^{-1}$	0.491 / 2.448	0.412 / 1.858	0.367 / 1.424
w^*, m^3/ day	15.19 / 50.21	7.79 / 22.19	3.85 / 10.92
L_2^* / L_0, %	45 / 35	38 / 33	38 / 33
III. Two digesters, in the first - mesophilic, in the second - thermophilic medium / in the first - thermophilic, in the second - mesophilic medium			
u_1^*, day $^{-1}$	0.149 / 0.402	0.128 / 0.341	0.112 / 0.268
u_2^*, day $^{-1}$	0.312 / 0.051	0.222 / 0.059	0.183 / 0.051
w^*, m^3/ day	15.35 / 25.12	6.61 / 11.42	3.26 / 5.42
L_2^* / L_0, %	30 / 34	29 / 35	26 / 32

Here, u^* are the optimal values of the relative rate of the substrate delivery; w^* is the corresponding daily average biogas yield; $\frac{L^*}{L_0}$ is the completeness of the processing of substrate nutrients.

Graphs of the biogas production rate are shown in Fig. 2.

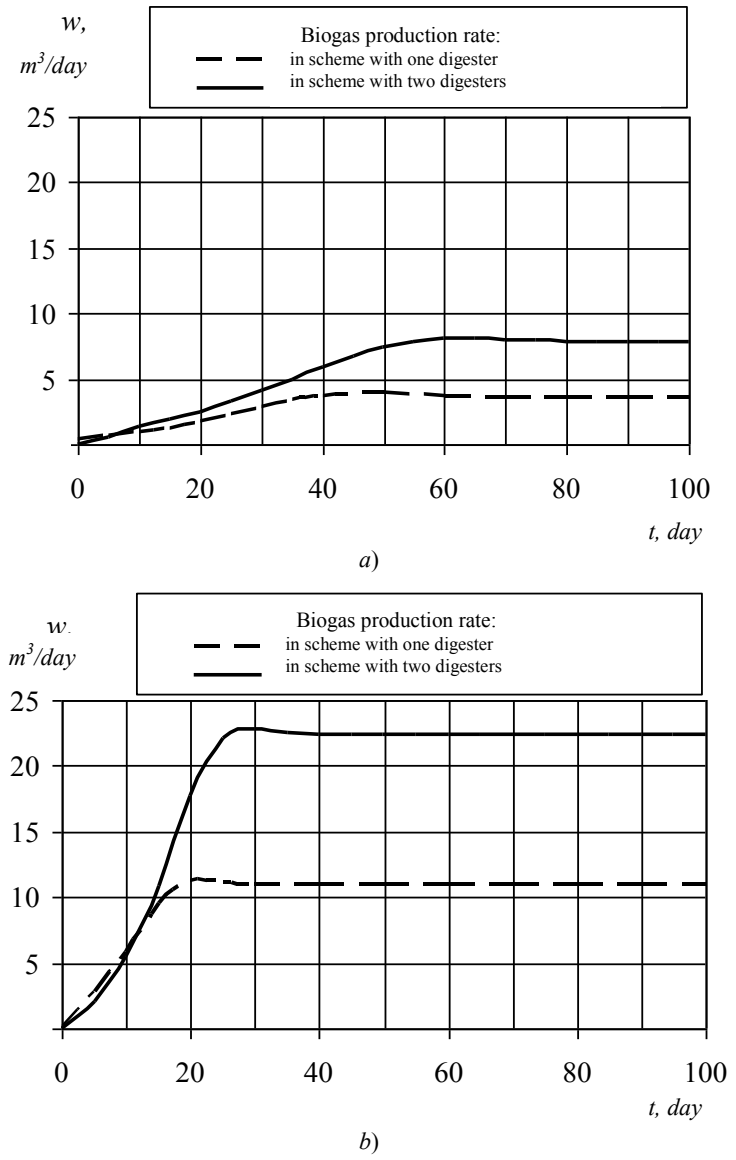

Fig. 2. Biogas production rate when using waste of pig farms for two digesters with mesophilic (*a*) and thermophilic (*b*) medium in each

III. Two digesters are used with downstream processing of the substrate, in which the temperature media are different.

Here, two cases are considered.

1) In the first digester, there is mesophilic medium, and in the second - thermophilic medium.

2) In the first digester, there is thermophilic medium, and in the second - mesophilic one.

See the optimal parameter values in Table 2.

Fig. 3 shows a graph of the biogas production rate.

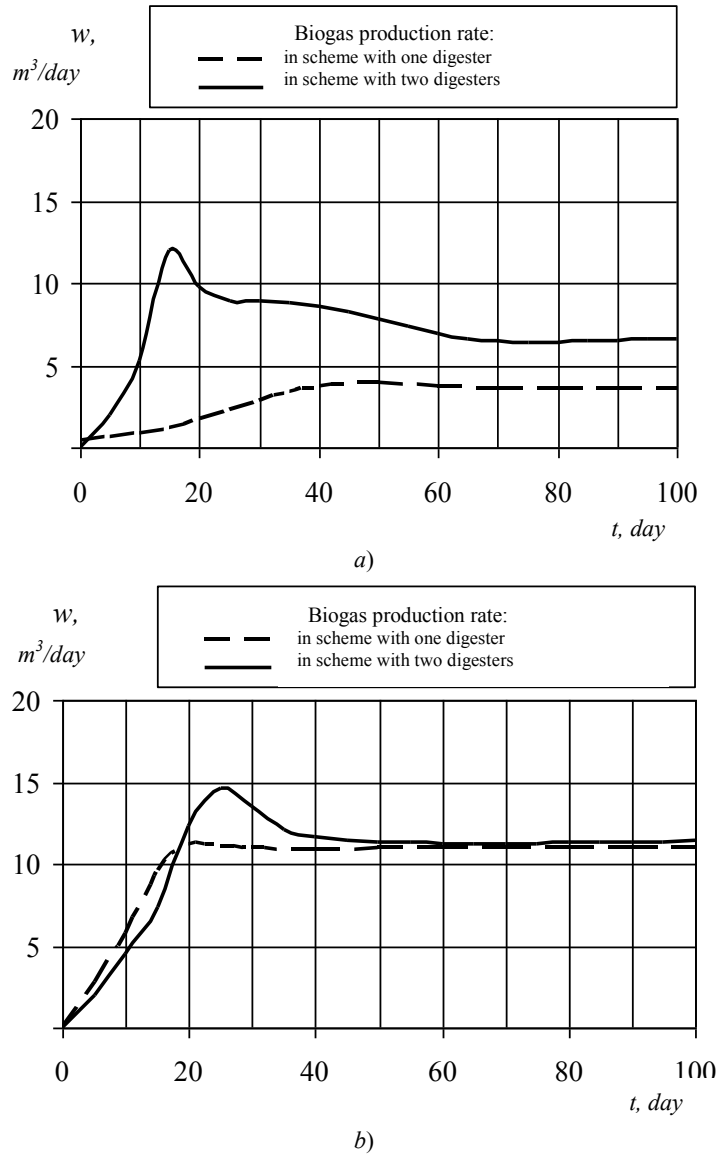

Fig. 3. Biogas production rate when using pig farm waste for two digesters: in the first digester there is mesophilic medium, in the second digester - thermophilic medium (*a*); in the first digester, there is thermophilic medium, in the second digester – mesophilic medium (*b)*

The use of a single digester in the continuous mode of fermentation enables to process the substrate nutrients by 40–45% for the mesophilic medium and by 50–55% for the thermophilic one.

When using two digesters with the same temperature media, the share of substrate processing increases by 10% for the mesophilic and by 5% for the thermophilic media. At this, the average daily production of biogas is almost doubled. The biogas production rate for the thermophilic environment is almost twice as high as for the mesophilic one.

Two digesters operating in different temperature media show different results. So, in the first case, the share of substrate processing is about 25% higher than when using a single digester with a mesophilic medium. In the second case, the share of substrate processing is 5–10% higher than when using a single digester with a thermophilic medium. Besides, the organization of the process in the first case provides a nearly twofold increase in the rate of biogas production (when compared to a single digester with a mesophilic medium). In the second case, a significant increase in speed is not observed (if compared to a thermophilic medium). It follows from the above that the second case is not advisable.

The first option loses somewhat in the rate of biogas production in case of using two digesters with a mesophilic medium in each, although it provides a higher (by 10–15%) degree of the substrate processing. This is due to the fact that with the use of two digesters with a mesophilic medium, the optimal values of the relative (and therefore absolute) rates of substrate input are higher, that is, more of the substrate is processed per unit of time. The rate of biogas generation for the second option is twice as low as for the case of using two digesters with a thermophilic medium.

Discussion and Conclusions. Mathematical models are developed that describe the methanogenesis during the downstream substrate processing in two digesters when the temperature media in them coincide and differ. These models correspond to the problem of optimal control of the methanogenesis process on the basis of the Pontryagin maxi-

mum principle. The paper describes an algorithm for its solution. The control parameters are relative rates of the substrate delivery into the digesters.

The numerical study results show that the sequential application of two digesters with the same temperature media allows for an increase in the degree of substrate processing by 5–10%. At the same time, the rate of biogas production is doubled. The degree of processing of the substrate for the mesophilic mode is also 5–10% higher than for the thermophilic one. At the same time, the biogas production rate in a thermophilic medium is almost twice as high as in a mesophilic one. This is due to the higher intensity of the process (higher than the optimal value of the relative rate of the substrate delivery).

The results of the operation of digesters with different temperature media are also shown. In the first case, the substrate is first processed in a mesophilic medium, and then enters the digester with a thermophilic medium. In the second case, on the contrary, the substrate from the digester with a thermophilic medium enters the digester with a mesophilic medium. In the first case, more substrate is processed. When compared to the use of a single digester with a mesophilic medium, the advantage is about 25%. When compared to the use of a single digester with a thermophilic medium, it is 5–10%. In the first case, the rate of biogas production is almost twice as high as in the case of a single digester with a mesophilic medium. In the second case, the rate of biogas production is almost the same as when using a single digester with a thermophilic medium. Thus, the second case is impractical.

In the first case, the biogas formation rate is somewhat lower than in the case of using two digesters with a mesophilic medium in each, but at the same time, the degree of substrate processing is 10–15% higher. In the second case the biogas production rate is twice as low as when using two digesters with a thermophilic medium in each, which again shows the inefficiency of the second case.

References

1. Gyunter, L.I., Goldfarb, L.L. Metantenki. [Digesters.] Moscow: Stroyizdat, 1991, 128 p. (in Russian).

2. Korolev, S.A., Maykov, D.V. Vliyanie klimaticheskikh usloviy na teplovoy rezhim raboty biogazovoy ustanovki. [Influence of climatic conditions on the termal mode of a biogas plant.] Vestnik Izhev. gos. tekhn. un-ta, 2011, no. 2 (50), pp. 209–213 (in Russian).

3. Vohmin, V.S. Issledovanie konvektivno-induktsionnogo nagreva pri anaerobnom sbrazhivanii otkhodov zhivotnovodcheskikh ferm. [Research of convective induction heating in anaerobic fermentation of animal farms waste.] Scientific Journal of KubSAU, 2011, no. 70, pp. 123–135 (in Russian).

4. Sakhmetova, G.E., Shinibekova, R.A. Masshtabirovanie i opredelenie parametrov reaktora-modulya biogazovykh ustanovok blochno-modul'nogo tipa. [Scaling and determination of parameters of reactor-module of biogas modular plants.] Priority directions of science and education development, 2016, no. 3 (10), pp. 95–99 (in Russian).

5. Reshetnikova, I.V., et al. Biogazovaya ustanovka s dozirovannym SVCh-nagrevom: patent 2490322 Ros. Federatsiya. [Biogas plant with dosed microwave heating.] RF patent, no. 2490322, 2013 (in Russian).

6. Golenkovsky, I.M., Gumirov, M.F., Nurutdinov, R.F. Ustroystvo dlya polucheniya metana pri pererabotke biomassy: patent 132439 Ros. Federatsiya: C02F 11/04 [Device for methanation in the biomass processing.] RF patent, no. 132439, 2013 (in Russian).

7. Svalova, M.V., et al. Biogazovaya ustanovka: patent 2404240 Ros. Federatsiya: C12M 1/107 [Biogas plant.] RF patent, no. 2404240, 2010 (in Russian).

8. Batstone, D.J., et al. The IWA Anaerobic Digestion Model No 1 (ADM1). Water Science and Technology, 2002, vol. 45, iss. 10, pp. 65–73.

9. Delgadillo-Mirquez, L., Hernández-Sarabia, M. Mathematical modelling and simulation for biogas production from organic waste. International Journal of Engineering Systems Modelling and Simulation, 2018, vol. 10, iss. 2, pp. 97–102. DOI: 10.1504/IJESMS.2018.10013112.

10. Korolev, S.A., Maykov, D.V. Identifikatsiya matematicheskoy modeli i issledovanie razlichnykh rezhimov metanogeneza v mezofil'noy srede. [Identification of a mathematical model and research of the various modes of methanogenesis in mesophilic environments.] Computer Research and Modeling, 2012, vol. 4, no. 1, pp. 131–141 (in Russian).

11. Rusyak, I.G., Korolev, S.A., Maykov, D.V. Issledovanie statsionarnykh resheniy i optimizatsiya parametrov matematicheskoy modeli metanogeneza. [The research of stationary solutions and the optimization of parameters of the mathematical model of methanogenesis.] Tomsk State University Journal of Mathematics and Mechanics, 2012, no. 3 (19), pp. 15–21 (in Russian).

12. Cortes, L.G., Cortes, S.K., Cortes L.E. Optimal Control Scheme on Anaerobic Processes in Biodigesters. Chemical engineering transaction, 2018, vol. 65, pp. 433–438. DOI: 10.3303/CET1865073.

13. Bayen, E., Cots, O., Gajardo, P. Analysis of an optimal control problem related to anaerobic digestion process. Journal of Optimization Theory and Applications, 2018, vol. 178, pp. 627–659. DOI: 10.1007/s1095.

14. Dvoretsky, D.S., et al. Komp'yuternoe modelirovanie biotekhnologicheskikh protsessov i system. [Computer simulation of biotechnological processes and systems.] Tambov: TSTU Publ. House, 2005, 80 p. (in Russian).

15. Yevtushenko, Yu.G. Metody resheniya ekstremal'nykh zadach i ikh primenenie v sistemakh optimizatsii. [Methods for solving extremum problems and their application in optimization systems.] Moscow: Nauka, 1982, 432 p. (in Russian).

16. Korolev, S.A., Maykov, D.V. Metod identifikatsii parametrov modeli metanogeneza v vide sistemy differentsial'nykh uravneniy na osnove geneticheskogo algoritma. [Method of identifying parameters of the model of methanogenesis as a system of differential equations based on genetic algorithm.] Intellektual'nye sistemy v proizvodstve, 2012, no. 1, pp. 29–35 (in Russian).

Submitted 29.03.2019
Scheduled in the issue 08.04.2019

Authors:

Korolev, Stanislav A.,
associate professor of the IT Systems Software Department, Kalashnikov Izhevsk State Technical University (7, Studencheskaya St., Izhevsk, 426069, RF), Cand. Sci. (Phys.-Math.), associate professor,
ORCID: https://orcid.org/0000–0002–8399–1385
stkj@mail.ru

Maykov, Dmitry V.,
mathematics teacher, Izhevsk Trade and Economics College (20a, Voroshilov St., Izhevsk, 426000, RF) ,
ORCID: https://orcid.org/0000-0002-8198-742X
MaykovD@yandex.ru